N O T I C E

THIS DOCUMENT HAS BEEN REPRODUCED FROM MICROFICHE. ALTHOUGH IT IS RECOGNIZED THAT CERTAIN PORTIONS ARE ILLEGIBLE, IT IS BEING RELEASED IN THE INTEREST OF MAKING AVAILABLE AS MUCH INFORMATION AS POSSIBLE

UNIVERSITY OF ILLINOIS
URBANA

AERONOMY REPORT
NO. 92

ROCKET MEASUREMENTS OF ELECTRON TEMPERATURE
IN THE E REGION

by

R. K. Zimmerman, Jr.
L. G. Smith

April 1, 1980
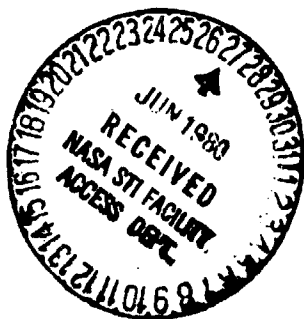
Aeronomy Laboratory
Department of Electrical Engineering
University of Illinois
Urbana, Illinois

CITATION POLICY

AERONOMY   REPORT

NO. 92

ROCKET MEASUREMENTS OF ELECTRON TEMPERATURE

IN THE E REGION

by

R. K. Zimmerman, Jr.
L. G. Smith

April 1, 1980

Aeronomy Laboratory
Department of Electrical Engineering
University of Illinois
Urbana, Illinois

ABSTRACT

The rocket-borne equipment, experimental method, and data reduction techniques used by the Aeronomy Laboratory in the measurement of electron temperature in the E region are fully described. Electron temperature profiles from one daytime equatorial flight and two nighttime midlatitude flights are discussed. The last of these three flights, Nike Apache 14.533, showed elevated E-region temperatures which are interpreted as the heating effect of a stable auroral red (SAR) arc.

TABLE OF CONTENTS

LIST OF TABLES

LIST OF FIGURES

1. INTRODUCTION

The Aeronomy Laboratory is engaged in a wide-ranging investigation of the lower ionosphere (50 to 200 km) using sounding rockets. Specific studies have included the winter anomaly in the D region, the formation of layers (including sporadic-E layers) by the action of the neutral winds and the production and loss of ionization (particularly the effects of energetic particles). This report is concerned with one aspect of the program: the measurement and analysis of electron temperature in the E region.*

Data from three Nike Apache rocket flights are presented. The first, Nike Apache 14.532 was launched from Chilca, Peru at 1526 LST (Local Standard Time) on 28 May 1975 as part of the NASA launch operation Antarqui. The second and third (Nike Apaches 14.534 and 14.533, in that sequence) were launched from Wallops Island, at 0001 EST on 10 August 1977 and at 0001 EST on 5 January 1978, respectively. The value of the 3-hour planetary index of geomagnetic activity (Kp) had the value, for the interval including the launch, of 2-, 4 and 5, respectively, for the three launches.

A Nike Apache rocket, of the type used in this investigation, is shown, in Figure 1.1, on a military rail launcher at Wallops Island.

Chapter 2 contains a general discussion of E-region electron temperatures during daytime and nighttime and, more specifically, of the role of energetic particles and a particular phenomenon: the stable auroral red (SAR) arc.

The use of Langmuir probes for *in situ* measurements in the ionosphere is described in Chapter 3 in terms of existing theories and regimes of operation. This chapter also contains a general description of the probes flown on the three rocket flights.

Details of the implementation of the experiment are given in Chapter 4. The equatorial launch (14.532) used both nose-tip and boom-mounted probes while the two midlatitude launches used only a nose-tip probe. Chapter 5 includes procedures for data reduction from digital data tapes.

The errors in the determination of electron temperature are discussed in Chapter 6 together with procedures (mainly in the software) that have been developed to minimize them.

---

*Although the ionospheric E region is conventionally defined as the altitude range of 90 to 160 km we will here, for convenience, use the term to include altitudes to 200 km.
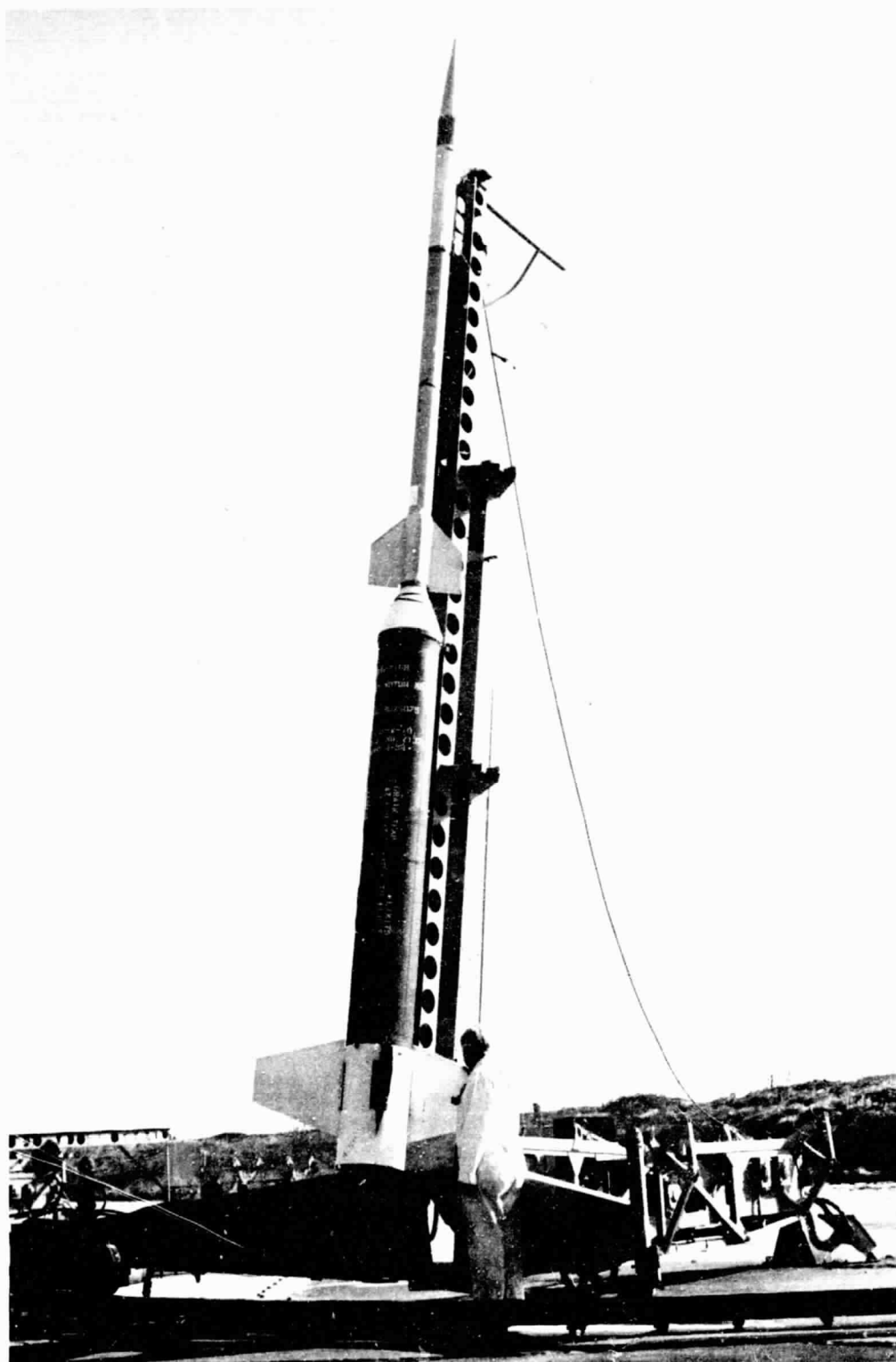
Figure 1.1 Nike Apache prior to nighttime launch at NASA Wallops Island range.

The equatorial launch was planned to allow a comparison between electron temperature measured independently by two rocket-borne probes and by the incoherent-scatter radar at Jicamarca. The results are presented in Chapter 7.

The observations from the two nighttime midlatitude launches are presented in Chapter 8.

Finally, Chapter 9 contains a summary of the study, some conclusions and suggestions for future work.

2. ELECTRON TEMPERATURE IN THE E REGION

2.1 *Heating Sources and Cooling Processes*

The ionospheric E region is composed of three interpenetrating fluids, these being the neutral gas, the positive ions (atomic and molecular), and the free electron gas. Additionally, in the lower E region, there are small numbers of negative ions formed through the process of electron attachment to neutral species. These negative ions are of no importance in terms of the E-region thermal balance because of their low concentration and will be ignored. Each of these three fluids has a characteristic temperature, a specific heat, and is in thermal contact (to a greater or lesser degree) with the other two components through collisional processes. At all altitudes and under all conditions most of the thermal energy is contained in the neutral gas.

2.1.1 *Lower E region.* At altitudes less than about 130 km there are sufficient collisions that the three fluids have the same temperature $(T_n = T_i = T_e)$. Evidence for this position has been obtained by incoherent-scatter radar studies of the lower E region by many researchers, for example: *Carru et al.*, 1967a, b; *Evans*, 1967; *Wand and Perkins*, 1968, 1970; and *Salah et al.*, 1975. At these altitudes the electron temperature will immediately follow any changes in the neutral gas temperature, and the question of heating and cooling the electron gas reduces to asking what processes heat and cool the neutral gas.

During the day solar ultraviolet radiation in the range 1026-1750 $\overset{o}{A}$ is absorbed by molecular oxygen causing photodissociation. The atomic oxygen produced in this manner liberates energy mainly as heat upon recombination. Solar X-rays ($\lambda > 1$ nm) are also important.

Another source of heating between 95 and 140 km is the dissipation of internal gravity waves, with periods between 5 minutes and 10 hours, propagating upward from the mesosphere. These waves yield energy to the neutral atmosphere up to heights of about 110 km by creating turbulence which eventually degrades to heat. At higher levels turbulence ceases [*Blamont and de Jager*, 1961]; the upper boundary of this region of mixing is called the turbopause.

Above the turbopause the dissipation of gravity-wave energy is due to molecular kinematic viscosity. The estimated heating rate due to these waves at midlatitude are 10 K/day at 95 km, 30 K/day at 105 to 110 km

and 100 K/day near 140 km [*Hines*, 1965]. If Hines is correct in these
estimates, then the heating due to gravity-wave dissipation is comparable
to heating due to solar-radiation absorption in the lower E region. Hines
has put this forth as an explanation of the rapid rise of temperature (with
increasing altitude) that occurrs in the E region.

Another major heat source is adiabatic compression of the atmosphere
by tidal motions. The tides are thought to be driven by the heating of
stratospheric-mesospheric ozone by UV radiation during the day [*Butler and
Small*, 1963; *Lindzen and Chapman*, 1969] and are often called thermal tides
to emphasize this point. Most of the energy of the ozone driving mechanism
goes into the first semidiurnal (2,2) tidal mode causing an upward and
downward propagating 12-hour pressure oscillation. The downward propagating
wave continues to the earth's surface and is observed there as a semidiurnal
pressure oscillation. The upward traveling (2,2) wave does not propagate to
the E region, becoming evanescent below the mesopause (at about 80 km).
However, there is mode mixing in the mesosphere, coupling the (2,2) mode
energy to the (2,3), (2,4) and (2,5) semidiurnal tidal modes. The (2,4)
mode, having a smaller equivalent depth than the (2,2) or (2,3) modes, can
propagate into the lower E region. As the wave passes through a given
altitude level, it causes a 12-hour rise and fall of the neutral gas
temperature T_n due to adiabatic compression and expansion. This modulation
of the temperature has been observed by the incoherent-scatter radar
facilities at Millstone Hill (42° N) and at St. Santin (45° N). It typically
amounts to an 11% variation in the mean temperature at 116 km but on occasion
as much as 20% variation is found [*Salah and Wand*, 1974].

There are other sources of heat in the midlatitude lower E region which
usually are not comparable in importance with the sources already discussed.
These include forms of chemical heating (other than the oxygen heating),
joule heating due to ionospheric dynamo electric currents, and heating due
to energetic-particle precipitation during times of moderate to severe
magnetic disturbance. This last effect might very well be more important
than previously assessed, particularly as an ionization and heating sources
at night. The Aeronomy Laboratory is currently engaged in a study of
energetic-particle flux in the E region using rocket-borne solid-state
particle detectors and data available from several orbiting satellites

[*Smith et al.*, 1974; *Voss and Smith*, 1979]. This source will be discussed separately in Section 2.2.

In all cases discussed here the neutral gas is colled by downward conduction of heat to the mesosphere. Above the turbopause this heat conduction is accomplished by molecular diffusion. At the turbopause and below the mechanism for heat conduction is eddy diffusion which carries heat through the temperature minimum at the mesopause and deposits the energy finally at heights of about 50 km.

Other sources of cooling such as radiative cooling by photoemission and chemical cooling by transport of atomic oxygen out of the region of production may also be significant.

2.1.2 *Upper E region.* At these altitudes the principal source of energy is also solar extreme ultraviolet radiation (EUV). At midlatitudes during the day there are no other competing sources of heat. Photoionization occurs, peaking at about 150 km, mainly due to absorption of radiation in the spectral range 140-796 Å [*Schunk and Walker*, 1973]. The energy of the ionizing photons well exceeds that required for ionization, the excess energy ₋oing into ion and electron kinetic energy, and electronic excitation of the resultant ion. The ion electronic excitation energy is typically less than 4 eV, leaving some tens of electron volts to be transferred to ion and electron kinetic energy. Most of the kinetic energy is carried by the electron, because of the large mas ratio between the ion and electron, resulting in hot photoelectrons. ⁻hese photoelectrons provide the entire heat input to the ambient electron gas. The route by which the photoelectrons share their energy with the population of thermal electrons is complicated, the general outline being given in Figure 2.1. Each photoelectron gives up most of its energy by effecting impact ionization of ambient neutrals, creating other excited ions and hot electrons. This will happen repeatedly and may be thought of as an energy cascade, since each impact ionization will remove 25 eV (mean) [*Pharo et al.*, 1971] from the photoelectron. Between impact ionizations the photoelectron loses energy in a continuous manner by elastic Coulomb collisions in the ambient thermal electron gas. The many hot electrons due to impact ionization also yield energy to the thermal population by Coulomb scattering, which is highly efficient because the masses of the scattering particles are equal. At altitudes less than
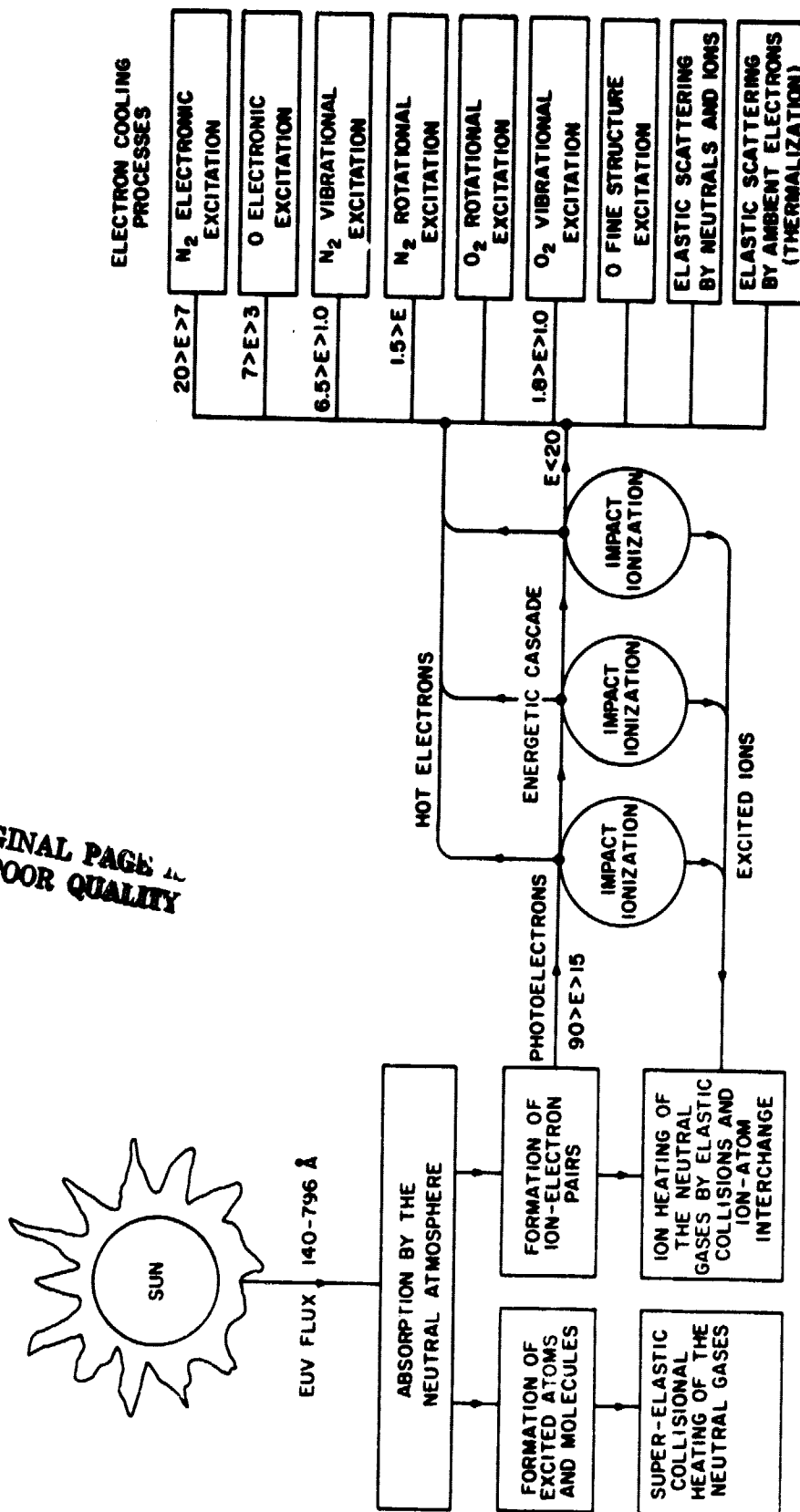
Figure 2.1 Energy flow in the E region. The photoelectron energy is degraded by successive impact ionization events, each requiring an average of about 25 eV. Energy levels shown are in eV.

200 km heating the thermal electron gas in the above manner is strictly a local heating process, meaning that the energy of the photoelectron will be dissipated within one neutral scale height of its origin site.

Solar EUV also causes direct heating of the neutral gas by formation of excited atoms and molecules. This energy is degraded and shared with the ambient neutral and ion gas by super-elastic collisions. Another less important source of heat for the neutral gas is excited photoions and hot ions created by photoelectron impact. If a general accounting of the heat input to the atmosphere is done, it is found that most of the heat input from solar EUV goes directly into warming the neutral atmosphere - the heat input to the neutral gas is roughly an order of magnitude greater than the heat input to the electron gas [Schunk and Walker, 1973]. However, the specific heat capacity of the electron gas is several orders of magnitude smaller than that of the neutral gas. It is expected, then, that the electron temperature T_e should be greater than the neutral gas temperature T_n, provided that the thermal contact between the two gases is weak enough to permit this to occur. This is precisely what happens, as satellite measurements in Figure 2.2 demonstrate. The lack of thermal equilibrium between the electron and neutral gas is the most striking difference between the ionosphere above 130 km and that below 130 km. Thermal nonequilibrium was first indicated by the rocket measurements performed in 1958 by Boggess et al. [1959] and verified since then by rocket, satellite, and radar studies. Energy flow from the hot electron gas to the warm neutral gas is moderated by the rather poor thermal contact between the two gases due to the neutral-electron collisional frequency decreasing with height.

Positive ions receive kinetic energy during the day in the ionization process and from Coulomb interactions with hot electrons. However, the ions are immersed in a sea of neutrals for which energy transfer by collision is a most efficient process, again, because of equal masses. This excellent thermal contact constrains the ion temperatures to be approximately equal to each other and equal to T_n. Often the ion temperatures for specific species T_i^j are all taken to be the same and are simply given as T_i. During the day ($T_i - T_n$) is usually no more than 10 K at 200 km, although sometimes it is as much as 100 K. A recent effort to measure T_n, T_i, and T_e simultaneously from the Atmosphere Explorer-C (Explorer 51) satellite is described in Brace et al. [1976]. Figure 2.2 is from this work, showing
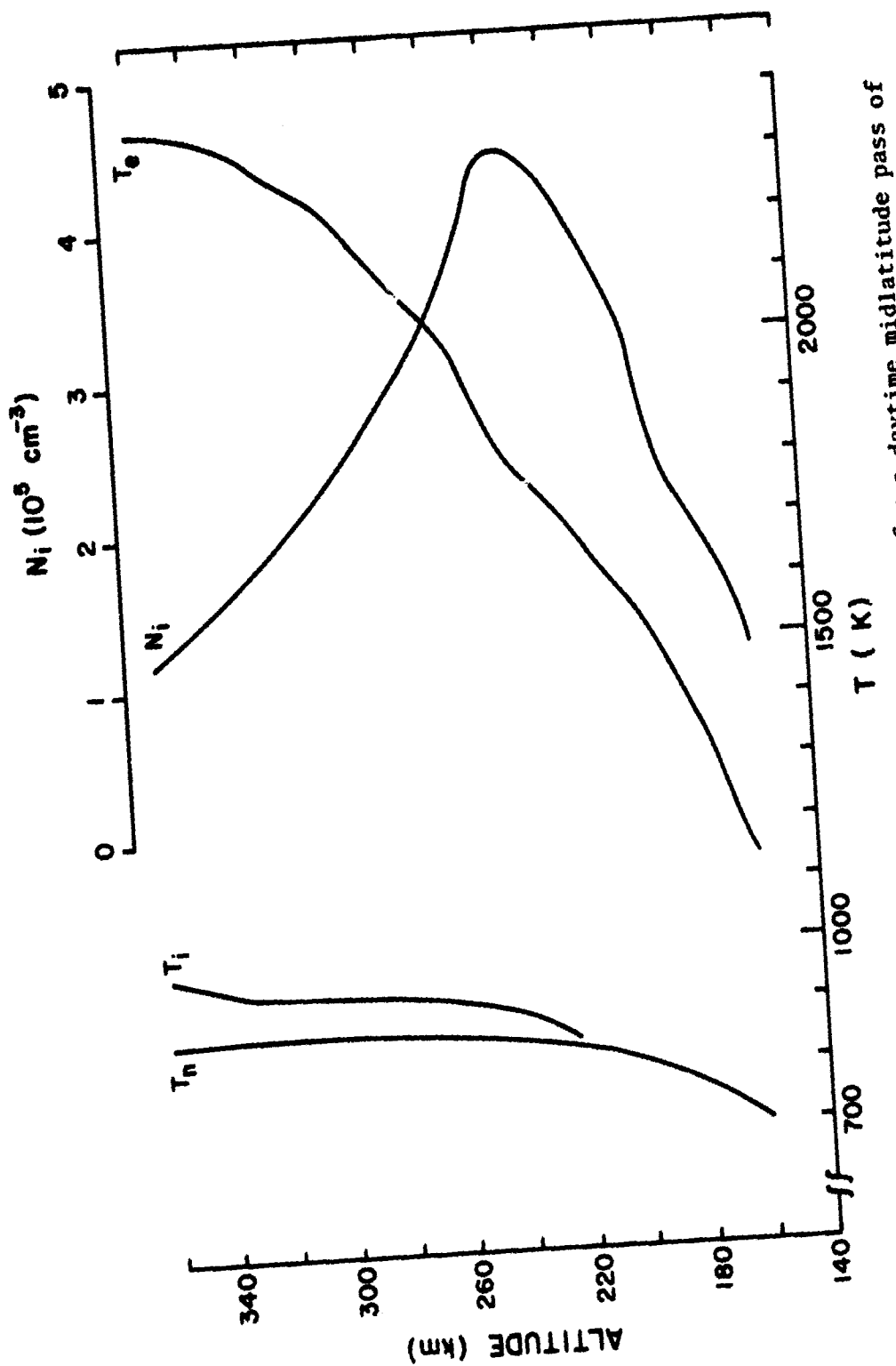
Figure 2.2 T_n, T_i, T_e, and ion concentration, N_i, for a daytime midlatitude pass of Atmosphere Explorer-C [Brace et al., 1976].

T_n, T_i, T_e and the ion concentration near perigee for a midlatitude pass during February. At 200 km the latitude was 33° N, the local time 1200 hr, and the solar zenith angle 48°. The pass occurred under moderately quiet geomagnetic conditions, the three-hour geomagnetic planetary index (Kp) being 2+. At 160 km the ion and neutral gas temperatures are the same at approximately 700 K. The electron temperature at the same altitude is about 1150 K. It is also clear from the diagram that in the F region the full heating and cooling theory for ions must be considered, as there is a significant departure from thermal equilibrium between ions and neutrals. However this is above the region of interest of this report.

The electron gas is cooled by a variety of processes which are indicated in Figure 2.1. Excitation of the fine structure levels of atomic oxygen is the dominant cooling mechanism for the electron gas. The fine structure levels are so closely spaced that they are easily excited even by thermal electrons, the energy then going into infrared radiation at 63 μm. Also important is the rotational excitation of N_2 and O_2. At elevated electron temperatures, say greater than 1500 K, cooling of the electron gas due to vibrational excitation of N_2 and O_2 must also be considered. Table 2.1, from *Schutz et al.* [1975], is a list of quantitative cooling formulas commonly used in modeling the thermosphere.

The ultimate fate of the electron gas thermal energy is to be transferred to the neutral gas, or to be lost as radiation at wavelengths for which the thermosphere is transparent. The former process has a small but significant effect on the neutral atmospheric temperature. Heat input to the neutral gas from the electron gas comprises roughly 15 percent of the total neutral gas heat influx [*Herman and Chandra*, 1969a,b]. Once energy is absorbed by neutral atmosphere, it is conducted downward by molecular diffusion or is lost to atomic oxygen fine structure excitation with subsequent emission at 63 μm.

2.2 *Energetic Particle Precipitation and SAR Arcs*

The two preceding sections addressed the thermodynamics of the midlatitude E region during daylight hours. Conditions at night are markedly different. Without the ionizing radiation from the sun the electron concentration drops by roughly a factor of 100 (on a magnetically quiet night) within two hours after sunset. In the absence of solar radiation the

Table 2.1 Quantitative electron cooling formulas used in modeling the
thermosphere. Cooling rates are in units of (eV cm^{-3}s^{-1}).
Cross section calculations by *Hoegy* [1976] suggest the atomic
oxygen fine structure cooling coefficient should be reduced to
roughly 60% of that shown.

Atomic oxygen fine structure excitation [*Dalgarno*, 1969]

$$L = \frac{[e][O](3.4 \times 10^{-12})(T_e - T_n)(1.0 - 7.0 \times 10^{-5} T_e)}{T_n}$$

N$_2$ rotational excitation [*Dalgarno*, 1969]

$$L = \frac{[e][N_2](2.9 \times 10^{-14})(T_e - T_n)}{T_e^{1/2}}$$

O$_2$ rotational excitation [*Dalgarno*, 1969]

$$L = \frac{[e][O_2](6.9 \times 10^{-14})(T_e - T_n)}{T_e^{1/2}}$$

N$_2$ vibrational excitation [*Dalgarno*, 1969]

$$L = [e][N_2](6.25 \times 10^{-18})(T_n - 300)(T_e - T_n - 300)$$

O$_2$ vibrational excitation [*Lane and Dalgarno*, 1969]

$$L = [e][O_2](1.0 \times 10^{-12})10^{[(T_e-800)/700]}$$

solar thermal input to the electron gas is zero, and the electron temperature falls to the temperature of the neutral gas. Representative values for an altitude of 150 km are n_e equal to 3×10^5 cm^{-3} during the day and 3×10^3 cm^{-3} at night, and T_e equal to 700 K during the day and 500 K at night.

The nighttime electron concentration and temperature are strongly dependent on magnetic activity; presently this is thought to be due to energetic-particle precipitation. Nike Apache 14.439 was launched from Wallops Island on the night of a severe magnetic storm (Kp = 8; 0003 EST on 1 November 1972) and carried a Geiger counter in the payload. Energetic particles (>70 keV) were detected with a maximum flux of 1086 ± 26 cm^{-2} s^{-1} ster^{-1} at 140 km [Smith et al., 1974]. The energetic particles were presumed to be electrons until subsequent experiments were carried out using solid-state surface-barrier detectors with broom magnets. Instrumentation such as this aboard Nike Apache 14.533 (Kp = 5; 0001 EST on 5 January 1978) has identified the flux of particles as consisting of protons and possibly O^+ and He^+ ions [Voss and Smith, 1979].

Using electron-concentration profiles from nine nighttime midlatitude launches, Voss and Smith [1979] have calculated the corresponding ionization rates. These rates are plotted in Figure 2.3 as a function of magnetic activity. The solid line is a least-squares fit, with a correlation coefficient of 0.93 for the nine observations. The ionization rate appears to be causally related to the level of geomagnetic activity. Present data indicate that the upper limit for all ionization sources (other than energetic-particle flux) in the upper E region is 10^{-1} cm^{-3} s^{-1}. This supports the conclusion that energetic-particle precipitation is the principal source of ionization in the midlatitude E region on geomagnetically quiet nights as well as disturbed nights. (Even under the most disturbed conditions particle precipitation is insignificant as an ionization source during the daylight hours, amounting to less than 1 percent of the daytime ionization rate.)

With the nighttime ionization rate controlled by geomagnetic activity, it is clear the electron temperature will depend on Kp, for each particle ionization event ultimately puts about 35 eV of energy into the E-region electron gas. Smith et al. [1974] have analyzed electron temperature data from Evans [1973] at Millstone Hill and found the electron temperature at
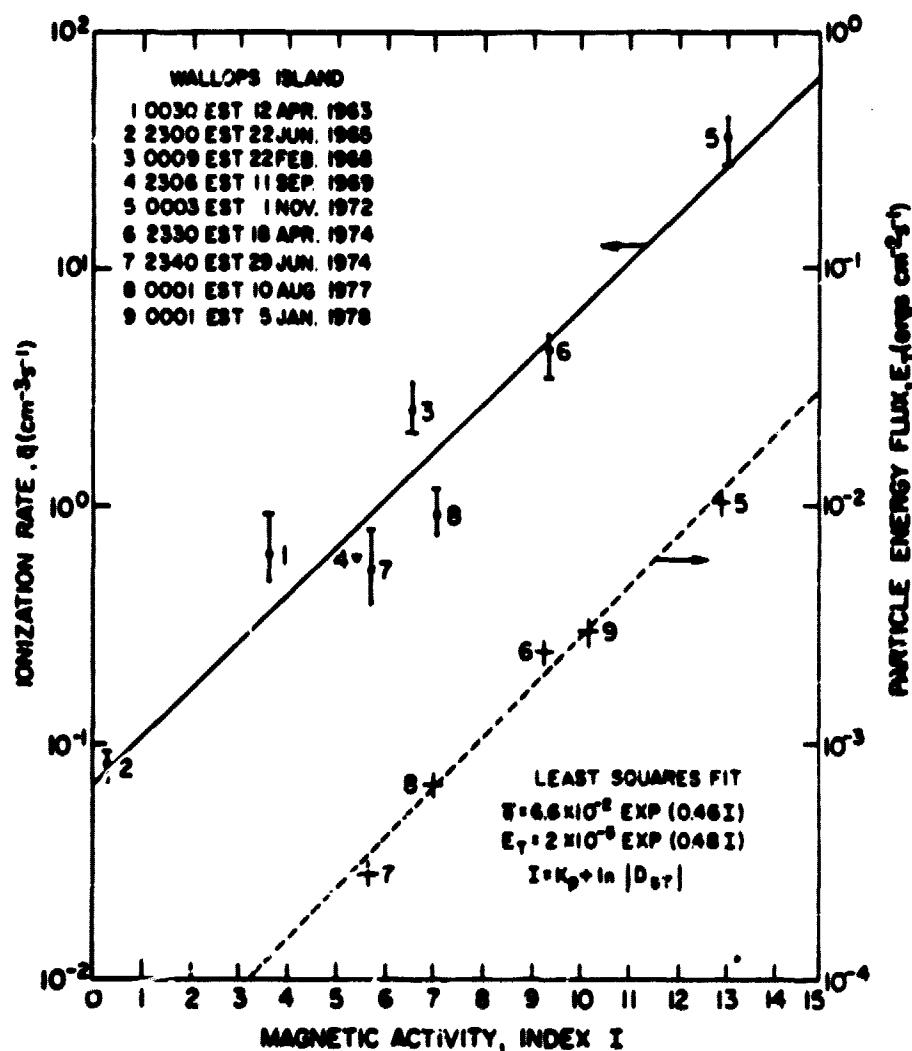
Figure 2.3   The variation with magnetic activity of the
            ionization rate in the upper E region near
            midnight [*Voss and Smith*, 1979].

200 km is well represented by (112 Kp + 588) K for a range in Kp of 1- to 5-. The correlation coefficient is 0.90.

Nighttime particle precipitation can qualitatively explain midlatitude E-region electron temperatures on quient and moderately disturbed nights. However, during geomagnetic storms with a Kp of 5 or greater another heating mechanism sometimes takes over, this being the stable auroral red (SAR) arc. The SAR arc (or M-arc, for midlatitude arc) was first observed in the night sky from southern France by Barbier in 1956 [Barbier, 1958]. The arc is a subvisual red aurora of amazing spectral purity; the wavelength of 6300 Å is the emission due to the atomic oxygen transition O I($^3P_2$ - $^1D_2$). The absence of other spectral lines, most notably the 5577 Å line of atomic oxygen (see Figure 2.4), implies low energy excitation of the oxygen atom since only 1.97 eV are required for the ^1D transition.

The arcs run east to west and extend around the night-side of the earth. The arc of September 1967 was viewed by the OGO 4 satellite and shown to be globe encircling [Reed and Blamont, 1968]. Generally, SAR arcs extend several hundred kilometers in the north-south direction. The position of SAR arcs is usually between the magnetic L shells 2 and 4 [Roach and Roach, 1963].

The mean altitude of the most intense 6300 Å emission has been found to lie near 400 km [Roach and Roach, 1963]. Tohmatsu and Roach [1962] have produced a normalized isophot.'¹ plot of a typical SAR arc in Figure 2.5.

The occurrence of SAR arcs is more than an occasional phenomenon. Their frequency follows the solar cycle; during the last solar cycle period SAR arcs were reported on 20 percent of the viewing nights at Fritz Peak, Colorado [Marovich, 1966].

There are two major atmospheric properties associated with SAR arcs: the arcs form within or on the equatorward edge of a general ionospheric electron-concentration depression. This is shown dramatically in Figure 2.6 [Clark et al., 1969] where the location of the arc, as determined by ground-based airglow observations, is indicated by the black bar. The electron-concentration data were obtained from the topside ionospheric sounder aboard the Alouette II satellite.

Secondly, there is a strong enhancement of the electron temperature compared with regions outside the arc [Norton and Findlay, 1969; Chandra

ENERGY LIFETIME

eV	SEC
4.19	0.74

5577Å 2978Å 2972Å 2958Å

^{1}S

^{1}D

1.97 110

6392Å 6364Å 6300Å

0.028
0.020
0

^{3}P
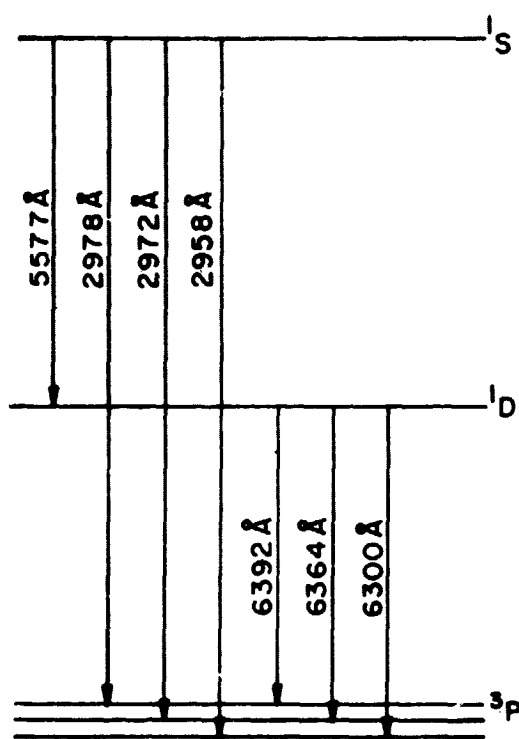
Figure 2.4   Low-lying transitions of atomic oxygen [*Rees and Roble*, 1975].
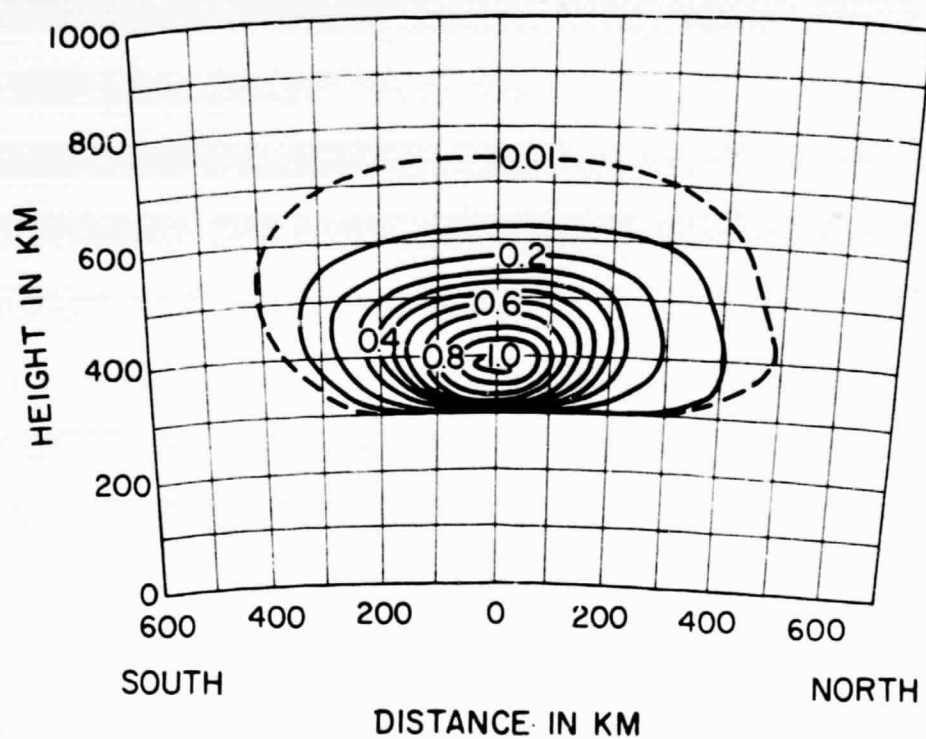
Figure 2.5 Normalized λ 6300 Å isophotal representation of an SAR arc cross section [*Tohmatsu and Roach*, 1962].
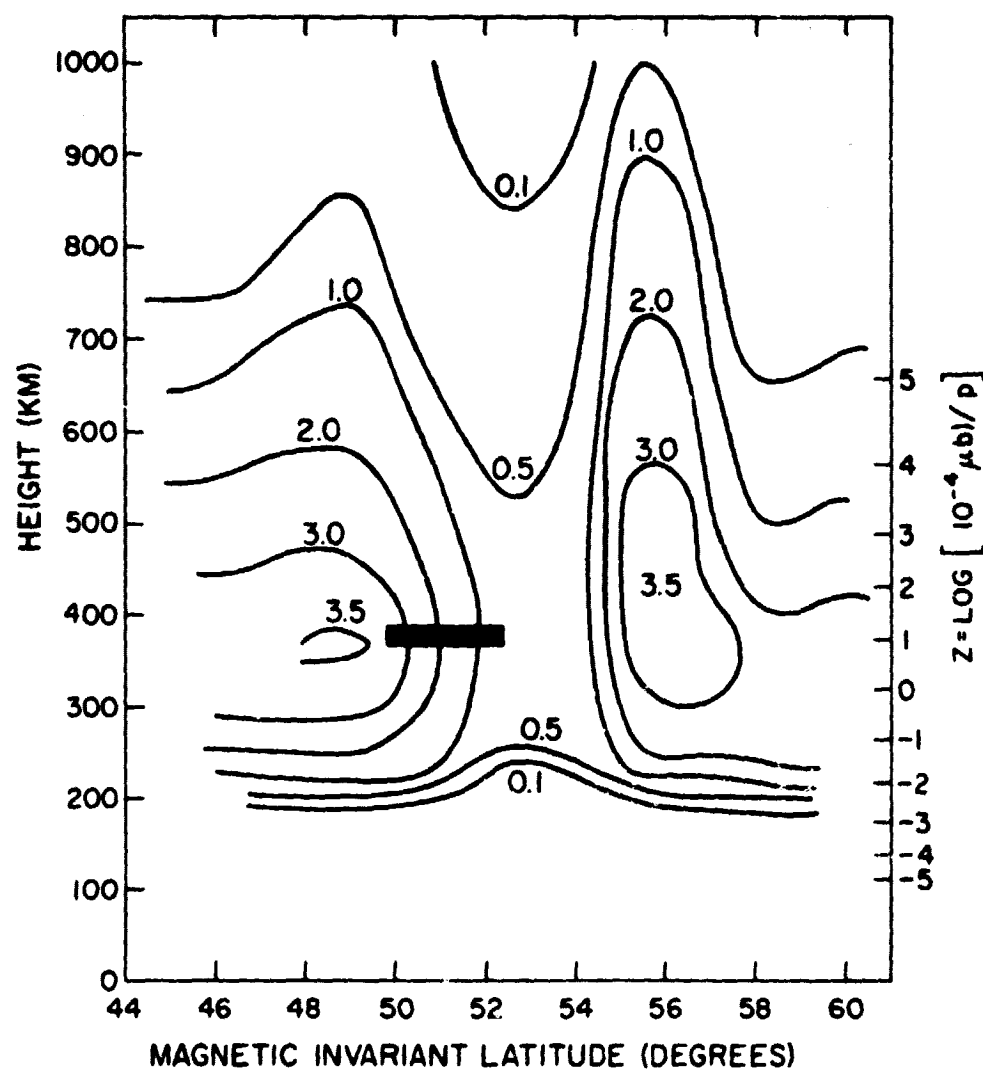
Figure 2.6 Electron-concentration contours (10^5 cm^{-3}) measured in the vicinity of the September 28-29, 1967, SAR arc. The bar indicates the photometric position of the arc. [*Clark et al.*, 1969].

et al., 1971; *Roble et al.*, 1971; *Nagy et al.*, 1972]. Satellite temperature
measurements above SAR arcs are shown in Figure 2.7 [*Roble et al.*, 1971].
In each case the electron temperature peaks just above the photometric
location of the arc. These measurements were taken at roughly 1000 km, but
a marked warming would also be expected in the upper E region due to downward
heat conduction. One of the launches analyzed in this report (Nike Apache
14.533) is believed to have flown beneath an SAR arc and detected elevated
electron temperatures due to this mechanism.

SAR arcs occur on magnetic sheets which pass through the plasmapause
region [*Carpenter*, 1971; *Chappell et al.*, 1971; *Hoch and Smith*, 1971].
Given the worldwide character of SAR arcs, most researchers agree that
heating does not originate in or immediately above the ionosphere, but takes
place in the magnetosphere with the proton ring current as an energy source
as shown in Figure 2.8 [*Rees and Roble*, 1975]. This presents a difficult
transport problem: how does the energy reach the ionosphere in sufficient
amounts to excite the arc and cause general heating, while not providing too
much energy (which would excite other spectral lines than just the oxygen
6300 Å line)? Presently there are four hypotheses which separately or
collectively may explain SAR arcs. All agree on the necessity of a
geomagnetic disturbance initally. And all agree that ultimately there are
electron energies of 2 eV in the upper F region, with consequent collisional
excitation of atomic oxygen to the ^{1}D state, and spontaneous emission at
6300 Å. They differ regarding the transport mechanism.

Cole [1975] claims Coulomb interaction between plasmaspheric electrons
and energetic ring particles (H^+, He^+, O^+) is the dominant heat source. The
electrons then carry their heat to the ionosphere by traveling along magnetic
flux tubes due to the high thermal conductivity along field lines.

Rees and Roble [1975] believe that intense ion-cyclotron waves are
generated in the equatorial region due to the overlap between the ring
current and the plasmasphere. These plasma waves give up their energy to
plasmaspheric electrons by Landau damping. These hot electrons then stream
down into the ionosphere along field lines, as in Cole's hypothesis.

The hypothesis of *Cornwall et al.* [1971] is that the initial interaction
in the equatorial ring current in Coulomb interaction, warming the ambient
electrons. After some warming ion-cyclotron wave generation begins. The
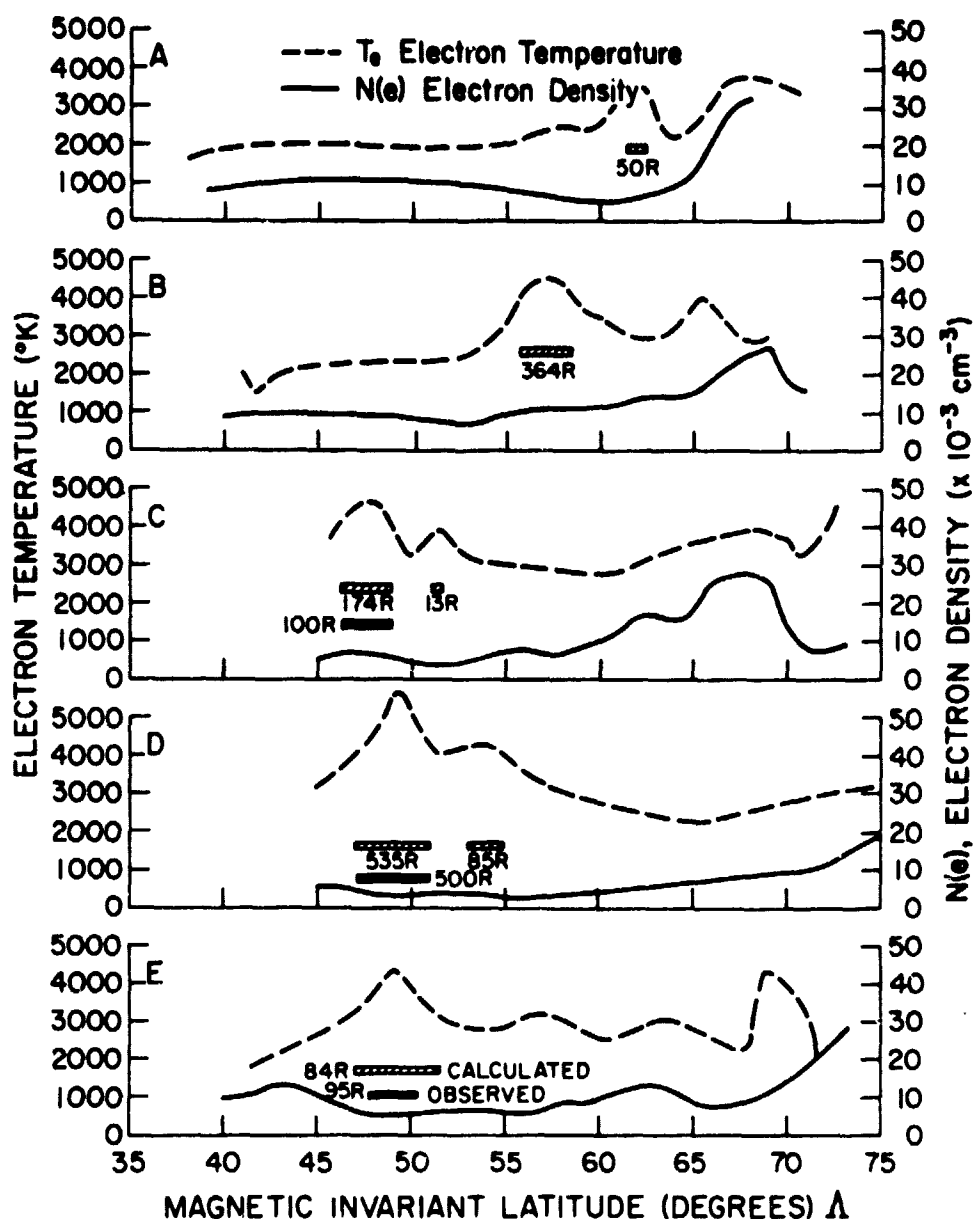
Figure 2.7   The electron temperature and electron density measured by
             the Alouette 2 satellite as a function of the magnetic
             invariant latitude.   Curves A-E were measured at different
             times during the geomagnetic storm of October 29-November 2,
             1968.   The hatched areas indicate the calculated λ6300
             emission rate in Rayleighs, and the solid areas indicate
             the λ6300 emission rate measured from airglow observatories
             [*Roble et al.*, 1971].
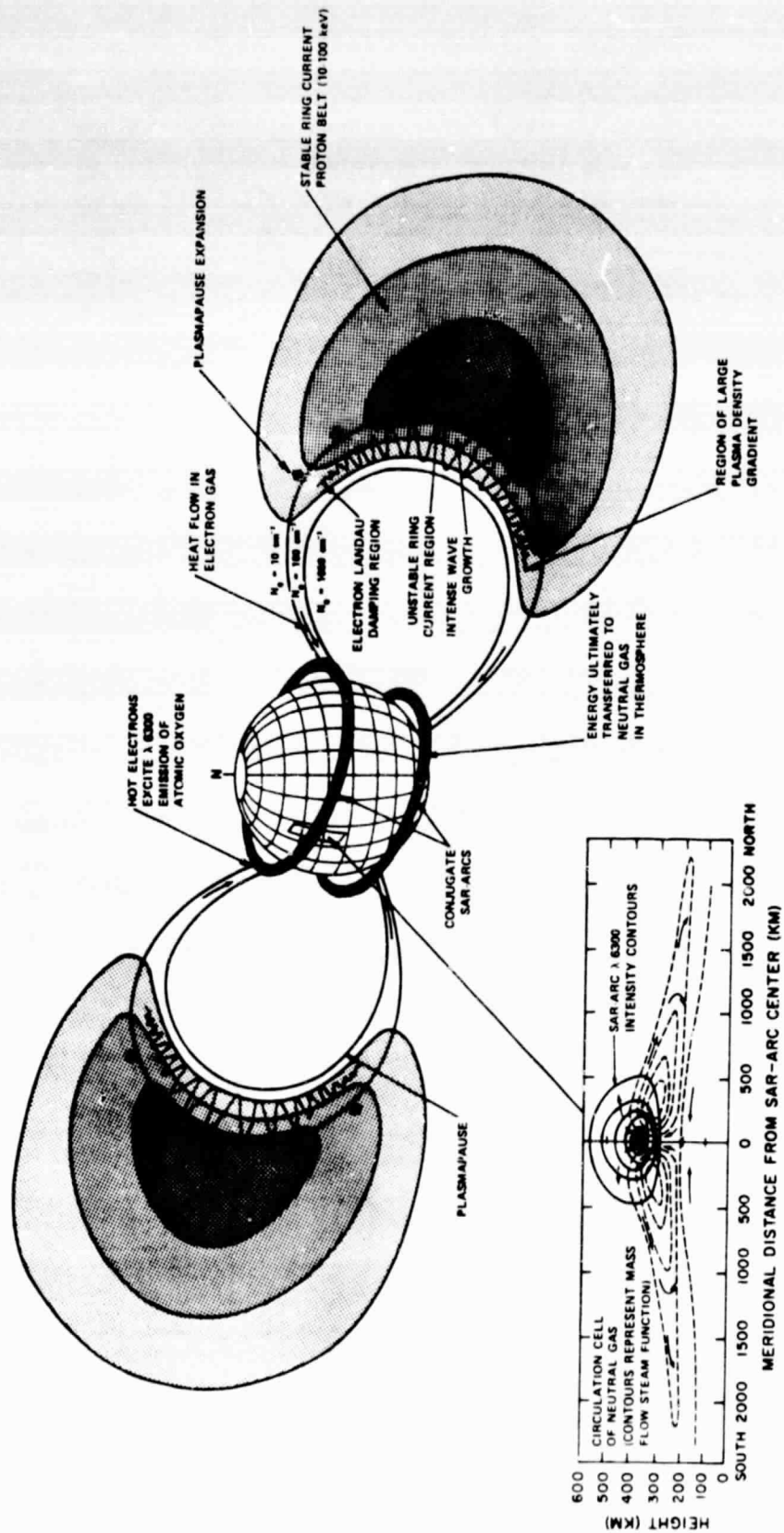
Figure 2.8 Schematic diagram of processes acting within an SAR arc according to *Rees and Roble* [1975].

energy from the ion-cyclotron waves is lost to the electrons by Landau damping again. Cornwall et al. argue that Landau damping is not effective until the electron gas has been preheated by the Coulomb interaction. When Landau damping becomes effective they call it Landau resonant energy exchange. Once the electrons are heated they carry the energy to the ionosphere along magnetic field lines.

Hasegawa and Mima [1978] have an hypothesis radically different from the previous three. They argue that due to two processes (magnetohydromagnetic surface wave generation and plasma drive wave instabilities) kinetic Alfven waves are created. This is a type of shear Alfven wave with an electric field parallel to the geomagnetic field. Electrons are heated by resonant energy exchange at the plasmapause and transported to the ionosphere by the parallel electric field. They show the kinetic Alfven wave wavelength is comparable to the length of a geomagnetic field line and that such long distance transport of hot electrons is quite reasonable due to the parallel electric field.

3.   LANGMUIR PROBES ON SOUNDING ROCKETS

3.1   *Plasma in the Region 100 to 200 km*

The region 100 to 200 km has electron concentration of the order of 10^5 cm^{-3} during the day. The neutral particle concentration at 150 km is about 5×10^{10} cm^{-3} (see Table 3.1) so that the region is only slightly ionized: a very tenuous plasma. In the context of plasmas generated in the laboratory the ionosphere may be considered quiescent since the characteristic time of change is of the order of an hour if we exclude the transient phenomena occurring at sunrise, sunset, and during solar eclipses.

Because of the hypersonic velocity of sounding rockets, typically 1.5 km s^{-1} at 100 km altitude, the positive ions and neutral gas impinge upon the rocket with a well directed flow velocity. However, the electron mean thermal velocities are 200 to 300 times greater than the ion thermal velocities, meaning that it is safe to assume the main electron population has an isotropic velocity distribution relative to the rocket vehicle. As *Boyd* [1968] has noted "... the supersonic or hypersonic velocity of the spacecraft gives rise to a situation in which the ion mean energy exceeds, by perhaps over an order of magnitude, the mean energy of the electrons -- a complete reversal of the situation to which the classical Langmuir papers are addressed." A further complication resulting from the high rocket velocity is local aerodynamic heating, though this is limited to the lower E region.

A plasma is described by several characteristic distances, the most important of these being the electron Debye length λ_D. This length, also called the Debye shielding length or (erroneously) the plasma sheath thickness, is the approximate range of Coulomb forces in plasma. Normally, one thinks of the Coulomb (electric) field due to a net charge as having an infinite range. This is not the case in a plasma where the free electrons (and to some extent, the ions) redistribute themselves around a net charge so as to shield the electric field from the distant plasma. Thus, when a conducting body is placed in a plasma it will generally have a space charge layer, the plasma sheath, surrounding it. Within the sheath charge neutrality does not hold, allowing electric fields to be maintained across the sheath.

Table 3.1 Some nominal daytime values of basic plasma parameters in near space for mean solar activity [*Boyd*, 1968]. Research in the past decade indicates $T_e = T_+ = T_n$ at 100 km.

PLASMA PROPERTY		ALTITUDE (km)		
		100	150	200
n_o	(cm^{-3})	10^{13}	5×10^{10}	8×10^9
n_e	(cm^{-3})	10^5	3×10^5	4×10^5
T_n, T_+	(K)	200	700	1100
T_e	(K)	250	1000	2000
$\bar{v}_+$	(m s^{-1})	400	700	1000
$\bar{v}_e$	(m s^{-1})	10^5	2×10^5	3×10^5
λ_D	(cm)	0.3	0.4	0.5
λ_o	(cm)	40	8×10^3	5×10^4
λ_{e+}	(cm)	4×10^4	5×10^5	10^5

The Debye length may be considered in a rough sense as the electrical "range of disturbance" in plasma due to a rocket body or electric probe, although it is important to keep in mind that the Coulomb field does not suddenly drop to zero at a distanct of λ_D. By placing a sensing probe more than several Debye lengths from the rocket body, for instance, one can be reasonably sure that the probe is immersed in the ambient plasma. This is with the provision that the neutral gas dynamics does not cause the probe to be in a region of rarefaction (the wake).

The electron Debye length is given by the formula

$$\lambda_D = (kT_e/4\pi n_e e^2)^{\frac{1}{2}} = 6.9(T_e/n_e)^{\frac{1}{2}} \qquad (3.1)$$

in c.g.s. units, where k is Boltzmann's constant, T_e is the electron temperature in Kelvin degrees, n_e is the electron concentration in cm^{-3}, and e is the electronic charge. Debye lengths for different altitudes of interest are given in Table 3.1, in each case being less than 1 cm.

Following the Debye length in importance is the neutral-neutral or ion-neutral mean free path λ_o (they are assumed equal), and the electron-ion mean free path λ_{e+}. These lengths are indicative of the collisional coupling between the plasma particles and are important in the following sense: if the mean free paths are much greater than the plasma sheath thickness, then any disturbance to the plasma due to particles emitted by the probe surface, reflected from the probe surface, or absorbed by the probe surface will be slight due to the large volume of plasma involved. Large volume here means that the collisional volume is much greater than the volume of the plasma sheath. Since the response of an electric probe primarily depends on the plasma within the sheath, the measurement errors are minimized if λ_o and λ_{e+} are much greater than λ_D. This situation is usually referred to as the thin sheath case.

From Table 3.1 we see that λ_o and λ_{e+} are much greater (by factors >20,000) than λ_D at 150 and 200 km. However at 100 km $\lambda_o/\lambda_D \approx 100$. Although this is still considered to be a thin sheath case, some caution in the use of conventional Langmuir probe theory is warranted, for to an increasing extent collisions are occurring within the plasma sheath. As alluded to earlier, there is the possibility in this situation of collisional heating within the sheath volume.

Before leaving this section it is necessary to emphasize that the most important plasma parameters are the ion and electron temperatures and the electron concentration. The Debye length and mean free paths have been discussed first because they are important concepts in understanding qualitatively how errors are introduced in probing plasma with a practical probe.

The electron temperature is the quantity which (to those not working with plasma) is most alien to our senses. For example it is initally surprising to find that the electron temperature within a typical fluorescent lamp is well in excess of 20,000 K. First, then, we must separate our association of heat with temperature, for it requires very little energy to greate very high electron temperatures in a plasma. This is due to the very small heat capacity per unit volume of electron gas, which is given by $(3/2)kn_e$ (c.g.s. units). The heat capacity of one cubic kilometer of the E region during the day (with $n_e = 10^5$ cm^{-3}) is 2×10^4 ergs/K; which is comparable with the heat capacity of the head of a pin (3.6×10^4 ergs/K for one cubic millimeter of iron).

Energy deposited in the midlatitude E region by energetic-particle precipitation does not cause any perceivable effect during the day. However, when the heat capacity decreases at night the particle energy flux, although small, is reflected in an elevated electron-temperature profile. Clearly, the electron temperature is a very sensitive ionospheric parameter and can be affected by even minor sources of energy.

The mean kinetic energy of an electron in the population is given by

$$\frac{1}{2} m_e \overline{v_e^2} = \frac{3}{2} kT_e = (1.293 \times 10^{-4}) \ T_e \ \text{(eV)} \tag{3.2}$$

Sometimes T_e is called the electron kinetic temperature, emphasizing this point and distinguishing it from other possible definitions of temperature. A 1000 K plasma, then, has a mean electron energy of only 0.13 eV and an r.m.s. electron velocity of 213 km s^{-1}. If a Maxwellian velocity distribution is appropriate, as it is in the case of electronic thermal equilibrium, then the electron temperature conveys much more information. Figure 3.1 gives the velocity distribution for a 1000 K Maxwellian plasma.
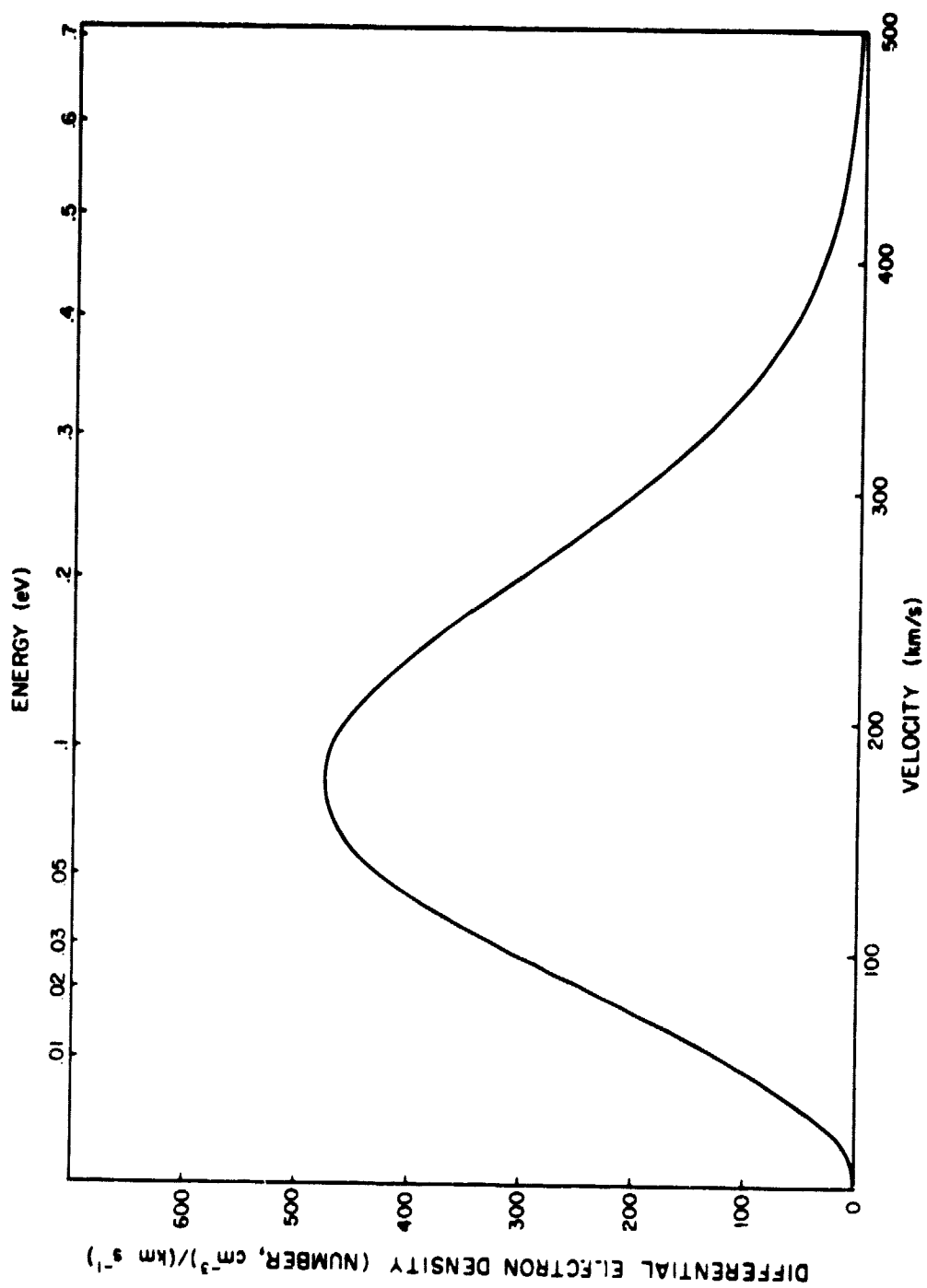
Figure 3.1   Velocity distribution for a 1000 K Maxwellian plasma, $N_e = 10^5$ cm^{-3}.

3.2 *Langmuir Probes*

The Langmuir probe (or electrostatic probe) was among the first experiments to be carried into the upper atmosphere when the American rocket program got underway in 1946 using German V-2 rockets. The probe is simple, consisting of a conducting material that is inserted into the plasma on an insulating mechanical support. The potential of the probe is varied with respect to the rocket body and the resulting current flow to the probe is recorded on board the vehicle or telemetered to ground on a telemetry link of sufficient bandwidth. The resultant current/voltage curve, the probe I-V characteristic, depends mainly on the ion and electron temperatures and the plasma concentration and, to some extent, on the magnetic field, the flow velocity, and the condition of the probe surface.

The Langmuir probe is capable of making direct local measurement of plasma parameters. This is of great importance in the study of aeronomic phenomena which may be transient or small-scale, for other rocket and ground-based techniques involved spatial or time integrating (averaging) methods necessitated by signal-to-noise considerations. If care is taken in the design of an electrostatic probe and its associated electronics package, spatial and time resolution of 1 m and 1 ms can be achieved from a vehicle traveling 1 km/s.

The essential simplicity of the Langmuir probe is somewhat offset by difficult theory and a variety of experimental problems which may beset the experimenter. Probe theory is complicated because the probe surface is a boundary to the ambient plasma and near boundaries the equations that govern plasma behavior change. There is no general theory for the Langmuir probe response under arbitary plasma conditions, and many of the experimental problems have yet to be adequately addressed. However, the promise of the Langmuir probe (direct measurement of local properties) is great and the theory is relatively simple over the altitude range 100 km to 800 km.

3.2.1 *Probe-operational regimes.* Probe-operational regimes are usually described with the ratios λ_D/R, λ_o/R, and λ_o/λ_D, where R is the characteristic dimension of the probe, λ_o is a representative mean free path, and λ_D is the Debye shielding length. These ratios determine the domains of probe operation, which are: collisionless/collisional, thin/thick sheath, orbital motion limited current; etc. The various probe-operational regimes are

shown in Figure 3.2, along with a curve indicating the various plasma conditions which are attained in the ionosphere.

Most of the D region of the ionosphere (specifically the range 50 to 85 km) is contained in the collisional-sheath domain. Here the current to the probe is controlled by collisional processes occurring within the plasma sheath. This is the problem of a flowing continuum low-density plasma which *Chang and Laframboise* [1976] have numerically solved for specified plasma conditions and probe geometries (sphere in flow, and cylinder in cross flow). As might be expected the solutions in this region depend strongly on probe geometry, vehicle velocity, and (for the cylindrical probe) angle of attack. For given plasma conditions and flow velocity Chang and Laframboise were able to calculate the total probe current, each calculation for a given probe potential requiring 20 minutes of numerical computation on a CDC 6600 computer. While it may be argued that it should be possible to solve the reciprocal problem (that of determining D-region plasma parameters from a Langmuir probe characteristic using first principles), it is not reasonable to do so at the present. Furthermore, a sensitivity analysis might indicate that this approach would never be worthwhile as a research technique. For example, at an altitude of 50 km the Debye length (λ_D) might be 40 cm, meaning that the plasma sheath due to the rocket body could be over a meter in thickness. It is a simple enough matter to create an isolated probe in a digital computer model, but quite a different affair to do so in the D region from a small sounding rocket.

It should be noted that the present use of Langmuir probes in the D region is restricted to a technique developed by *Smith* [1963] for measuring fine structure (on a scale of meters) in electron concentration. No attempt is made in this method to determine electron concentration from probe current using first principles. Rather, the probe current is recorded as a function of altitude with a constant positive potential on the probe. The assumption is made that the probe current and electron concentration are related by a constant factor, n_e/i which changes only slowly with altitude. This calibration factor is obtained from an independent experiment, usually a radio-propagation experiment.

Referring to Figure 3.2 again, at about 85 km is the transitional sheath probe regime. Some effort has been made to deduce electron temperature from

λ_0/λ_D

1200

ORBITAL
MOTION
LIMITED

800

COLLISIONLESS
THIN
SHEATH

200

150

100

90

TRANSITIONAL SHEATH

1

80

COLLISIONAL SHEATH

75

0

1

R/λ_D
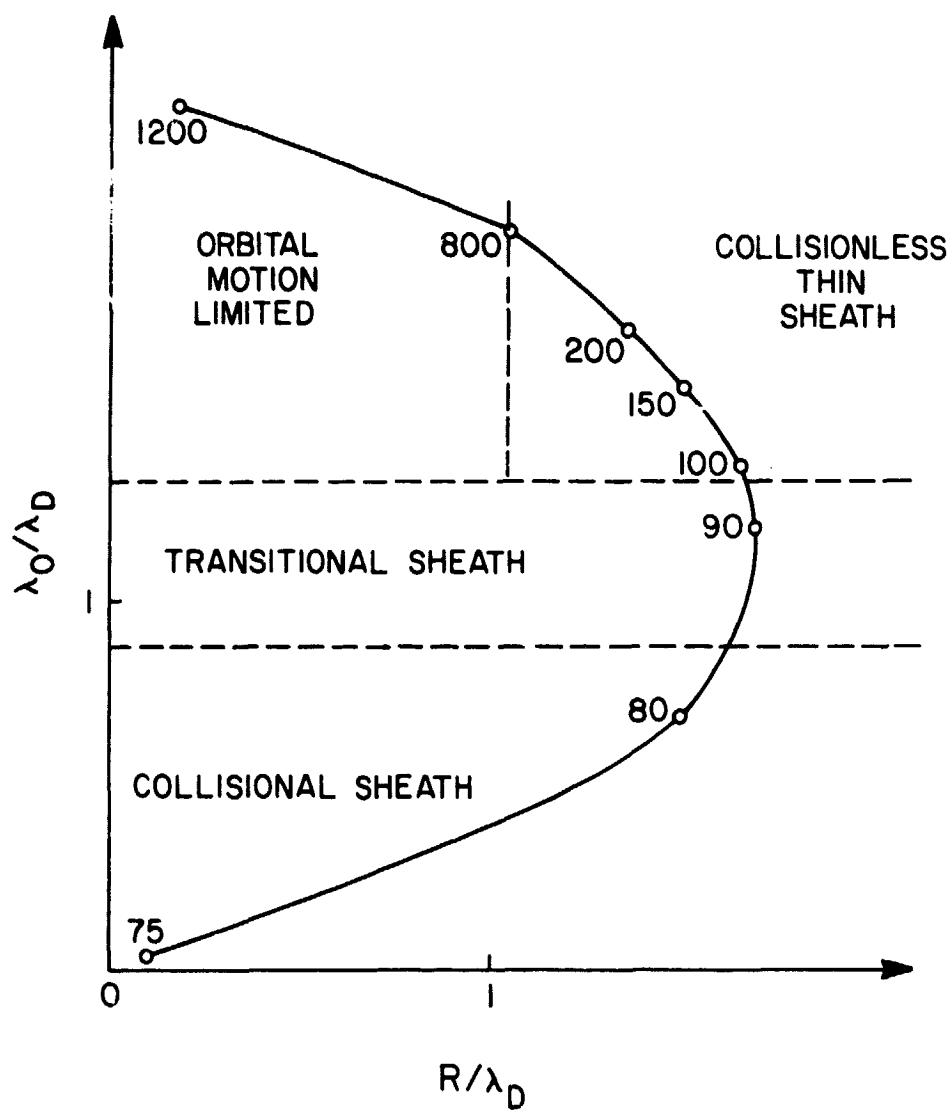
Figure 3.2 Two-dimensional representation of probe-operational
regimes. The smooth curve indicates the various
operational regimes for a Langmuir probe on a sounding
rocket as a function of altitude in km.

probe measurement in this region, although the results have not been
encouraging. Ion-neutral collisions are still numerous enough to render
the conventional Langmuir probe theory invalid.

Extending from approximately 100 km to in excess of 800 km is the region
where conventional Langmuir probe theory is valid. This is the thin sheath
region, mentioned in the previous section. Here the theory of Langmuir probe
operation is based on the kinetic theory of gases with the additional
assumption of there being no collisions within the plasma sheath. This is
an excellent assumption and results in the elegant and powerful theory,
described in detail in the following section (collisionless probe theory),
which is appropriate to most of the work described in this report.

Beyond 800 km the Debye shielding length begins to increase due to the
high electron temperature found in this region and the gradual decrease in
electron concentration (above the F-region peak). As λ_D increases, and in
the complete absence of collisions, particles which are attracted to the
probe tend to execute orbital motions about the probe for particular values
of energy and angular momentum. This increases the residence time of the
attracted particle near the probe. However, as in the thin sheath regime
at lower altitudes, the electron temperature is determined by analysis of
that portion of the probe characteristic where electrons are repelled from
the probe surface (retarding potentials). The retarding potential analysis
developed in the following section is applicable for the determination
of T_e in the orbital-motion-limited case also.

3.2.2 *Collisionless Langmuir probe theory*. The plasma sheath, in
addition to being dependent on the various plasma parameters, is a function
of the probe potential. There is a potential for which ions and electrons
adjacent to the probe are neither attracted to nor repelled from the probe
surface. This potential is called the *plasma potential* or *space potential*.
There is no space charge sheath surrounding the probe at plasma potential.
If one were to microscopically examine the plasma near such a probe, one
woudl find the distribution of speeds (for both positive and negative
particles) is identical with that in the ambient plasma. Adjacent to the
probe surface the particles are directed only towards the probe surface
(assuming the surface is perfectly absorbing and nonemitting) whereas the
particle velocities are isotropic in the ambient plasma, but this is of
minor importance.

When the probe is at plasma potential, the ion and electron currents to it are controlled strictly by the thermal velocities of the ions and electrons in the surrounding plasma. From the kinetic theory of gases the number of particles striking a unit area per second is $n\bar{v}/4$ where n is the particle concentration and $\bar{v}$ is the mean particle velocity. The magnitude of the electron and ion current density to the probe surface is given by

$$|j_e| = n_e e \bar{v}_e / 4 \tag{3.3}$$

and

$$|j_+| = n_+ e \bar{v}_+ / 4 \tag{3.4}$$

The assumption that the probe is perfectly absorbing (fully accommodating) is not always satisfactory, in which case it is necessary to reduce the current densities in equation (3.3) and (3.4) by experimentally determined accommodation factors ranging between 0 and 1. The assumption that the probe is nonemitting is very good. Probes can be made to emit by applying excessive potentials or by heating the probe (thermionic emission), but that is not the intent of the present work.

The electron temperature may exceed the ion temperature because the energy of the photoelectrons is given to the electron gas. For the moment, however, assume that the ion and electron gases are in thermodynamic equilibrium. The ion mean energy is then equal to the electron mean energy

$$\tfrac{1}{2} m_e \bar{v}_e^{\,2} = \tfrac{1}{2} \bar{m}_+ \bar{v}_+^{\,2} \tag{3.5}$$

The ratio of electron to ion mean velocity is, therefore,

$$\bar{v}_e / \bar{v}_+ = (\bar{m}_+ / m_e)^{\tfrac{1}{2}} \tag{3.6}$$

or about 170, depending on the ion composition at a given altitude. Throughout the E region there is strict charge neutrality, so that, $n_e = n_+$. This fact, together with equation (3.6) above, indicates that when a probe is at plasma potential the electron current to its surface will exceed the ion current by a factor of about 170 (greater in reality, where there is not thermodynamic equilibrium). Clearly, the probe must take in a considerable electron current if it is to remain at plasma potential.

If measurements are to be made on a rocket with an electrostatic probe at plasma potential, it will be necessary to provide a means to balance the

net current which the probe collects from the plasma with an equal but opposite current elsewhere in the system. As mentioned earlier, plasma potential is a convenient potential to use since the current densities are immediately obtained from kinetic theory. Therefore, the return current is an important consideration.

Another special case occurs when the probe is biased so as not to draw any current. Since the ion and electron currents are then equal in magnitude (but of opposite sign) it follows that the ion and electron velocities adjacent to the probe are perturbed relative to the ambient plasma. This point may be seen by considering a probe, initially at plasma potential, which is then isolated electrically from the spacecraft. The electron flux to the probe initially exceeds the ion flux, and the probe quickly takes on a negative potential of such a magnitude as to make the ion and electron currents equal. In this situation the probe is surrounded by a negative plasma sheath which acts to accelerate positive ions to the probe surface while retarding electrons. The probe is at floating potential. It is relative simple experimentally to determine the probe floating potential with high resolution by sweeping the probe voltage with respect to the space vehicle and recording the applied voltage at which the probe current is precisely zero. The plasma potential is more difficult to measure. Fortunately it is possible to determine the electron temperature without an accurate knowledge of the plasma potential.

Since the probe electron current is more than two orders of magnitude greater than the ion current when the probe is biased near plasma potential, it is worthwhile initially to consider all the current as electron current. *Mott-Smith and Langmuir* [1926] developed the theory for the current to a probe in a Maxwellian plasma. For a probe of *any* geometry as its voltage is made negative with respect to plasma potential the electron current density will decrease exponentially:

$$j_e = j_{eo} \exp(eV/kT_e), \qquad\qquad V < 0 \qquad\qquad (3.7)$$

where, j_{eo} is the random electron current density given in equation (3.3) and V is the probe potential. Potentials more negative than the plasma potential are electron retarding potentials; only those electrons with energies greater than the retarding potential can strike the electrode.

When ion currents can be ignored, it is a straightforward matter to determine the electron temperature by analyzing the electron component of the probe current as a function of probe potential for retarding potentials.

If the active surface area of the probe is A then, in terms of the measured currents, equation (3.7) becomes

$$i_e = A \, j_{eo} \, \exp(eV/kT_e) \tag{3.8}$$

Taking the logarithm of both sides we have

$$\ln i_e = \ln(A \, j_{eo}) + eV/kT_e \tag{3.9}$$

Differentiating with respect to probe potential, V, gives

$$\frac{d}{dV} (\ln i_e) = \frac{e}{kT_e} \tag{3.10}$$

whence

$$T_e = \left[\frac{k}{e} \frac{d}{dV} (\ln i_e) \right]^{-1} \tag{3.11}$$

Therefore, if one makes a semilog plot of i_e versus V for electron retarding potentials the slope of the curve is inversely proportional to the electron temperature, from equation (3.9). This is the basis of electron-temperature measurement using retarding potential analysis, Figure 3.3.

The problems associated with the method just described are experimental. The positive-ion current cannot be ignored. It is difficult to determine the precise passage of the probe through plasma potential, there being no obvious change in the electrode current. Since the method is valid only for retarding potentials, there is the possibility of applying the analysis to data taken beyond plasma potential and obtaining erroneous results (although perhaps not obviously in error). And finally, any type of system or natural noise must be minimized.

To discuss experimental problems more fully and in preparation for Chapter 4, it is necessary to study the probe current-voltage relation more closely. This curve, Figure 3.4, is the probe characteristic. The electron current to a positively biassed electrode (or, the positive-ion current to negatively biassed electrode) depends on the probe geometry. For simple geometries exact expressions are available. For a planar electrode with
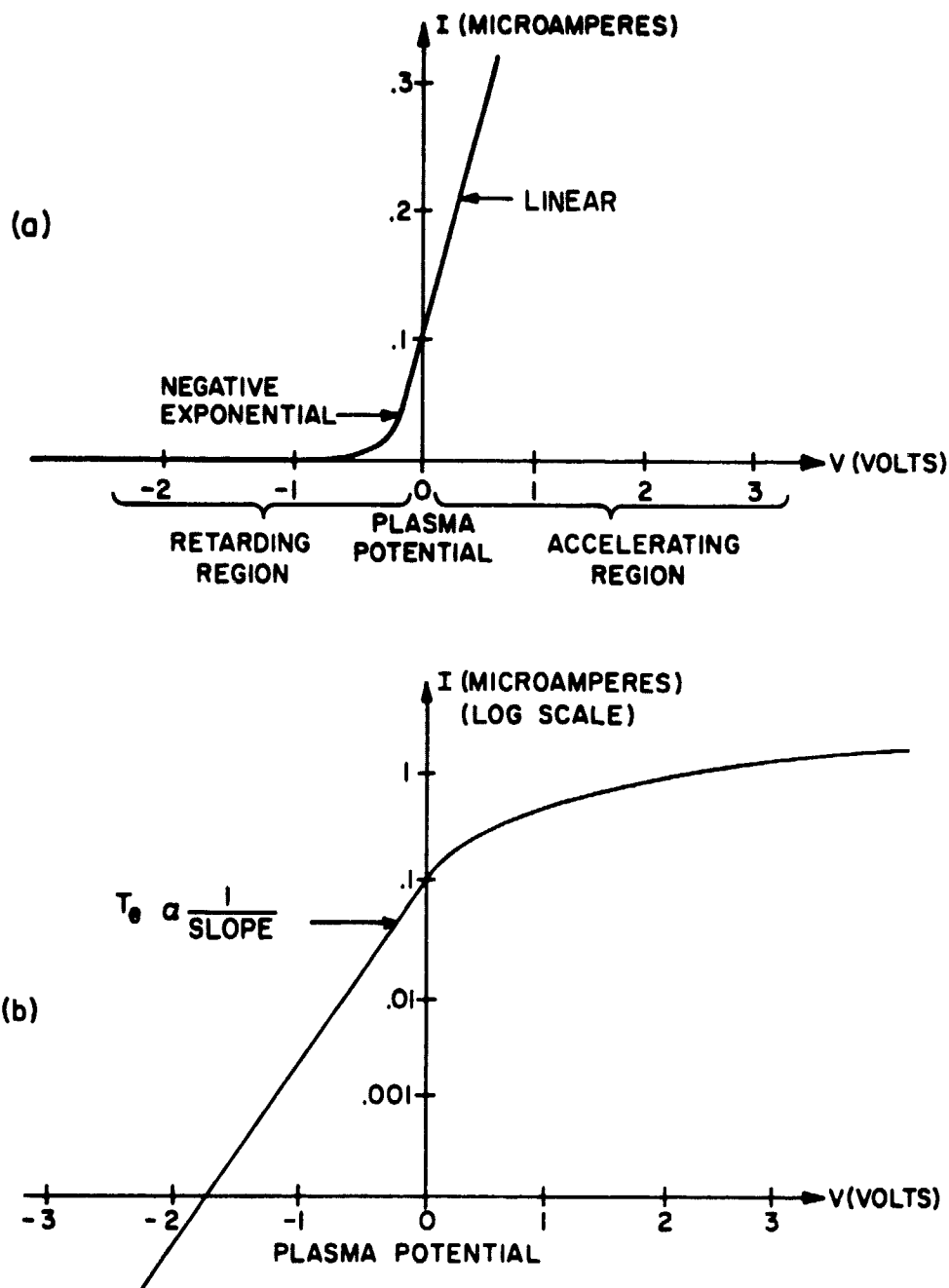
Figure 3.3 (a) Theoretical electron current versus electrode
voltage (spherical electrode); (b) Semi-logarithmic
theoretical electron current versus electrode
voltage (spherical electrode).
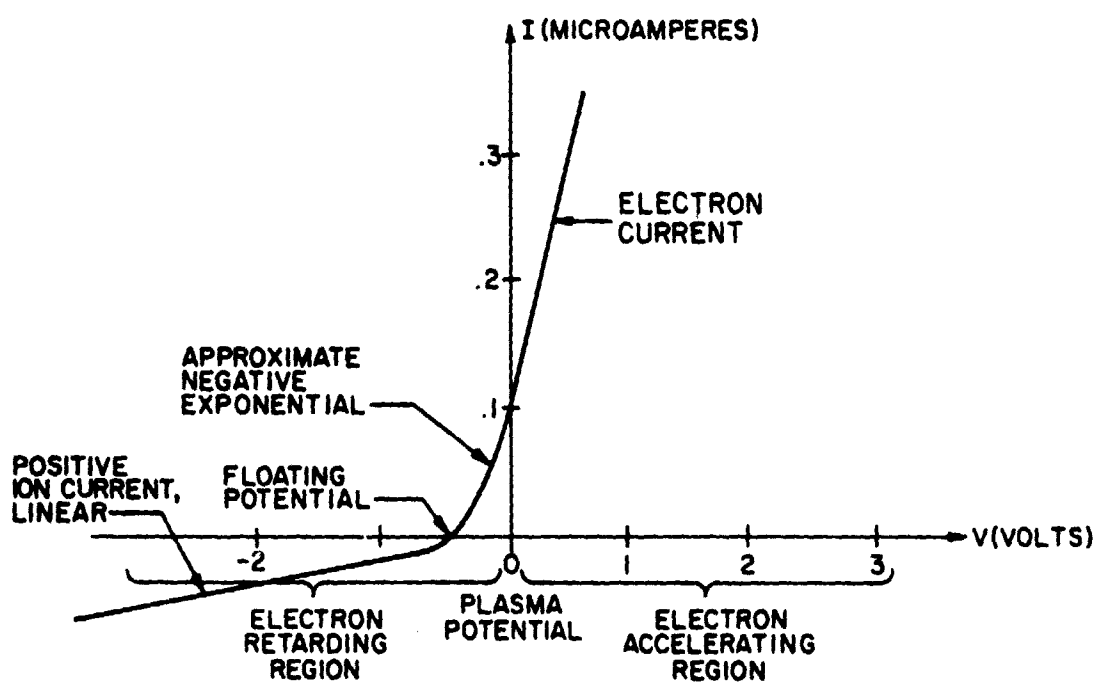
Figure 3.4   Total electrode current, including electron and
             positive-ion components.

dimensions which are large compared to a Debye shielding length, λ_D, the electron current for positive potentials is just the random current density

$$j_e = j_{eo} \qquad (3.12)$$

For a cylindrical electrode which is long relative to λ_D, and of small cross section,

$$j_e = j_{eo} \frac{2}{\pi^{\frac{1}{2}}} \left(\frac{eV}{kT_e}\right)^{\frac{1}{2}} + \exp\left(\frac{eV}{kT_e}\right) \text{erf}\left(\frac{eV}{kT_e}\right)^{\frac{1}{2}} \qquad (3.13)$$

For a spherical electrode of small radius the current for $V > 0$ is linear, as in Figure 3.3

$$j_e = j_{eo} \left(1 + \frac{eV}{kT_e}\right) \qquad (3.14)$$

The small spherical probe has an interesting characteristic: dj_e/dV is continuous through plasma potential. The plane and the small spherical electrodes are limiting geometries in that an electrode of any geometry will have a characteristic contained between these two characteristics. Equations (3.12)-(3.14) are due to *Mott-Smith and Langmuir* [1926] and apply equally well to positive ions by changing the e subscript to $+$. The equations are then valid for positive ions for $V < 0$ (i.e. accelerating potentials). The principal assumptions here are that the plasma has a Maxwellian velocity distribution, that the plasma is at rest relative to the probe, and that no magnetic field is present.

If we assume a spherical probe, we may readily calculate the magnitude of the retarding potential for which ion current becomes appreciable in comparison to electron current. Suppose the ion current is 10% of the electron current. Then

$$j_{+o} \left(1 - \frac{eV}{kT_+}\right) = 0.1 \, j_{eo} \exp\left(\frac{eV}{kT_e}\right) \qquad V < 0 \qquad (3.15)$$

The quantity $|0.1 \, j_{eo}/j_{+o}|$ is about 17. For convenience, assume once more that $T_+ = T_e = T$, so that

$$\ln\left(1 - \frac{eV}{kT}\right) = \ln 17 + \frac{eV}{kT} \qquad (3.16)$$

The solution is

$$\frac{eV}{kT} = -1.8 \qquad (3.17)$$

or

$$V = -1.8 \frac{kT}{e} = -1.55 \times 10^{-4} \ T \qquad (3.18)$$

Clearly, at low temperatures the ion current becomes appreciable even for very small retarding potentials. For $T = 300$ K the ion current is 10% of the electron current for $V = -47$ mV. This is critical in that the uncertainty in locating the plasma potential is typically about 50 mV. For $T = 1000$ K the ion current does not become 10% of the electron current until the probe is at -155 mV.

Until about 1965 the following technique was used to handle the positive-ion current. With the probe characteristic plotted as in Figure 3.4 the positive-ion component of the current (in the region between floating potential and plasma potential) was estimated by extrapolation of the curve obtained for large negative potentials, where it may be assumed the current is solely ion current. Subtracting the ion current from the total current yields the electron current in the retarding region which can then be analyzed by the standard semilog plot, as described previously. In addition to making the data analysis quite tedious, two sources of error limit the accuracy of this technique to about ±100 K. The method involves subtracting two quantities of comparable magntidue to obtain a small residual. Errors in locating the plasma potential will be reflected as errors in temperature measurement.

In 1967 a new technique for data reduction was developed [*Smith et al.*, 1968] which resulted in accuracies of ±25 K under optimal conditions. The total current to a Langmuir probe of area A for electron-retarding potentials is $i = Aj_t$ where j_t is the total current density, given by

$$j_t = j_e + j_+ = j_{eo} \ \exp \frac{eV}{kT_e} + j_+ \qquad (3.19)$$

Again, the explicit form of j_+ as a function of V and T_i is dependent upon the probe geometry. The derivative with respect to voltage is

$$\frac{dj_t}{dV} = \frac{j_{eo}\,e}{kT_e}\exp\frac{eV}{kT_e} + \frac{dj_+}{dV}$$ (3.20)

When $dj_t/dV \gg dj_+/dV$, equation (3.20) becomes

$$\frac{dj_t}{dV} = \frac{j_{eo}\,e}{kT_e}\exp\left(\frac{eV}{kT_e}\right)$$ (3.21)

Taking the logarithm of both sides of this equation, we have

$$\ln(dj_t/dV) = \ln(j_{eo}\,e/kT_e) + eV/kT_e$$ (3.22)

which is similar to equation (3.9)

A semilog plot of dj_t/dV will be a line with slope inversely proportional to electron temperature. As before, this is true only over a limited range in voltage from plasma potential down to the retarding potential where ion current becomes appreciable; this is precisely the constraint $dj_t/dV \gg dj_+/dV$. However, unlike before, the range of validity is easy to detect; a line may be fitted to the linear portion of the curve to immediately determine temperature. Figure 3.5 is a representative graph using this method of the data from Figure 3.4.

The increase in accuracy using this technique comes from two sources. First, the range of validity of theory is operationally more clear. Second, *Smith et al.* [1968] differentiated the probe current on board the vehicle using a capacitor. The displacement current in the capacitor (which is proportional to dj_t/dV) was then measured using a logarithmic electrometer, its output being telemetered to ground on a conventional FM/FM telemetry link. Compressing the data in this manner prior to transmission makes the data more immune to noise and easier to process. The importance of this experimental arrangement must be stressed since it is ultimately noise which limits the accuracy of retarding potential analysis. It is this technique employing partial on-board data analysis that is used in the present research.

The implementation of this experiment is described in the next chapter.
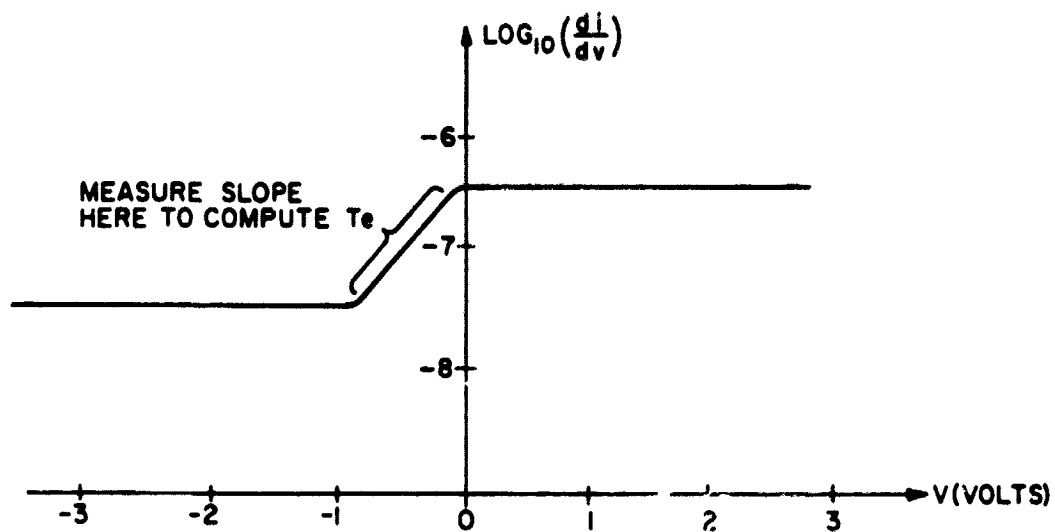
Figure 3.5 Representative graph of $\log_{10}(\frac{di}{dv})$ versus V.
Temperature is determined by measuring the slope
of the increasing segment of the curve.

4. EXPERIMENTAL TECHNIQUE

4.1 *Introduction*

The Langmuir probe experiment together with several other, related experiments are integrated into the rocket payload. For the three flights that are the concern of this report the rocket is the spin-stablized Nike Apache, having a payload diameter of 6.5 in (16.5 cm). The configuration of this two-stage vehicle is shown in Figure 4.1.

In addition to the experiments the payloads each include one or more batteries and their associated switching circuits and an FM/FM telemetry system having, typically, ten voltage-controlled subcarrier oscillators, (VCO's or SCO's), each representing one information channel. The frequencies of the various SCO's conform to IRIG standards.

The channel assignments for Nike Apache 14.532, as an example, are listed in Table 4.1. The signals transmitted from this rocket are from the propagation experiment [*Fillinger et al.*, 1976], the tip probe, including electron density fine structure [*Klaus and Smith*, 1978; *Smith and Klaus*, 1978], and the boom probe and RF probe [*Smith et al.*, 1978]. The magnetometer, mounted transverse to the spin axis, gives aspect information and spin rate (used in the propagation experiment).

The telemetry channel assignments for Nike Apache 14.533 are given in Table 4.2. This payload contained two energetic-particle spectrometers, using solid-state detectors. One spectrometer (EES) was sensitive to electrons and protons; the other (EPS), by using a magnet in front of the detector, was sensitive only to protons. The payload of Nike Apache 14.534, launched earlier, was similar but included only one spectrometer, with no magnet.

The emphasis of both flights was on airglow (391.4 nm) and energetic-particle flux. Some of the data relating to the energetic particles has been presented by *Voss and Smith* [1979]. The most significant result is the identification of the energetic particles as protons; they had earlier been assumed to be electrons.

4.2 *Probe Description*

The instrumentation for the Langmuir probe experiment consists of three main parts: (1) the electrode and its supporting structure; (2) a programmed voltage applied to the electrode; and (3) a current-measuring device (electrometer) which may also include logarithmic compression and differentiation.
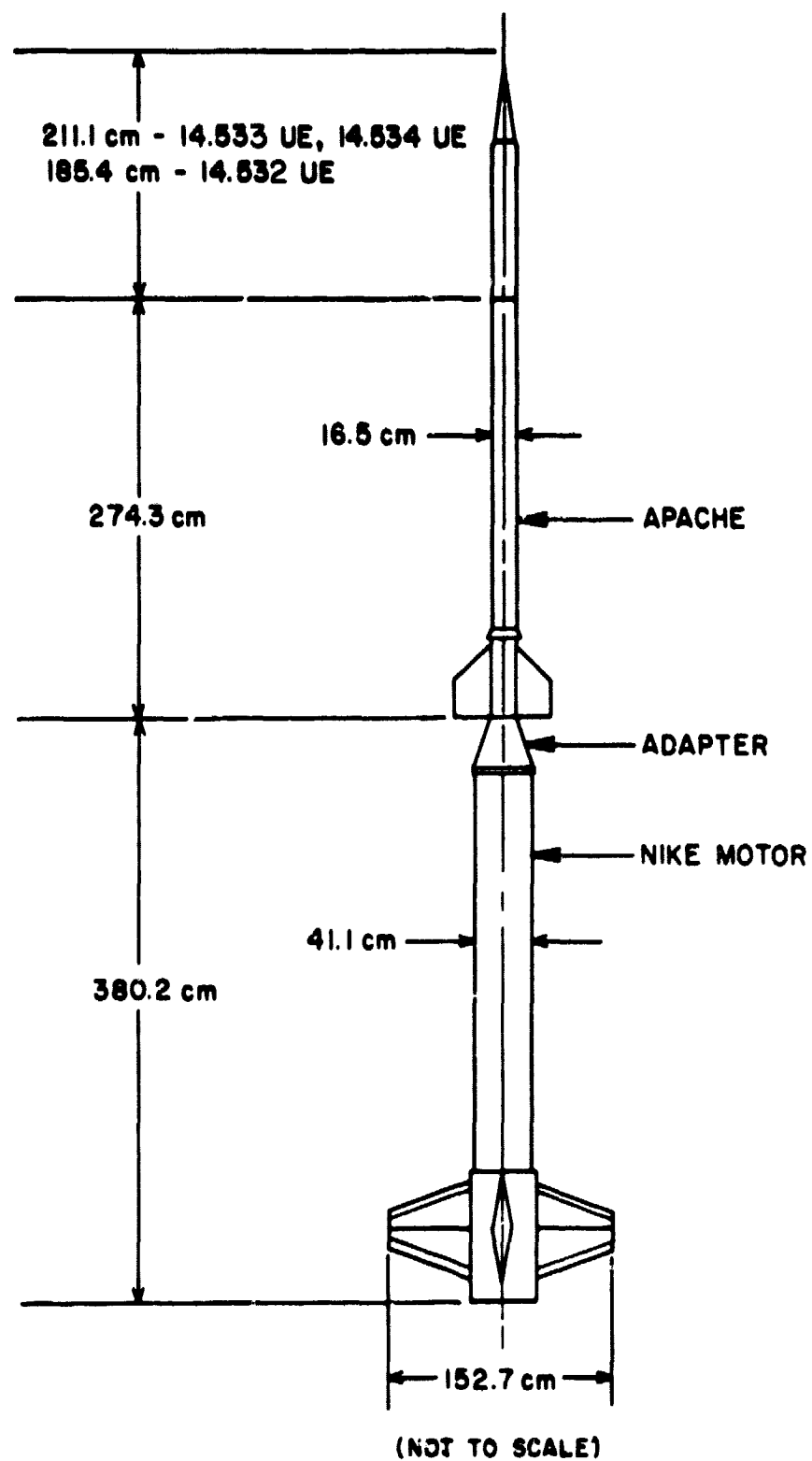
Figure 4.1 Nike Apaches 14.532, 14.534, and 14.533.

Table 4.1 Telemetry channel assignments for Nike Apache 14.532.

Channel Number	Center Frequency* (kHz)	Information Bandwidth** (Hz)	Signal
19	93	1395	RF probe, output
18	70	1050	Tip probe, fine structure
17	52.5	790	Receiver #1, modulation
16	40	600	Receiver #2, modulation
15	30	450	Tip probe, log output
14	22	330	Boom probe, log output
13	14.5	220	Boom probe, linear output
12	10.5	160	RF probe, monitor
11	7.35	110	Receiver #1, AGC
10	5.4	81	Receiver #2, AGC
9	3.9	59	

*deviation = ±7.5%
**modulation index = 5

Table 4.2 Telemetry channel assignments for Nike Apache 14.533.

Channel Number	Center Frequency* (kHz)	Information Bandwidth** (Hz)	Signal
21	165	2475	Photometer, output
20	124	1860	EES, output #1
19	93	1395	EPS, output #1
18	70	1050	Tip probe, fine structure
17	52.5	790	Receiver #1, modulation
16	40	600	Receiver #2, modulation
15	30	450	Tip probe, log output
14	22	330	EES, output #2
13	14.5	220	EPS, output #2
12	10.5	160	EES, output #3
11	7.35	110	Photometer, filter temperature
9	3.9	59	Magnetometer
7	2.3	35	EPS, output #3

*deviation = ±7.5
**modulation index = 5

All three flights used the nose-tip electrode as shown in Figure 4.2. It has a base diameter of 1.08 in (2.75 cm) and a height of 1.50 in (3.81 cm). It is fabricated from a low-sulphur stainless steel (304 CRES), intended for vacuum applications. To minimize outgassing during the flight it is baked in vacuum at a temperature between 900° and 1000° C for 30 minutes and then allowed to cool in the vacuum.

The nose tip is the perferred location for a Langmuir probe because it minimizes, at least on ascent, the possibility of disturbance of the ambient plasma and of direct modulation of the probe current by the wake of the rocket as the rocket spins and precesses. On descent the rocket remains essentially upright to an altitude of about 100 km before beginning to turn over. Some effects of rarefaction in the wake are noticeable in the descent data [*Smith*, 1969].

Electrons in the E region have only a very slight mobility across geomagnetic field lines. This is due to the rarity of collisions which would scatter electrons across field lines. Hence, electrons are constrained in their motion to follow helical trajectories along magnetic field lines with a radius of gyration (Larmor radius) of about 1 cm. At midlatitudes the rocket flight path places the rocket axis roughly parallel to the magnetic field. However, this is not always the case because of launch constraints and, in any event, the rocket will precess during flight so that the cross-sectional area of the probe projected in the direction of the magnetic field will vary with time. To first order it is the projected area which is the effective probe area for electron sensing [*Smith*, 1969]. To minimize the sensitivity of the probe current to rocket attitude the tip electrode is ogival in shape. (An ogive is a solid formed by revolving an arc of a circle.) The height is chosen to yield a nearly constant cross-sectional area for forward angles.

The tip probe is used for two types of data: electron temperature and electron concentration. To determine electron temperature the probe voltage is swept from 0 to 4.05 V with respect to the rocket body. This voltage range is sufficient to ensure the probe voltage has passed through plasma potential. Between probe sweeps is a period when the probe voltage is held at 4.05 V. In this constant-voltage mode the probe current is proportional to the ambient electron concentration. In conjunction with a radio-propagation experiment in the same payload (which serves to determine
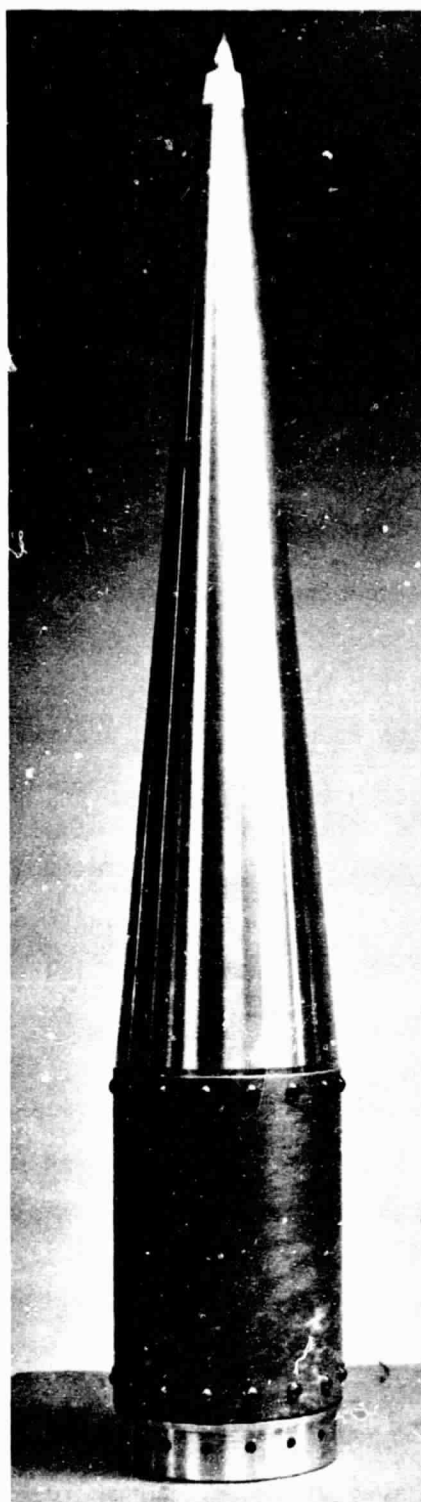
Figure 4.2 Nose-tip electrode.

the proportionality constant between probe current and electron concentration) this mode of probe operation permits absolute measurement of the electron concentration with a spatial resolution of 1 m. Figure 4.3 is a graph of probe voltage versus time showing the periods over which temperature and concentration data are recorded. The tip-probe cycle period is 2 seconds with the swept-mode period being, here, 0.3 s (earlier 0.5 s was used). Since the rocket velocity is about 1.5 km s^{-1} at 100 km, there is one temperature measurement every 3 km. As the rocket travels upward the velocity continuously decreases resulting in an increased altitude resolution in the temperature measurements.

In addition to a tip probe Nike Apache 14.532 (but not 14.533 and 14.534) also carried a boom-mounted probe as shown in Figure 4.4. The three-section boom is folded inside the payload at launch. A timer within the payload releases the boom cover plate when the rocket is at an altitude of about 60 km. The boom extends to a length of 80 cm by centrifugal force. At the end of the boom a spherical aluminum electrode, 1 cm in diameter, and coated with Aquadag (colloidal graphite) is mounted on an insulator. The boom-mounted probe should have no magnetic aspect dependence since the electrode is spherical. The boom-probe on this flight was used only to measure electron temperature. The boom-probe sweep program is also shown in Figure 4.3. The boom-probe voltage is swept from -1.35 to 4.05 V over a period of 0.5 s, with a repetition rate of 1.7 Hz.

All current to the Langmuir probe must return to the plasma by way of the rocket body. It is desired that the ratio of rocket surface area to probe electrode area be large enough that even when the probe is positive relative to the plasma (and considerable electron current is being drawn by the probe) the floating potential of the rocket will not be significantly disturbed. In the E region the ratio of electron to positive-ion random current density is about 200. In order to restrict the voltage shift of the rocket relative to the plasma, it is usual to design rocket experiments such that the ratio of rocket surface area to probe area is at least an order of magnitude greater than j_{eo}/j_{+o}, or about 2000. The total area of an Apache second stage plus payload is about 2.6×10^4 cm^2 while the projected area of the ogive tip probe is 5.9 cm^2. This is an area ratio of 4400. To maintain this high area ratio and ensure a low impedance current path to the plasma, the Apache and instrumented payload are left unpainted.
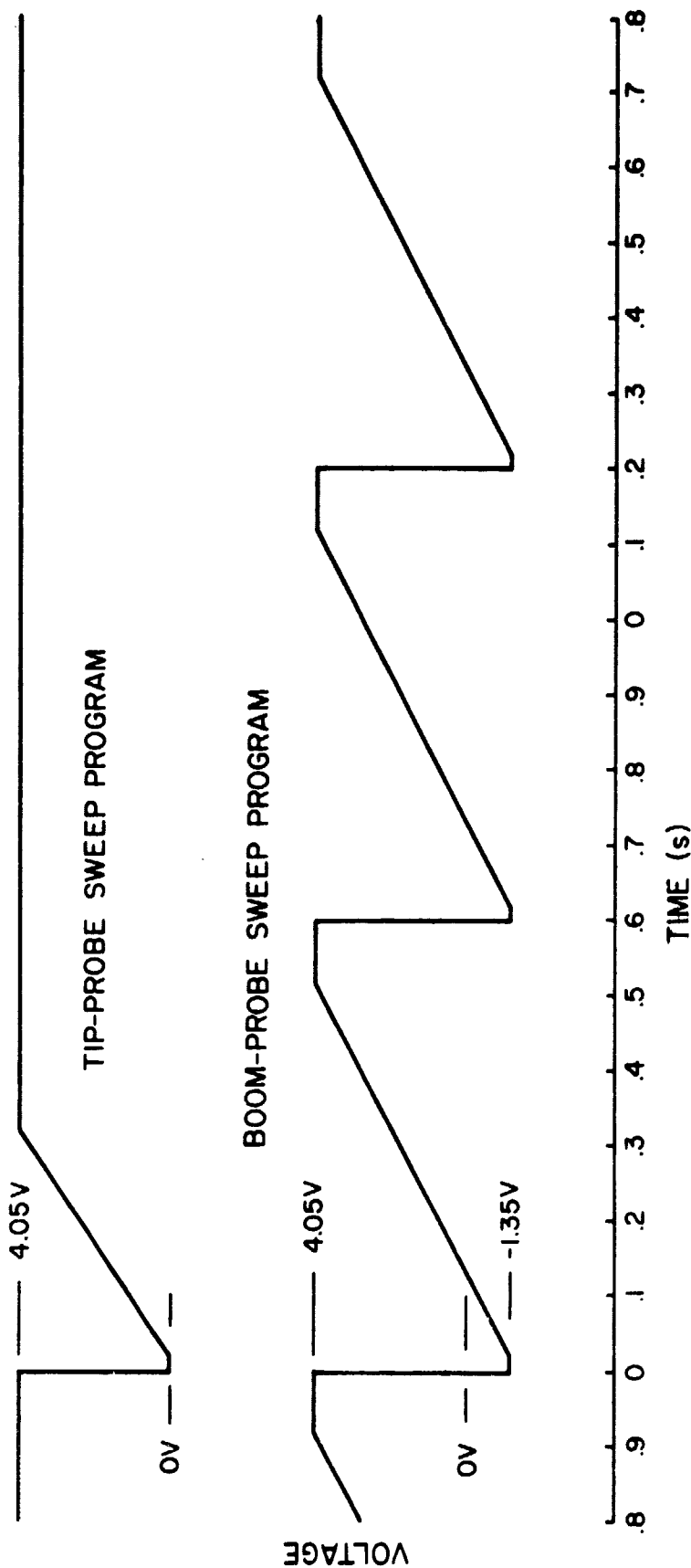
Figure 4.3 Top curve, tip-probe sweep program. Probe sweeps from 0 to 4.05 V in 0.3 s, resulting in a sweep rate of 13.5 V s-1. The sweep recurs every 2 s. There is a 15-ms dead period at the beginning of each sweep. Bottom curve, boom-probe sweep program. Probe sweeps from -1.35 to 4.05 V in 0.5 s, resulting in a sweep rate of 10.8 V s-1. The sweep recurs every 0.6 s. There is a 15-ms dead period at the beginning of each sweep.
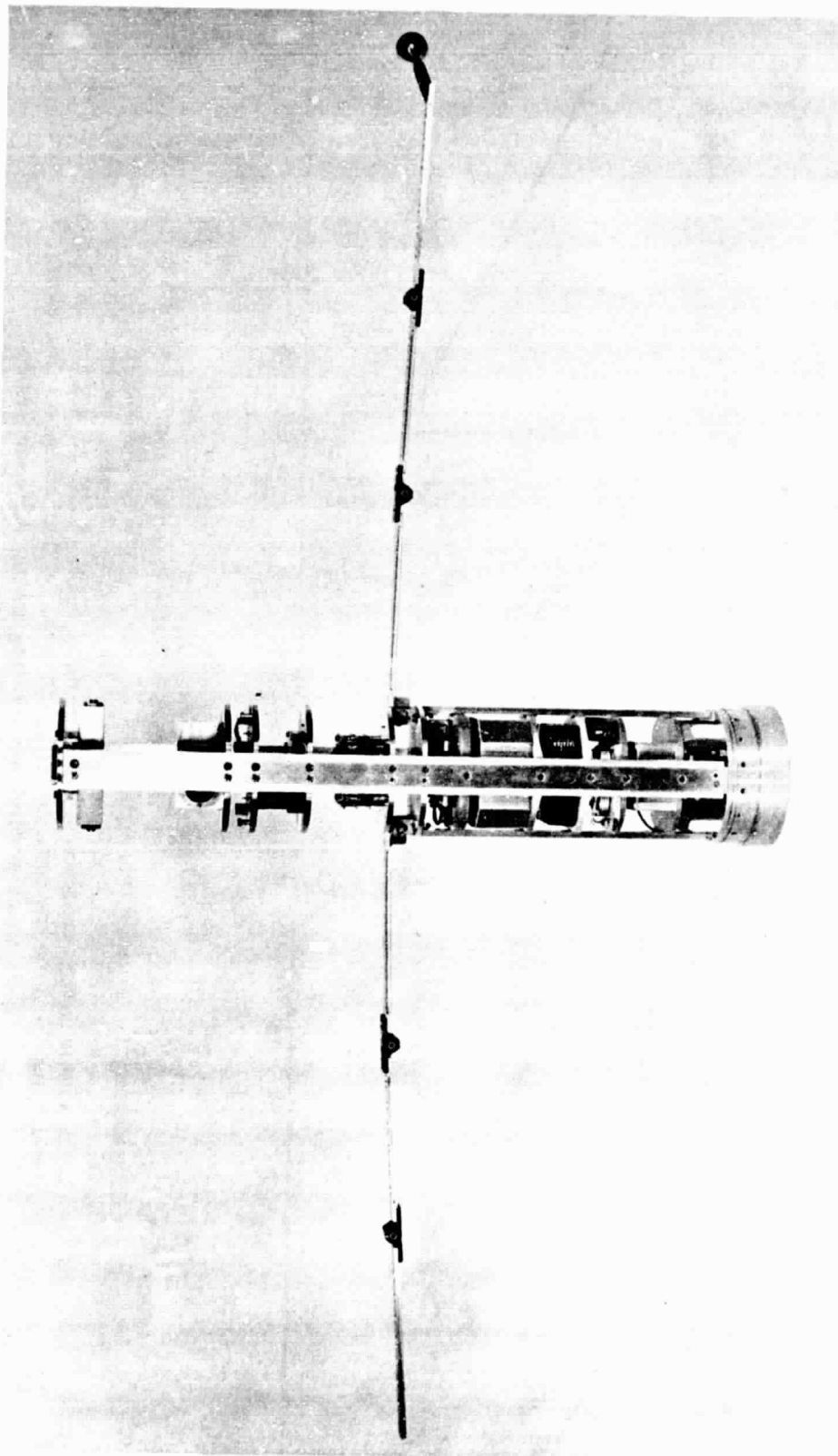
Figure 4.4 Boom probe in extended position.

The full geometric area of the Apache and payload is used in this calculation
(rather than the end-on area) because all the area is accessible to positive-
ion current. This is due to the large Larmor radii of the positive ions
($\sim$40 m for N_2^+ and O_2^+).

4.3 *Probe Circuit and Operation*

The Langmuir probe circuit is shown in block form in Figure 4.5.
With both relays in the positions shown a constant 4.05 V is applied to the
probe. In this state the logarithmic electrometer monitors the probe current
at constant potential. The output voltage is adjusted to fall in the range
0 V to 5 V in order that it may be conveniently telemetered using conventional
FM/FM telemetry equipment. This signal is used to obtain the electron-
concentration profile as discussed earlier (Section 4.2). The output from
the logarithmic electrometer also is coupled through a capacitor to an
amplifier. As the rocket passes through small-scale plasma irregularities,
or if a propagating plasma wave is present in the rocket environment, its
spectrum will be contained in the output of the amplifier.

After a period of 1.7 s the double-pole relay is energized for a period
of 0.3 s by a trigger circuit which simultaneously enables the ramp generator.
The probe voltage increases linearly with time over the 0.3 s from 0 to
4.05 V. The probe current is monitored by the linear electrometer and applied
to the logarithmic electrometer by way of a differentiating capacitor. In
this mode the output from the logarithmic electrometer is $\log(di/dV)$, the
quantity which contains the electron temperature information.

The above paragraphs refer to the tip-mounted probe. The boom-mounted
probe in Nike Apache 14.532 does not use the constant-voltage mode. The
ramp generator was enabled every 0.6 second and the double-pole relay was
omitted. The boom probe and tip probe were not synchronized.

All instruments are calibrated in flight by substituting a calibration
resistor for the probe electrode. This is done by a calibration relay which
is energized for two periods of about 5 seconds each. This relay is
controlled by two barometric switches, the first being closed for altitudes
greater than 40,000 feet (12 km) while the second is closed for altitudes
less than 70,000 feet (21 km). With these switches in series the calibration
relay is energized between 40,000 and 70,000 feet on both ascent and descent.
The calibration resistor is typically 10^6 Ω for daytime flights (14.532 and
10^7 Ω for nighttime flights (14.533, 14.534). In addition to the in-flight
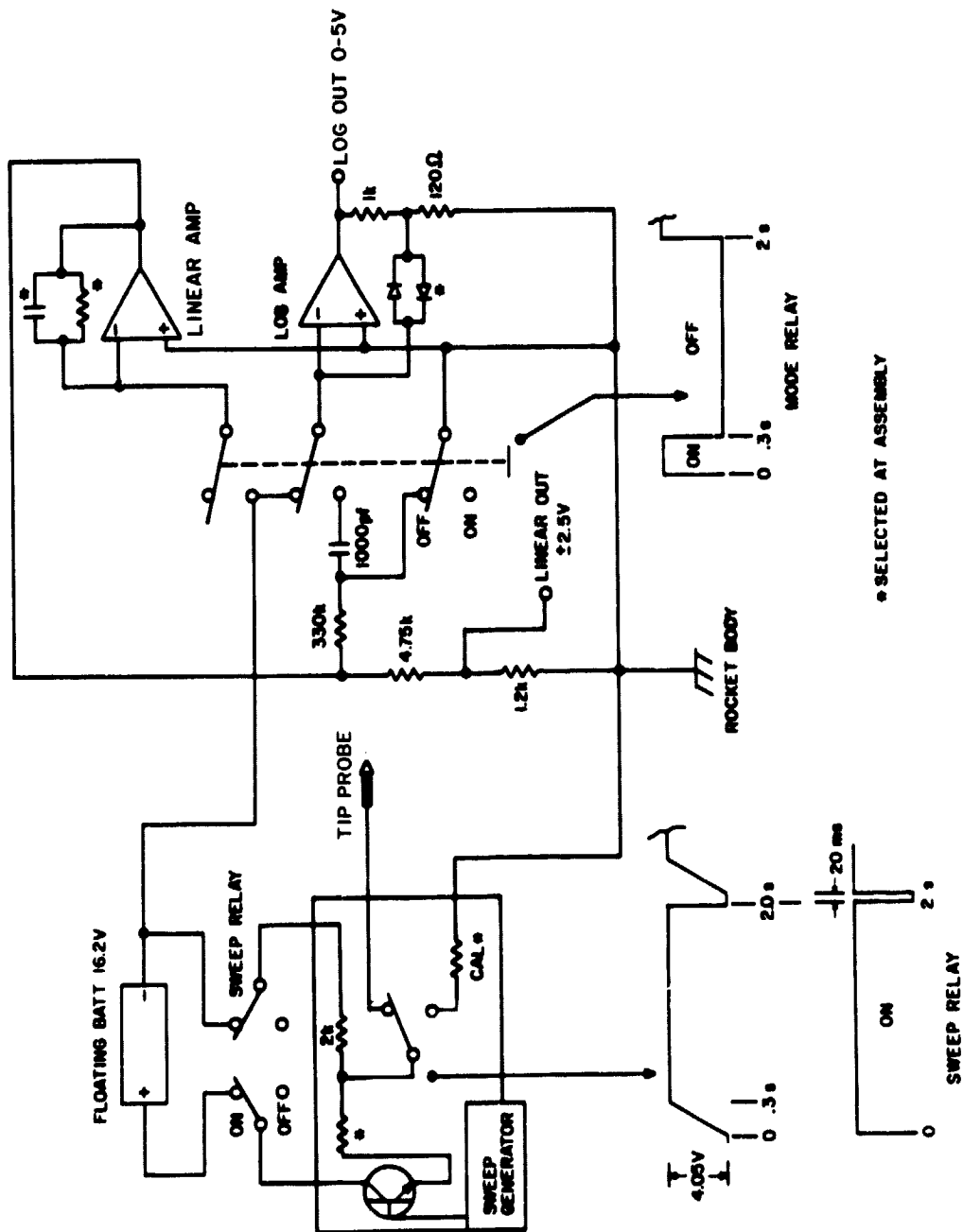
Figure 4.5 Langmuir probe instrumentation block diagram

calibration an extensive calibration was performed prior to each launch. This consisted of sequentially connecting resistors with values between 10^{10} and 10^4 Ω between the electrode and ground.

The electronic circuits of the probes, whether using the nose-tip or boom-mounted electrodes, are essentially identical. As noted above they differ principally in the waveform of the voltage applied to the electrode; this is determined by the timer circuit.

The probe timer circuit is shown in Figure 4.6. The unijunction transistor Q1 and associated circuit sets the repetition rate of the sweep-fixed voltage sequence. Transistor Q2, which is normally conducting, energizing the relay in the sweep circuit, is cutoff for 20 ms after the period set by Q1. In setting up the times R2 is adjusted to give the 20 ms cutoff; then R8 is adjusted for 2 s (for the nose-tip probe) or 0.6 s (for the boom-mounted probe). These times are not critical and no attempt is made to temperature-compensate the circuit.

The part of the circuit including transistors Q3, Q4, and Q5 is used to energize the mode relay for the duration of the sweep (0.3 or 0.5 s).

The circuit including transistor Q6 is used to inhibit the sweep. Q6 is in parallel with Q2 and, when conducting, prevents the sweep relay being de-energized and thus the sweep is not triggered. The sweep-inhibit circuit is controlled by a timer elsewhere in the payload. It is used in the nose-tip probe circuit to obtain a continuous (fixed-voltage) profile to an altitude of 120 km, after which the probe reverts to the alternating sweep/fixed-voltage mode. The sweep inhibit is turned on by the 70,000 ft (21 km) baroswitch so that the pre-flight and calibrated periods are also obtained in the fixed-voltage mode.

The waveform generator which applies the voltage to the probe is shown in Figure 4.7. Since this circuit is inserted between the probe and the electrometer (current-to-voltage converter) it cannot be connected directly to ground. Accordingly it is powered by mercury batteries (12 cells of 1.35 V each). Until power is applied to the payload the sweep relay K1 is not energized, disconnecting the batteries from the circuit. When power is applied to the circuit by energizing K1, the output voltage (developed across R7 by the current is Q2) begins to rise at a linear rate determined by R1 + R3 and C1. After 0.3 or 0.5 s, the value chosen for the sweep duration by adjusting R5, the voltage remains constant. It is adjusted by R6 to be 4.05 V

52
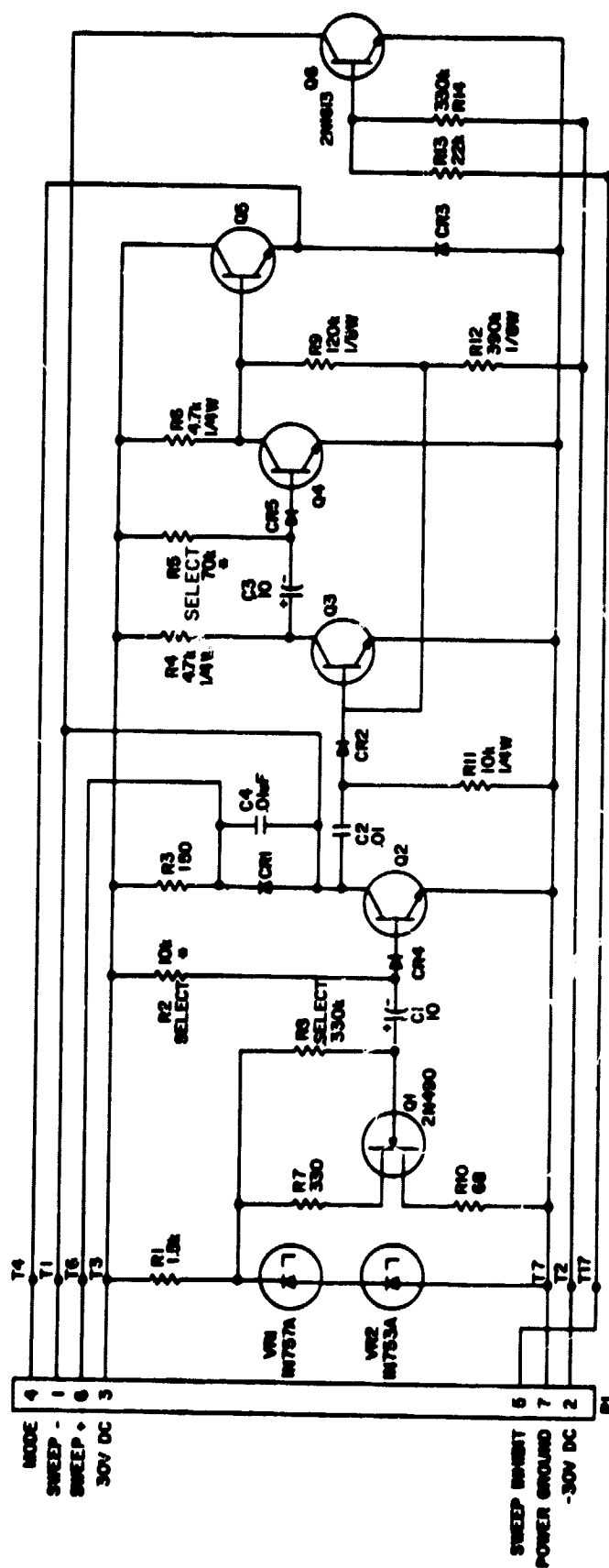
Figure 4.6   Probe timer schematic.
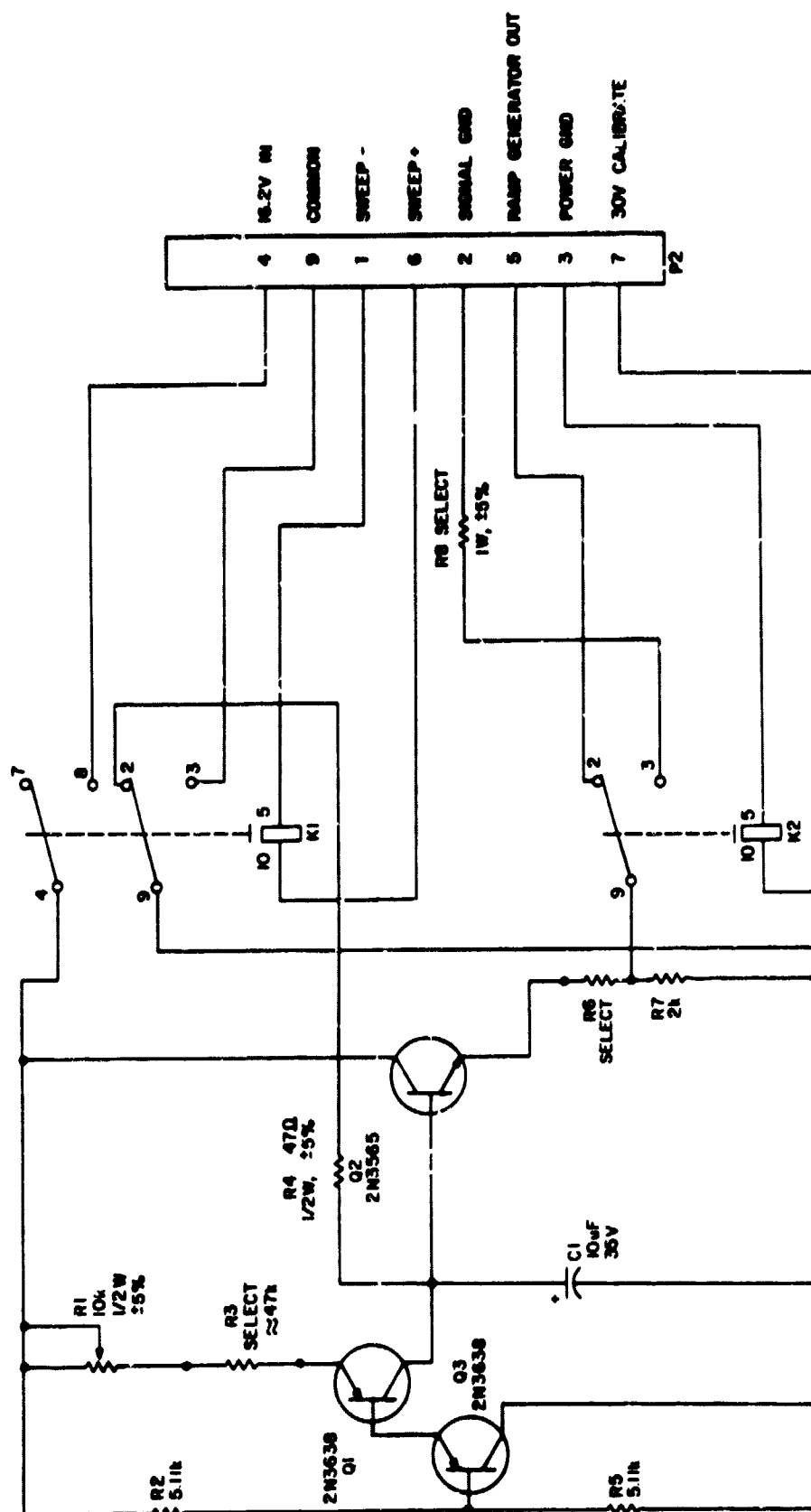
Figure 4.7 Probe ramp generator.

(chosen because it can also be obtained by three mercury batteries).

When K1 is de-energized (for 20 ms) by the timer circuit, capacitor C1 is discharged through resistor R4 (which limits the current).

The relay K2, on being energized, disconnects the waveform generator from the electrode and substitutes a calibration resistor R8. As noted earlier this calibration period is controlled by baroswitches.

The two arrangements of the floating-battery circuit are shown in Figure 4.8. The nose-tip probe usually has a 0 to 4.05 V sweep and the boom-mounted probe has a -1.35 to 4.05 V sweep.

The PROBE IN terminal on the battery pack is connected to the input of the log-linear electrometer circuit, shown in Figure 4.9. Relays K1 and K2, when energized by the timer circuit, switch the input to the linear electrometer and connect the output of the linear electrometer through the differentiating capacitor C2 to the input of the log electrometer. When the sweep ends and the relays are de-energized the input is connected directly to the log electrometer, and the linear electrometer is disconnected from the circuit by opening the input.

The linear electrometer uses a Fairchild F-418A operational amplifier with an RC feedback network. The resistor, R6, establishes the sensitivity: typical values are 1 MΩ for daytime flights and 10 MΩ for nighttime flights. The parallel capacitor C3, has a value of 330 pF for daytime flights and 33 pF for nighttime flights giving an upper 3 dB frequency for the electrometer circuit of about 500 Hz. The electrometer is followed by a 741 op amp connected as a unity-gain inverting amplifier.

The log electrometer uses a Keithley 302 operational amplifier with diodes in the feedback circuit to give the logarithmic characteristic. The voltage divider formed by R2 and R3 multiplies the voltage across the diodes by about 10 allowing a full-scale output greater than 5 V.

The frequency response of the log electrometer varies with current. It is shown in Appendix I that the frequency response is better than 500 Hz for currents greater than 2×10^{-8} A.

When the probe is used strictly for electron-temperature measurement and the probe is swept repeatedly (without an extended period at fixed-voltage), as for the boom-mounted probe on Nike Apache 14.532, then the mode-switching relays are not needed and the circuits are correspondingly simplified.

COMMON 6

PROBE IN 2

12 CELLS

+

16.2V 1

(a)

-1.35V 6

I CELL

PROBE IN 2

II CELLS

14.9V 1

(b)
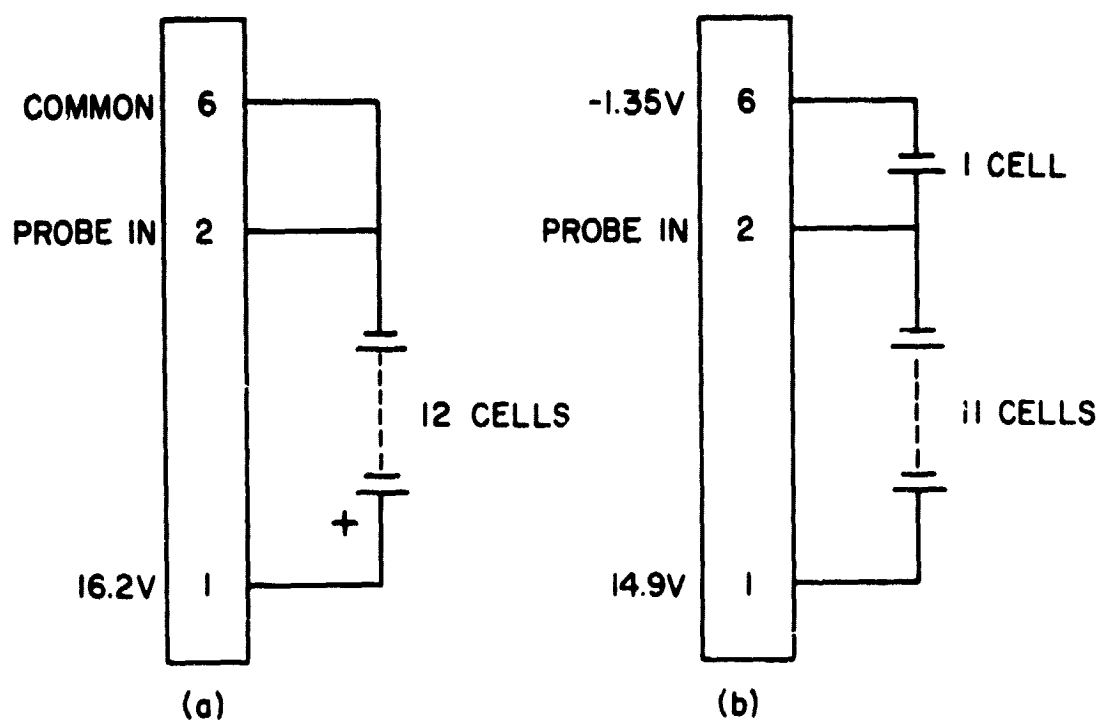
Figure 4.8 Floating-battery circuit for (a) nose-tip probe
and (b) boom-mounted probe.
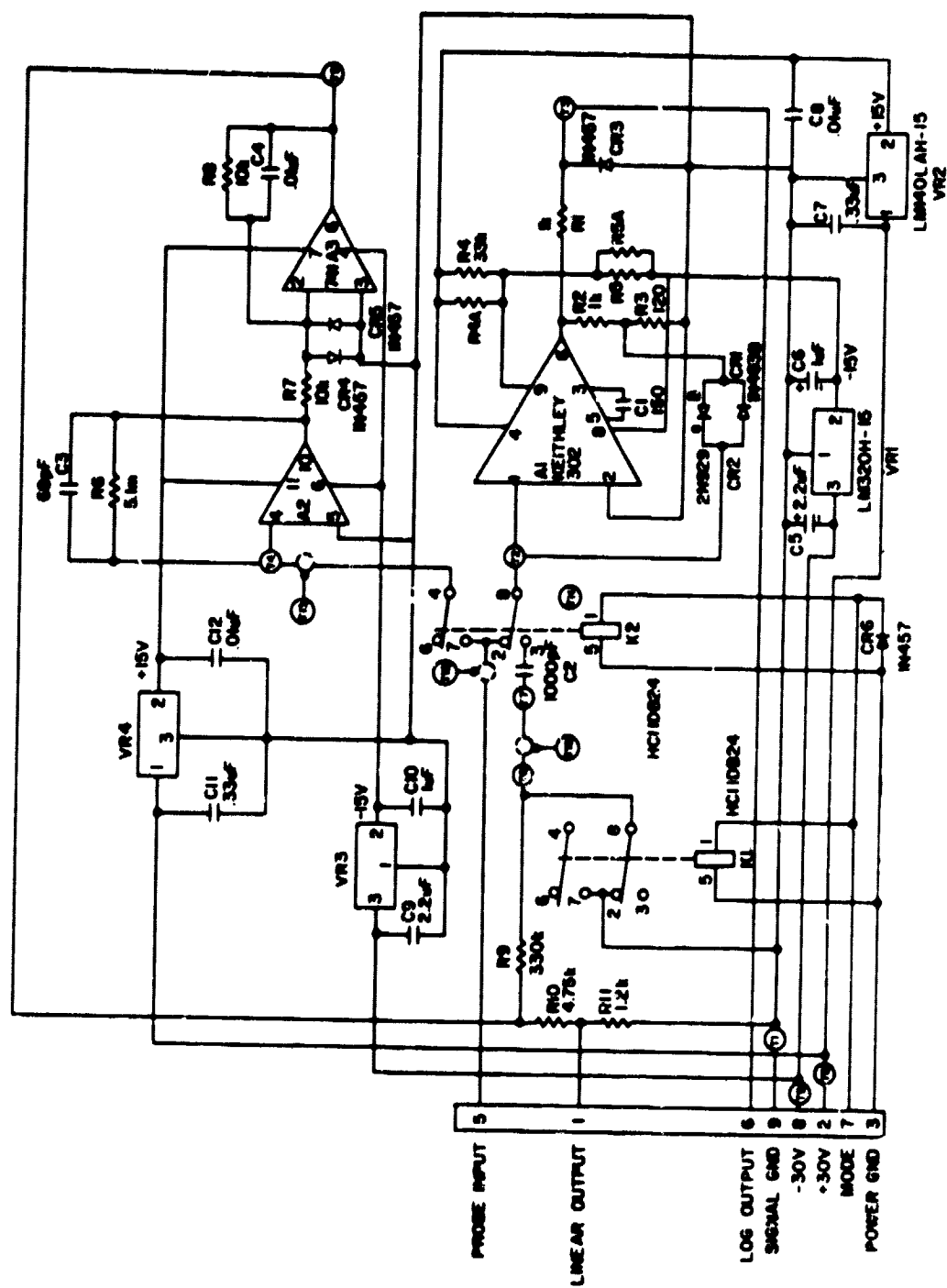
Figure 4.9 Circuit of the log linear electrometer.

The main power supply for the payload is a re-chargeable battery consisting of 20 HR-1 cells. This 30 V supply (actually closer to 28 V) is reduced to 15 V (or other appropriate value) by voltage regulators in the individual experiments. A DC-to-DC converter is used to provide a -30 V supply for the payload. Again this is reduced by voltage regulators in the different circuits.

5. DATA REDUCTION

5.1 *Introduction*

On board the rocket the signal which carries the temperature information is developed as a voltage in the range 0 to 5 V. This voltage is applied to a voltage-controlled subcarrier oscillator (VCO) whose output frequency modulates a 1 W transmitter. The frequency of the transmitter is P band (about 240 MHz) or S band (about 2.2 GHz). On the ground this telemetry signal is received by a high-gain tracking antenna, demodulated, and recorded on an analog magnetic tape, together with timing and other signals. As the analog magnetic tape is being produced the demodulated signal is also applied to frequency-to-voltage converters (discriminators) whose outputs reproduce the signals applied to the VCOs in the rocket. These varying dc signals are digitized and recorded on another magnetic tape. At any time after a launch has occurred the analog tape may be played back, discriminated, and digitized to produce additional digital recordings.

The digitizer operates at a rate of 5 kHz and is preceded by a five-channel commutator. Every fifth data sample to be digitized and recorded is electron temperature data; the other four data samples are taken from other information channels. This results in a digitization rate of 1 kHz per data channel.

Before digital computers were widely available, all rocket data reduction was accomplished by hand. The recovered voltage from the telemetry discriminator was recorded on a high-speed stripchart recorder. For each probe sweep a temperature could be determined by measuring the slope of the log (di/dv) signal using a straight edge and protractor. Figure 5.1 is a stripchart record demonstrating this technique. Data reduction was straightforward, although tedious, and quite satisfactory under optimal conditions.

The initial desire to computerize the data reduction process was to save time and reduce errors. After software was created to handle the digital magnetic tapes other advantages became apparent, foremost being the capability to incorporate simple noise-reduction algorithms. This permitted the recovery of temperature information from data recorded under less than optimal conditions.

The software must be able to perform several tasks:

ORIGINAL PAGE IS
OF POOR QUALITY

SWEEP NO. 13
10 in/s

NIKE APACHE 14.534
450 Hz LP

ELECTRON TEMPERATURE = CONST./tan θ
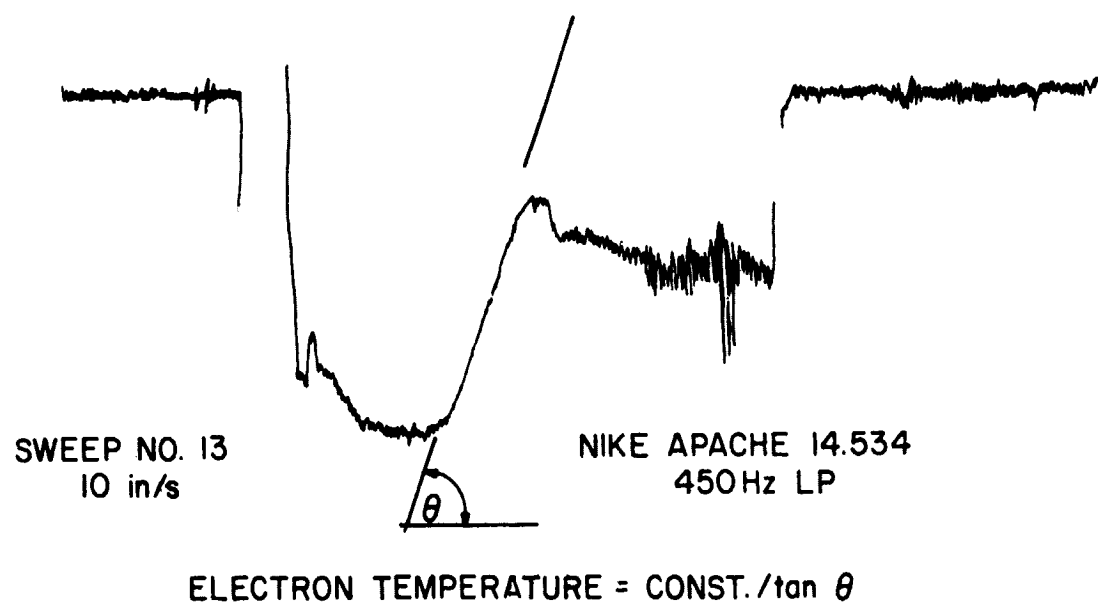
Figure 5.1 Stripchart record demonstrating manual technique of recovering electron temperature information.

1. The program must efficiently scan the digital magnetic tape
    and recognize probe sweep data;

2. The probe voltage sweeps linearly from 0 to 4.05 V. Only
    data generated while the probe is within (roughly) 100 mV
    of plasma potential are meaningful for temperature
    determination. Other data must be ignored;

3. Once the proper data have been located the temperature
    determination must be made. This entails fitting a line
    to a limited number of data points. Data which show
    evidence of systematic error must be corrected at this stage
    or eliminated; and

4. With rocket trajectory information supplied by NASA the
    program must assign an altitude to each temperature
    measurement.

After the temperature data have been generated they should be printed in
tabular form and, ultimately, plotted as a graph of temperature versus altitude.

5.2 *Data Reduction Software*

The program to obtain electron temperature is ELTEMP. Before proceeding
with a detailed description of the function of each subroutine in ELTEMP it
is necessary to describe the organization of information on the digital tapes.
Each digital tape consists of one file containing records of various lengths.
At the beginning of each tape are four header records, each containing 45
words of identifying information. Each word contains 16 bits, the equivalent
of an IBM 360 half-length integer. Alpha-numeric information is encoded
using the IBM Corporation EBCIDIC convention.

Following these header records are five calibration records, each
containing 1005 words. These records are the digital levels corresponding
to the five analog telemetry levels, 0 V, 1.25 V, 2.50 V, 3.75 V, and 5 V.
The remaining records are all data records, containing 2008 words each.
This organization is demonstrated in Figure 5.2.

The data record structure is displayed in Figure 5.3. Each of these
records contains five channels of data running cyclically through the 2008
words, beginning with word 6 and ending with word 2005. Words 1 through 5
of each record are not used. Words 2006, 2007, 2008 contain binary-coded
decimal time as explained in Table 5.1. The time recorded in these three
words is the time of word 6 in the following record. Note that there is a
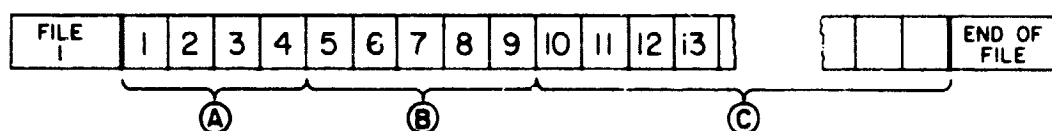
(A) Four header records of length 45 words containing tape identification, e.g., AMQ1 NIKE APACHE 14.532.

(B) Five calibration records of length 1005 words. These records are the digital levels corresponding to the five analog telemetry levels LBE(-7.50%), LBH(-3.75%), BAND CENTER, UBH(+3.75%), and UBE(+7.50%).

(C) Data records of length 2008 words.

Figure 5.2 Organization of data on a digital tape.
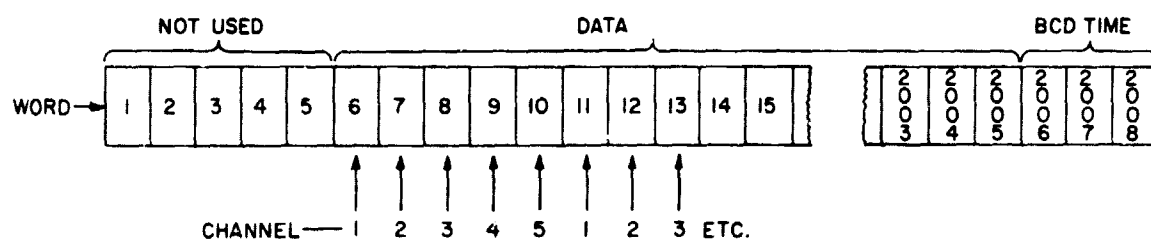
Figure 5.3 Organization of information within one record.

Table 5.1   NASA format for BCD time encoding.

Word 2006	bits	
	1 - 4	tenths of milliseconds
	5 - 8	one of milliseconds
	9 - 12	tens of milliseconds
	13 - 16	hundreds of milliseconds
Word 2007	bits	
	1 - 4	ones of seconds
	5 - 7	tens of seconds
	9 - 12	ones of minutes
	13 - 15	tens of minutes
Word 2008	bits	
	1 - 4	ones of hours
	5 - 6	tens of hours
	7 - 10	ones of days
	11 - 14	tens of days
	15 - 16	hundreds of days

constant increment of time between any two adjacent words in the same channel
of 1 ms, even between word 2005 of one record and word 10 in the following
record. Since each data record contains 2000 words of data digitized at 5 kHz,
one record corresponds to 0.4 second of data. This is 400 words of
temperature data and 1600 words from the other four channels.

Program ELTEMP consists of the nine major FORTRAN subroutines listed
in Figure 5.4 allowing it to operate on the control Data Corporation CYBER
computer. The main program is simply a calling program for the many
subroutines. The entire program is listed in Appendix II.

The tape information is read in subroutine LOAD and the logarithmic
electrometer information, log (di/dv), is transferred to the array LOG(M,N).
The data in the other channels are discarded. This array is dimensioned
$M = 3$, $N = 400$ permitting three data records of 400 points to be stored.
Each time LOAD is called one data record is read from the tape and stored
in LOG with M equal to 1, 2, or 3. LOG is a circular file in that it is
filled sequentially from the magnetic tape as shown in Figure 5.5.

Called from within LOAD are the subroutines CALTIM and BINARY. BINARY
converts the words 2006, 2007, and 2008 into binary representation. CALTIM
takes these three binary numbers and calculates the time using the timing
code in Table 5.1. This is the time (UT) in days, hours, minutes, seconds,
and fractional seconds. From this is subtracted the time of launch to give
the time after launch (in seconds). This is the tape record time which is
stored in RECTIM(M) upon returning to LOAD. Also, the tape record number
is stored as RECNUM(M).

The main program then calls subroutine TRSHLD which searches through
the data is array LOG for the beginning of a probe sweep. The signal
characteristic which indicates the beginning of a probe sweep is the sharp
transition (<5 ms) from a high signal value KMAX to less than a small signal
KMIN for 10 ms or longer. The values KMAX and KMIN are input variables
since they vary from flight to flight depending on the digitization constant
(digital units/analog volt) used at the ground telemetry station.

In practice it is a simple matter to have the contents of a portion of
data tape printed, observe a transition at the beginning of a probe sweep,
and choose appropriate values for KMAX and KMIN. A useful program for this
purpose is NASA listed in Appendix III. The signal must stay low for more
than 10 ms (10 points) to remove the possibility of a single low bad point
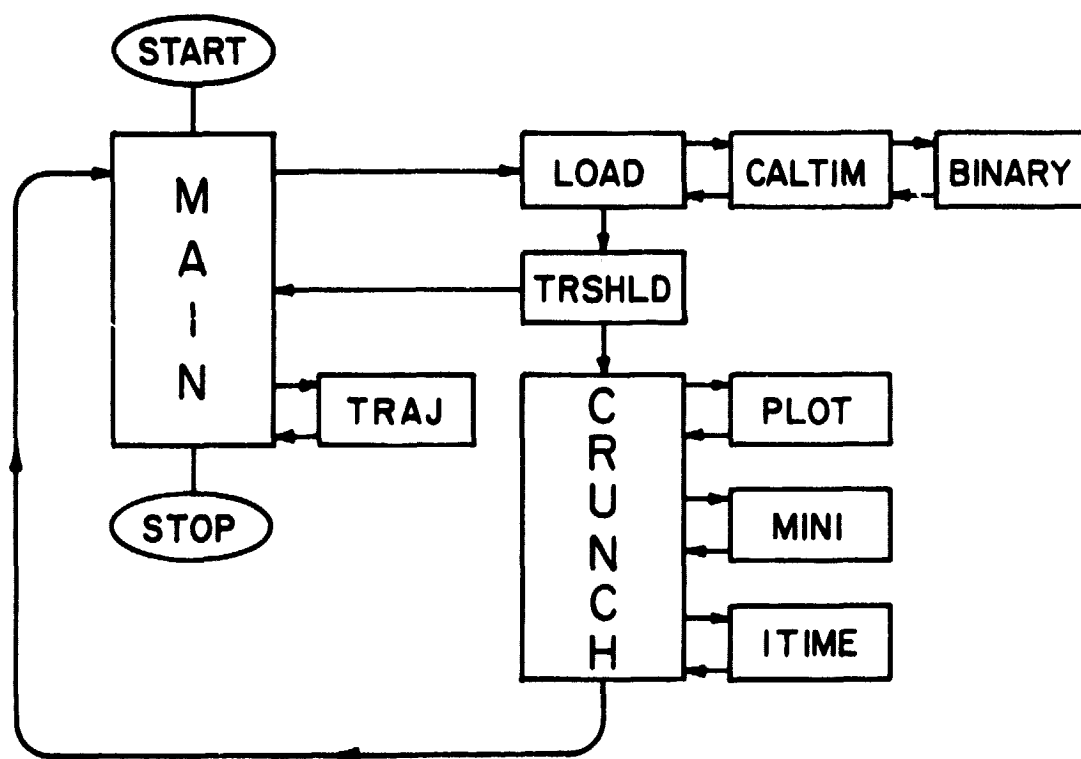
Figure 5.4 Program ELTEMP flow diagram.
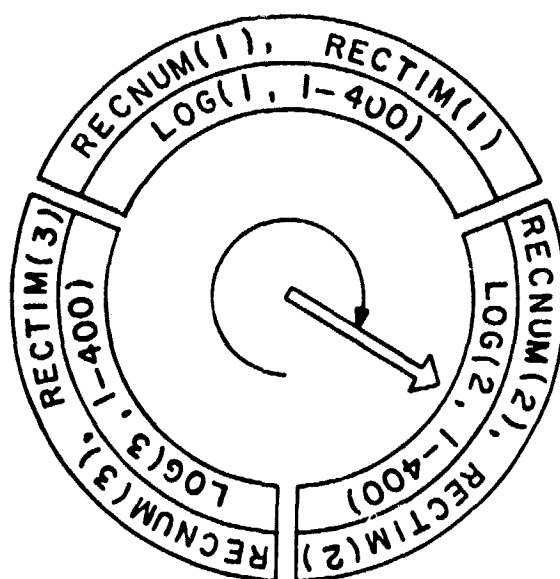
Figure 5.5 Circular data processing file. Logarithmic
electrometer data are shifted into array
LOG 400 points at a time. Associated with
each array LOG is RECNUM, the magnetic tape
record numbei, and RECTIM, the record time
in seconds after launch.

triggering the program falsely. The testing in TRSHLD is sufficiently general to operate across an array boundary, say between LOG(2,400) and LOG(3,1), if the transition should by chance occur there.

If TRSHLD does not find a sharp transition the program control returns to the main program. Here the central index M is incremented by 1. If $M = 3$, it is incremented to $M = 1$. Subroutine LOAD enters another record of probe data in array LOG. CALTIM calculates another time and TRSHLD is called once more.

When TRSHLD does locate the beginning of a probe sweep program control passes to CRUNCH, the most complex of the subroutines. The purpose of CRUNCH is to determine the slope of the log (di/dv) data about plasma potential (in the retarding potential region), take the reciprocal, and multiply by a calibration constant to recover the temperature in degrees Kelvin. The first action CRUNCH takes is to advance some number of points from the transition to the center of the probe sweep. The number of points advanced is an input parameter called OFFSET. During the rocket flight the vehicle acquires floating potential a few volts below plasma potential. When the probe sweep begins (at zero volts with respect to the vehicle) there is very little electron current because the probe is well below plasma potential. There is no reason to examine this portion of the probe characteristic. The OFFSET parameter locates the region of interest closer to the point when the probe passes through plasma potential.

The next 60 data points are that portion of the probe characteristic containing temperature information. As recorded on the digital tape this may bridge two data records and hence be transferred to two arrays by LOAD, say LOG(2,-) and LOG(3,-). For computational convenience CRUNCH transfers these points to one 60-element array LLOG. The calculating window was chosen to be sixty points in length; this much data permits one to get an intuitive feel for the probe characteristic. Also, using fewer data would cause the choice of the OFFSET parameter to be quite critical. As the rocket ascends it usually encounters higher temperatures causing the floating potential to be lower. This means the probe passes through plasma potential further into the probe sweep. For Nike Apache 14.532 and 14.534 the 60-point data window was wide enough that the OFFSET parameter did not need to be adjusted during the flight.

With the raw data now in array LLOG subroutine CRUNCH proceeds with a five-point line fit, first with points 1 through 5, then 2 through 6, and

so on. This generates 56 slopes which are stored in array SLOPEZ. The line fit is a least-squares fit and incorporates the following noise-reduction technique. Five points are used in the line fit. Then each point is checked to see how far it lies from the best-fit line. If this distance is less than the number SPREAD (usually 250 units), CRUNCH will proceed with the next five-point line fit. If the distance is greater than SPREAD, that point is thrown out and the line fit done again with four points. Again the points are checked to see how far off the line they lie. If any of the four points fall beyond SPREAD from the best-fit line, the slope for those points is set to 1 and CRUNCH proceeds with the next five point line fit.

When the line fitting is complete for a given probe sweep there are 56 slopes in the array SLOPEZ. A running average of the slopes (5 points at a time) in array SLOPEZ produces 52 smoothed slopes which are stored in SLOPEZ again. The reciprocal of each slope is multiplied by a calibration constant to yield the numbers in array TE, one of which is the electron temperature in degrees Kelvin. Subroutine MINI makes this choice by choosing the lowest temperature as representative. Although simple, this choice is completely satisfactory. Figure 5.6 shows the contents of arrays LLOG (in digital units) and TE (in degrees Kelvin) for a probe sweep during the flight of Nike Apache 14.532. As can be seen there is an extended region of 8 ms where the slope is constant and the temperature is well defined. Each probe sweep is printed in this fashion to verify the quality of the data and as a diagnostic when one temperature in a profile is far from the mean. The quality of the data is actually better than Figure 5.6 appears for the figure was produced on a computer drum printer resulting in a quantitzation of the data. The printer plot is produced by subroutine PLOT. The time of the temperature measurement is determined by subroutine ITIME by interpolating between the times given at the end of each tape record.

Each call to CRUNCH results in a time and temperature being returned to the main program. This continues until the tape recorder number matches the stop number given by the user. Subroutine TRAJ performs a parabolic interpolation using the NASA trajectory data to assign an altitude to each time/temperature pair. Finally a table of time, altitude, and temperature is printed.
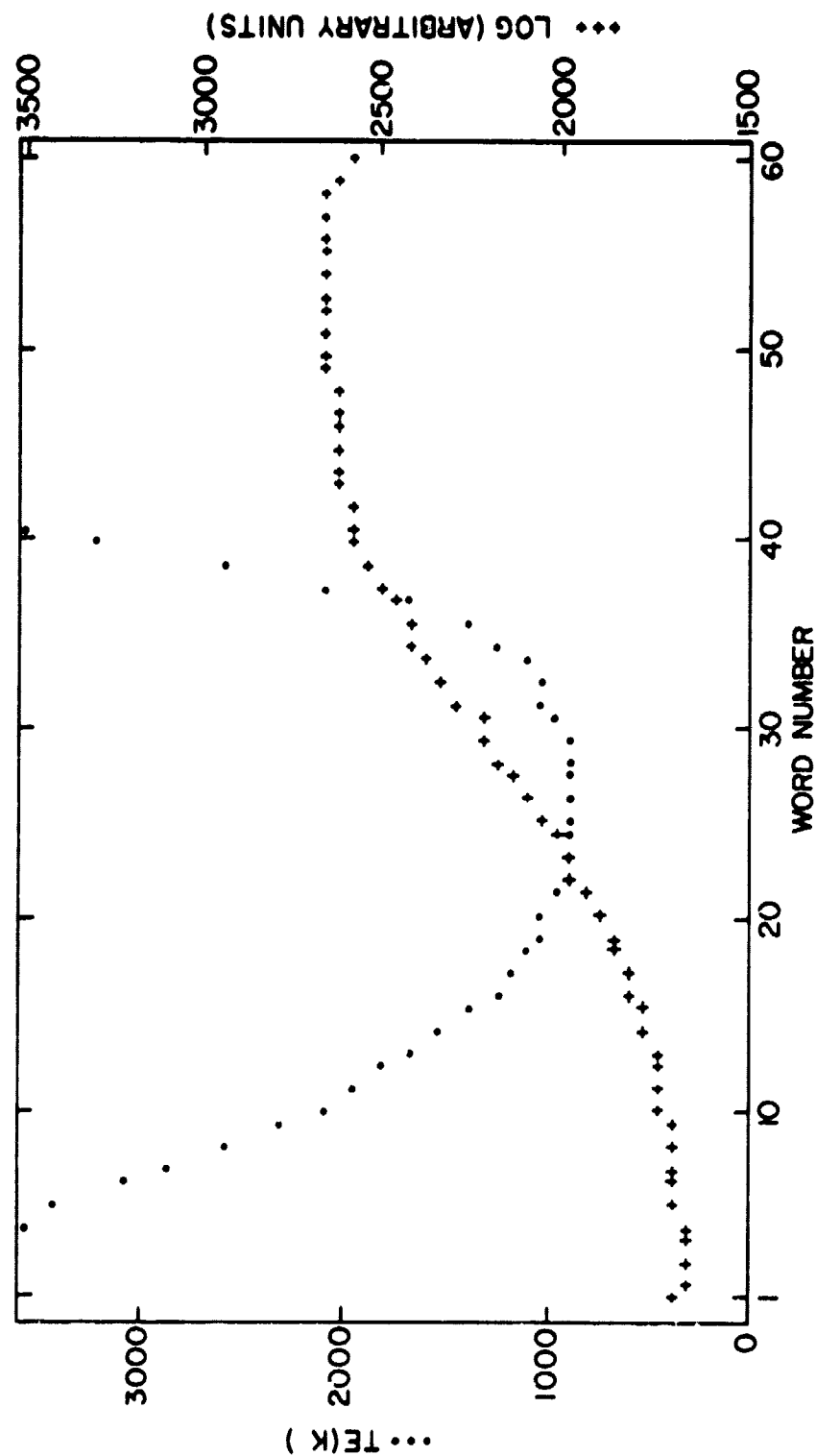
Figure 5.6 Contents of arrays LLOG (represented by +++) and TE represented by •••) plotted against word number. The minimum value in the center of the figure of the TE data is the electron temperature (K) during the probe sweep cycle. Note that one word corresponds to a one millisecond interval.

5.3 Calibration

In the retarding potential region for an electrode of any general shape the electron current density to the probe surface is

$$j_e = j_{eo} \exp\left(\frac{eV}{kT_e}\right) \tag{5.1}$$

where j_{eo} is the random electron current density to the probe surface with the probe at plasma potential, k is Boltzmann's constant, e is the electronic charge, and T_e is the electron temperature. The voltage V is negative voltage measured, strictly speaking, from the plasma potential. In the experiment the probe voltage is measured from the Apache rocket body which floats about 1 V negative with respect to plasma potential. As will be seen this offset is unimportant so long as it does not vary during a probe sweep.

The probe has an effective area for current collection, A, thus the total electron current to the probe is

$$i = A\, j_{eo} \exp\left(\frac{eV}{kT_e}\right) \tag{5.2}$$

The voltage applied to the probe is generated by a ramp generator (Figure 4.7). Let the voltage sweep rate be v_s and the time from the beginning of the sweep be t (the voltage is assumed to be 0 V at $t=0$; the actual value is inconsequential) then

$$i(t) = A\, j_{eo} \exp\left(\frac{ev_s t}{kT_e}\right) \tag{5.3}$$

This current is converted to a voltage by a linear electrometer with an effective (feedback) resistance R so that the output voltage of the linear electrometer is

$$v(t) = RA\, j_{eo} \exp\left(\frac{ev_s t}{kT_e}\right) \tag{5.4}$$

From the linear electrometer the signal passes through a capacitor which time-differentiates the signal. For a capacitance C the displacement current is

$$i(t) = C\frac{dv}{dt} = CRA\, j_{eo} \left(\frac{ev_s}{kT_e}\right) \exp\left(\frac{ev_s t}{kT_e}\right) \tag{5.5}$$

The current through the capacitor is converted to a voltage by a second electrometer, this one employing a diode as a feedback element to provide a

logarithmic scale. For a silicon diode with a forward current of less than 5×10^{-5} A the diode current is an exponential function of voltage. The transfer function of the log electrometer is

$$i = I_o \exp\left(\frac{v_o}{v_e}\right) \tag{5.6}$$

in which I_o has a value about 5×10^{-11} A, v_o is the output voltage of the log electrometer and v_e is the e-folding voltage, typically 0.4 V.

Thus
$$v_o = v_e \ln\left(\frac{i}{I_o}\right) \tag{5.7}$$

The input current is the capacitor displacement current so that the output voltage of the log electrometer is

$$v_c(t) = v_e \ln\left[\left(\frac{CRA \, j_{eo}}{I_o}\right)\left(\frac{ev_s}{kT_e}\right)\exp\left(\frac{ev_s t}{kT_e}\right)\right] \tag{5.8}$$

or

$$v_o(t) = v_e\left[\ln\left\{\left(\frac{CRA \, j_{eo}}{I_o}\right)\left(\frac{ev_s}{kT_e}\right)\right\} + \frac{ev_s t}{kT_e}\right] \tag{5.9}$$

This voltage is telemetered to ground.

At the ground telemetry station a voltage is recovered from the discriminator. It is related to the voltage on-board the rocket by $v = Gv_o + H$, where G is a scaling factor and H is a constant offset voltage. This voltage is carried over a coaxial cable to a digitizer operating at 1 kHz per data channel. The digitizer has a digitization constant p (digital units/analog volt) and a positive offset r. The number recorded on the digital tape is thus

$$u = p(Gv_o + H) + r \tag{5.10}$$

where v_o is the voltage given in (5.9).

To recover the electron temperature information from this signal the first step taken is to calculate the digital slope of the signal, i.e., the number of digital units increase per digital word. This eliminates the digitization offset r and the telemetry offset voltage H.

$$\Delta u = pG\Delta v_o = pG\left(\frac{q dv_o}{dt}\right) \tag{5.11}$$

where q is the interval between digital samples (i.e. 1 ms).

As explained in Section 5.1, Δu is obtained in subroutine CRUNCH by a 5-point line fit rather than by differencing adjacent data points. Dividing by p, the telemetry constant, yields analog volts per digital word. Dividing this by q, the digitization time increment, gives dv_o/dt (volts per second)

$$\frac{\Delta u}{pq} = G \frac{dv_o}{dt} \tag{5.12}$$

From equation (5.9)

$$\frac{dv_o}{dt} = v_e \left[\frac{d}{dt} \ln\left\{ \left(\frac{CRA\ j_{eo}}{I_o}\right) \left(\frac{ev_s}{kT_e}\right) \right\} + \frac{ev_s}{kT_e} \right] \tag{5.13}$$

In this equation C, R, I_o and v_s are constants. The effective area of the probe, A, may change slightly during flight due to changes in the probe surface. However, the probe sweep rate is about 70 ms V^{-1} and only 200 mV of data are required in the retarding potential region. This is about 14 ms of probe data for which the assumption that A is constant is justified. The random current density j_{eo} also changes during the flight, since it is a function of electron concentration. But again, with the vehicle traveling at less than 1.4 km s above 90 km there would have to be a large gradient in n_e in a distance less than 20 meters to significantly change j_{eo}. The only ionospheric structure capable of generating such a gradient is the sporadic-E layer. In all other cases j_{eo} can be regarded as a constant for the duration of the probe sweep. The only other variable is the electron temperature. There has recently been evidence indicating sharp temperature gradients within sporadic-E layers [Szuszczewicz and Holmes, 1977] and we must rule out the use of this technique in such circumstances. However, it is safe to say T_e is constant over the duration of a probe sweep in all other situations. The time derivative of the log term is thus zero for all of the E region except, perhaps, in the sporadic-E layers.

Combining equations (5.12) and (5.13) we have

$$\frac{\Delta u}{pq} = \frac{Gv_e ev_s}{kT_e} \tag{5.14}$$

whence

$$T_e = \frac{Gv_e ev_s pq}{k\Delta u} \tag{5.15}$$

The notation used is as follows: e is the electronic charge $(1.602 \times 10^{-19}\text{C})$, v_s is the probe voltage sweep rate (V s^{-1}), p is the digitization constant (digital units V^{-1}), q is the digitization time increment (s), k is Boltzmann's constant $(1.380 \times 10^{-23}\text{ J K}^{-1})$ and v_e is the measured logarithmic e-folding voltage. The telemetry constant G is, in practice, combined with p.

In subroutine CRUNCH the digital slope is calculated, its reciprocal taken and multiplied by CALIB, the calibration constant. From (5.15) it is seen CALIB is numerically equal to $Gv_e ev_s pq/k$. The probe voltage sweep rate v_s and the electrometer e-folding voltage v_e are measured while the payload is on the ground. The digital time increment q is 1 ms. Records 5 through 9 on each digital magnetic tape contain the information to determine Gp. (The two quantities need not be measured separately.) These records are the telemetry calibration records: record 5 is the digital level for 0 V, record 6 is the digital level for 1.25 V, and so on, with record 9 being the digital level for 5 V. To determine Gp for channel 1 one can average all 200 of the channel 1 values in record 9. Also average all the channel 1 values in record 5. The difference divided by 5 V is Gp for channel 1. Program CALIB, listed in Appendix IV, was designed for this purpose. It prints the average channel values for records 5, 6, 7, 8, and 9. Examples of the output are shown.

The e-folding voltage v_e is determined from calibrations performed prior to launch (see Section 4.3). The probe is connected to the vehicle ground by way of a series of test resistors ranging from $10^4 \Omega$ to $10^{10} \Omega$. For each resistor, R_{cal}, place in the circuit the resultant output voltage from the logarithmic electrometer is,

$$V = v_e \ln \frac{CRv_s}{R_{cal}I_o} \tag{5.16}$$

which may easily be seen by going back to equation (5.2) and starting with $i = V/R_{cal}$. A semi-log plot of V against R_{cal}^{-1} has a slope v_e allowing v_e to be obtained.

During the in-flight calibration periods a calibration resistor is substituted for the probe electrode. This gives a one-point check of the calibration. Experience in many flights has shown that this is sufficient verification of the system.

6. ERROR ANALYSIS

This chapter discusses noise encountered in rocket experiments with Langmuir probes and the specific efforts taken to reduce the effects of noise in the data analysis. Five types of noise (error) have been identified and are considered in the following sections.

1. Statistical scatter among data points.

2. Power line noise.

3. Systematic error in data handling and reduction (low-pass filtering).

4. Probe surface contamination (work function or contact potential).

6.1 *Statistical Scatter*

The simplest type of noise encountered is statistical scatter on the data points. The source of this noise is probably within the payloads' instrumentation, including the experiment itself and the telemetry system. The scatter is of such a magnitude that it is not satisfactory to take the difference of adjacent points to evaluate the slope of log (di/dv). Therefore subroutine CRUNCH determines the slope by a five-point least-squares fit described earlier. This technique appears to be completely satisfactory under normal conditions.

Severe scatter was observed on five rocket flights during 1974 and 1975 in which there was a partial failure of the P-band telemetry transmitters shortly after launch. During the first few seconds of flight it is usual for rockets to acquire a static charge due to rocket motor firing and, to a lesser extent, triboelectricity. This charge causes voltage on the order of 2 kV to develop on antennas or probes extending from the vehicle. The rocket flights on which transmitter failures occurred used telemetry transmitters without a dc shunt in the output stage. The high voltages encountered during the first five seconds of flight were sufficient to damage the transmitter output stage so that the rf output was reduced to a few milliwatts. This has been experimentally verified by Gilchrist [in *Edwards*, 1977] in a specially instrumented payload.

Nike Apache 14.532 was affected by such a failure. The telemetry signal was poor throughout the flight making the recovered signal very noisy. The boom probe log electrometer data was usable until 173 seconds after launch

(182 km) and then became much worse, as illustrated in Figure 6.1. Subroutine CRUNCH, in doing the line fitting to determine slope, threw out many data points as lying too far from the best-fit line. Even so, the data from each probe sweep had to be viewed by hand (using the plots generated by subroutine PLOT) to be assured the recovered electron temperatures were reasonable.

The telemetry transmitter has been redesigned and flown successfully on following flights. Also, it is worth noting that the charge acquired by the vechile early in flight is dissipated well below 50 km and in no way affects the Langmuir probe.

6.2 *Power Line Noise*

While using program ELTEMP on magnetic tape data from Nike Apache 14.534 it became clear the data were contaminated with a periodic signal not related to rocket spin or precession. A 16 or 17 ms variation can be seen in Figure 6.2 in the plot of reciprocal slope, although not in the data because of the poor resolution of the printer plot. In the telemetry building at Wallops Island Station the data lines are coaxial cables running from the telemetry discriminators through a patch panel to an A-to-D converter in the computer room, a distance of about 10 meters. It appears that somewhere along this cable run there was sufficient capacitive coupling to 60-Hz power lines (τ = 16.7 ms) to cause modulation of the analog data signals. To establish this, the telemetry step calibration at the beginning of two data tapes were plotted on an expanded scale. In Figure 6.3 are the telemetry step calibrations for Nike Apache 14.534 for the log electrometer channel, low pass filtered at 81 Hz. Figure 6.4 shows the telemetry step calibrations for the same channel on another tape, low pass filtered at 450 Hz. The traces are the digital values representing 0 V, 1.25 V, 2.50 V, 3.75 V, and 5.00 V and should be perfectly constant. Instead, a strong 60-Hz component is seen on both tapes. In Figure 6.3 the peak-to-peak deviation is about 24 digital units (32 mV). In Figure 6.4 the 60-Hz component is present at about the same mangitude, as well as a noticeable 120-Hz harmonic.

Figure 6.5 is a plot of a portion of the in-flight (ascent)calibration for Nike Apache 14.534 at 23 seconds after launch. In the lower trace the maximum peak-to-peak displacement is 52 digital units (67.5 mV). The seriousness of this can be understood by examining Figure 6.2 again. The plot of reciprocal slope may be read as temperature in degrees Kelvin on the right-hand scale. By chance, just where the minimum temperature should have
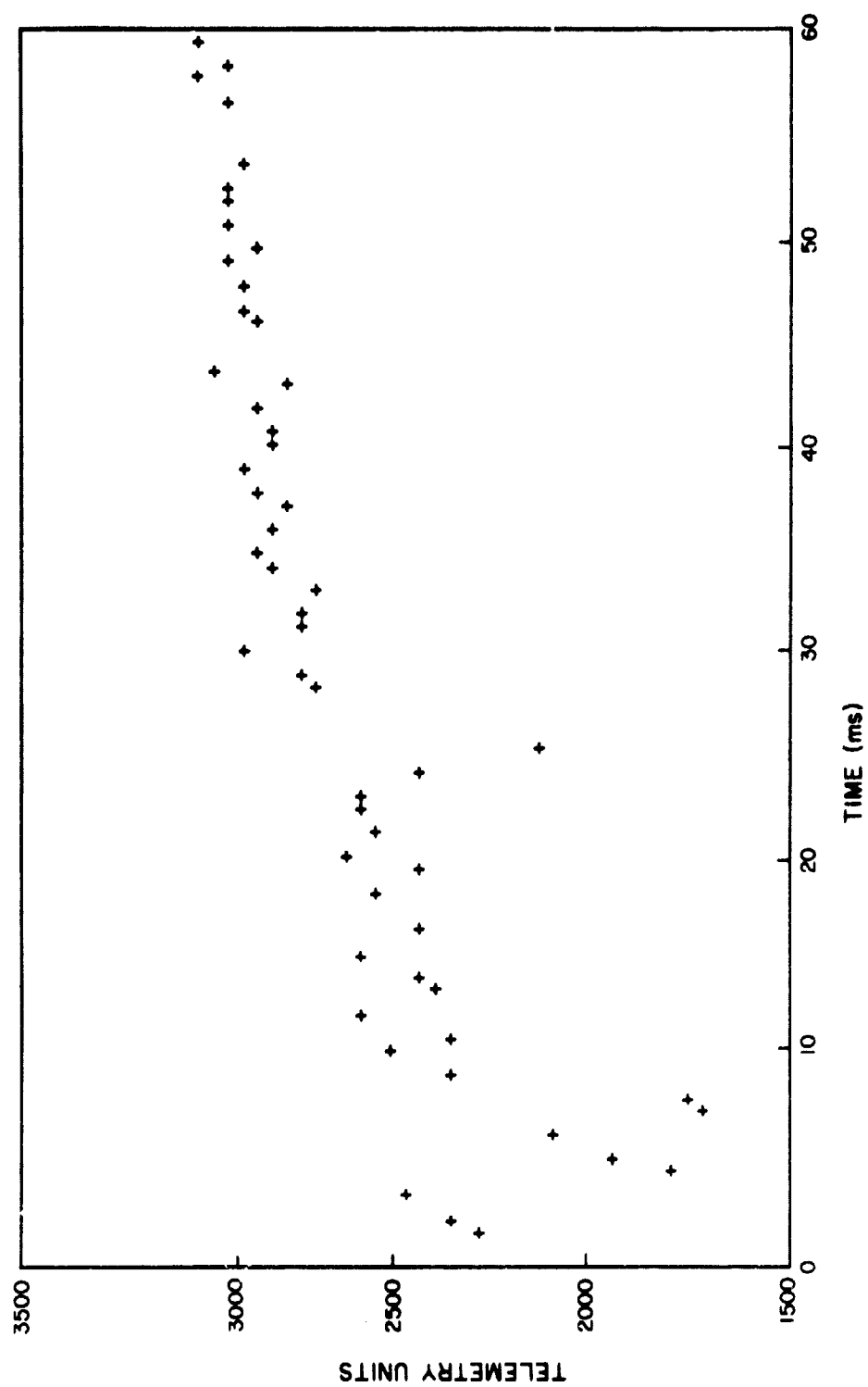
Figure 6.1 Reproduction of plot from record 479 from Nike Apache 14.532 showing noise (scatter).

77
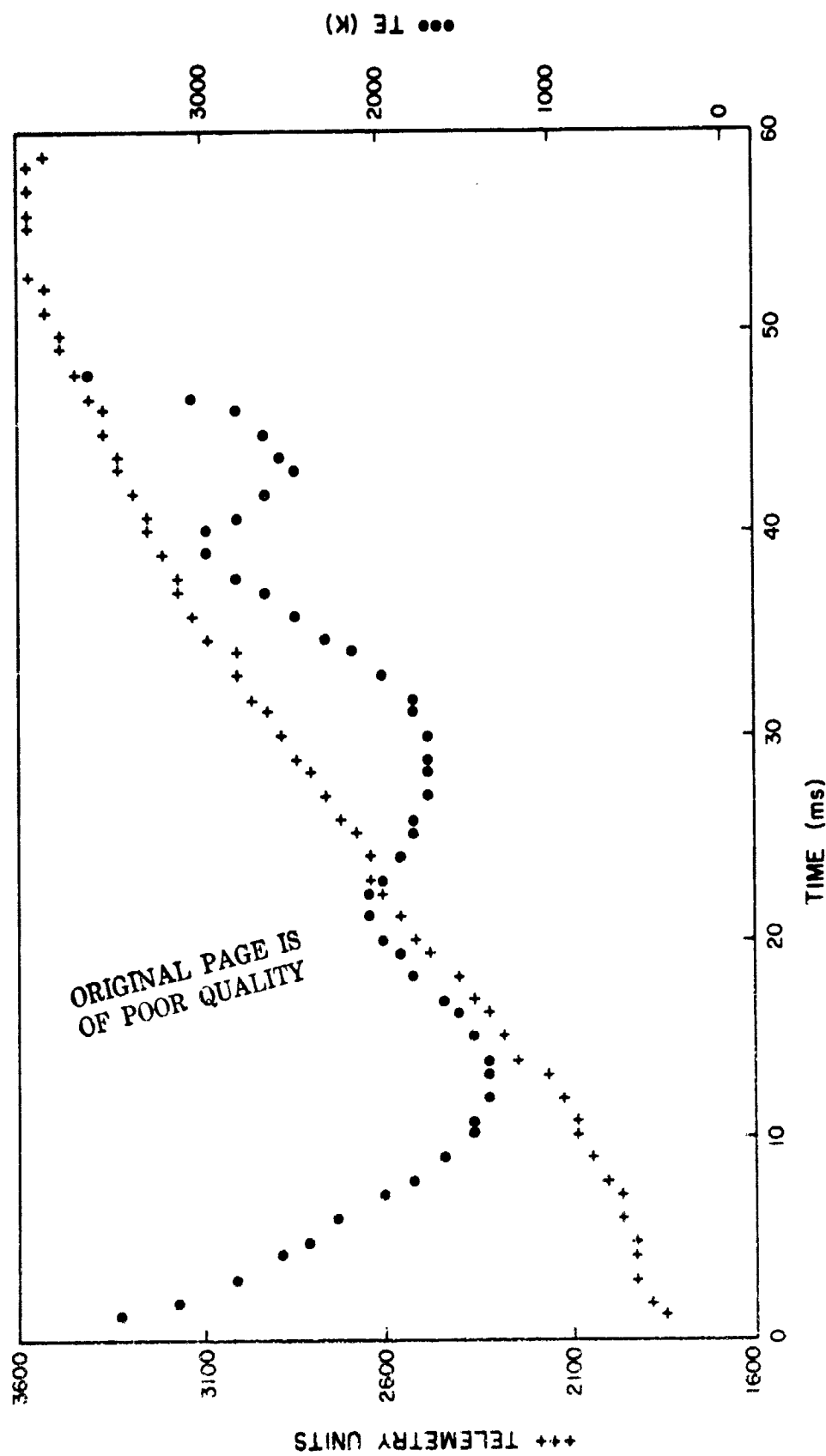
Figure (2 Reproduction of plot (sweep #25) Nike Apache 14.534 81 Hz LP showing hum evidence - periodic variation of reciprocal slope (no humbucking).
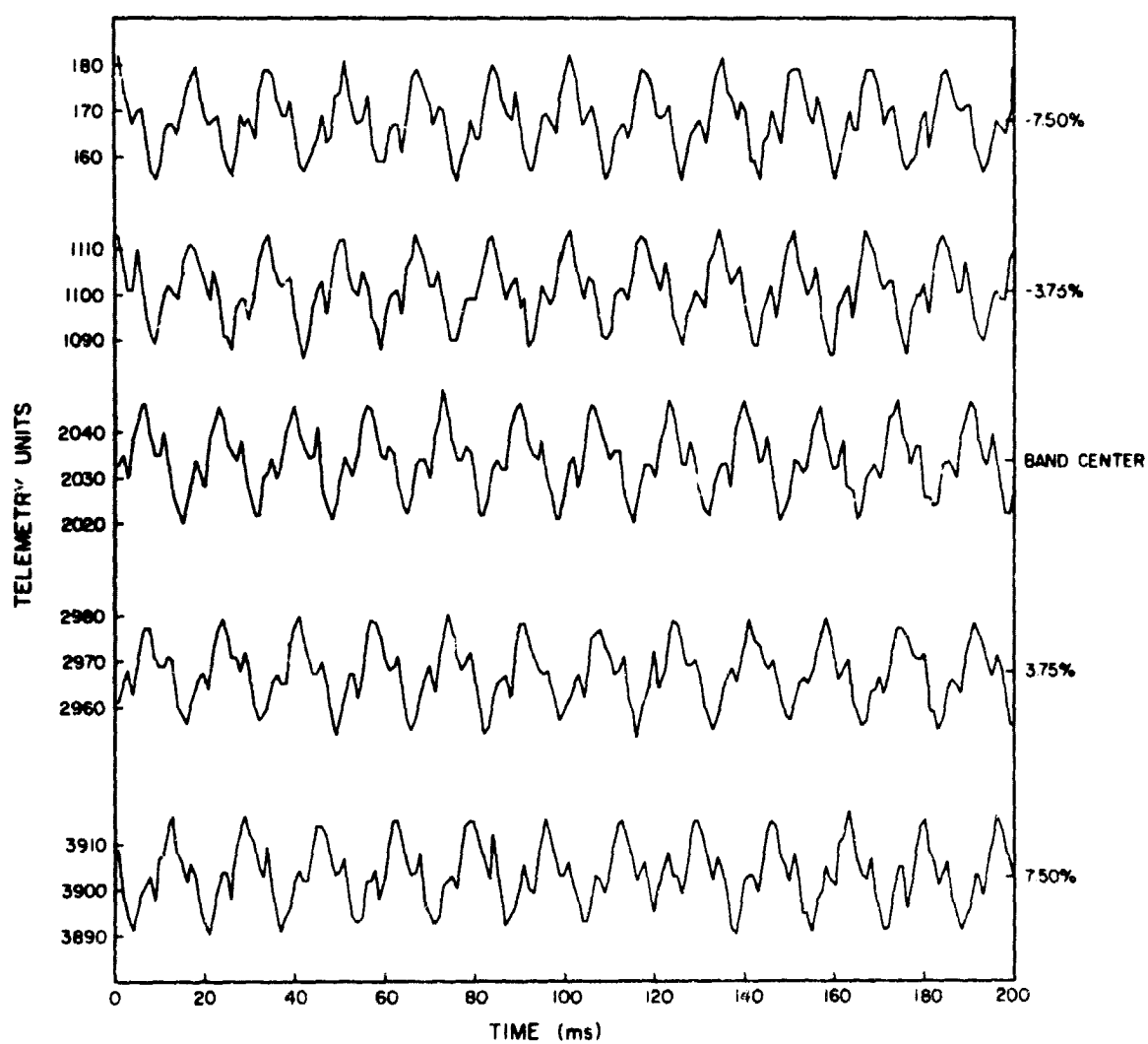
Figure 6.3   Plot of 60 Hz on the five-step TM calibration, 14.534
81 Hz LP filtered.
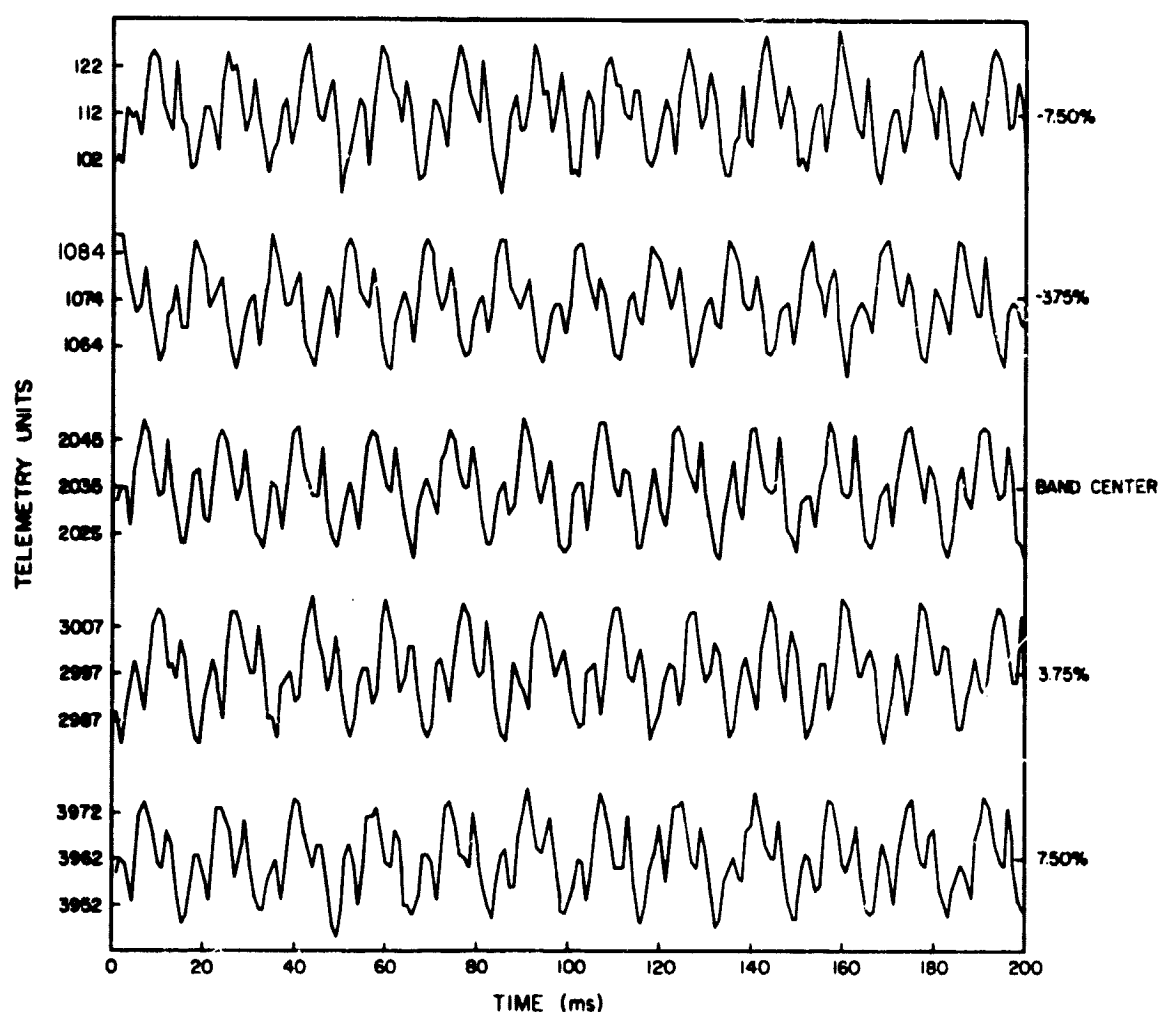
Figure 6.4   Plot of 60 Hz on the five-step TM calibration, 14.534
450 Hz LP filtered.
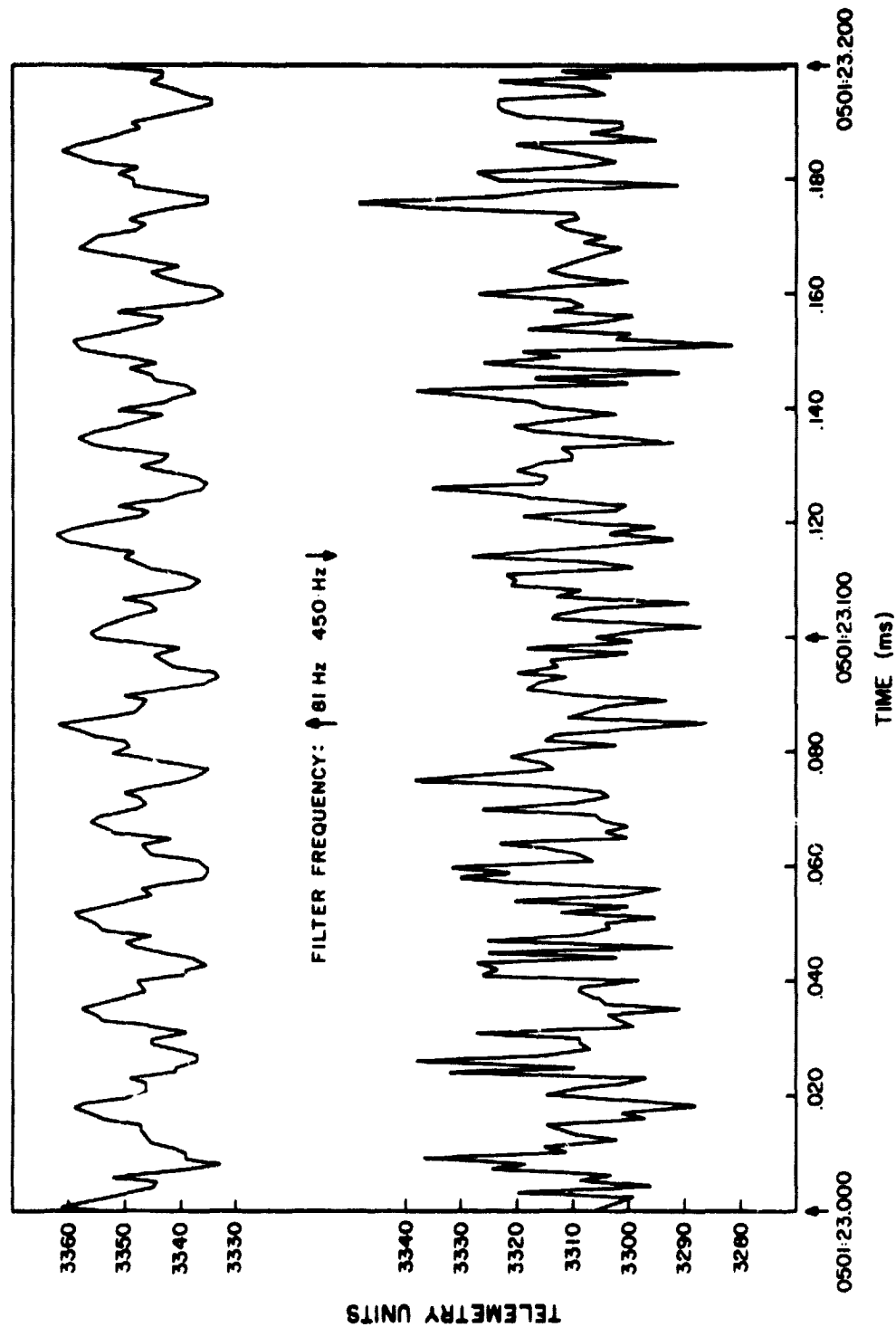
Figure 6.5 A portion of the inflight (ascent) calibration for Nike Apache 14.534. The trace should, ideally, be completely constant. The modulation of the signal, 67.5 mV p-p, occurred at the telemetry station through capacitive coupling between the data cable and 60-Hz power lines. The signal is shown using two low-pass filters (450 Hz and 81 Hz) in the telemetry play-back system.

occurred there is instead a bump, attributable to contamination of the signal at 60 Hz. (Compare with Figure 6.5, an example of a probe sweep without 60 Hz contamination.) It is clear, depending on the phase of the 60-Hz signal during the probe sweep, the recovered temperature can be elevated or depressed by as much as several hundred degree.

Tests conducted at the Wallops Island telemetry facility showed that, with the discriminator in the telemetry room and the digitizer in the computer room there was a 30-mV p-p 60-Hz signal on the cable at the discriminator input. When the discriminator and low-pass filter were relocated adjacent to the digitizer and a very short interconnecting cable was used, it was found that this reduced the hum pickup to 10-mV p-p. In both cases the telemetry discriminator was receiving a band-center signal and was followed by a 59-Hz low-pass filter. Considering the short length of cable in the second case, it is likely that the residual hum originated within the discriminator or digitizer.

Rather than redigitize the tapes at the 10-mV noise level, the decision was made to use the given tapes with software designed to tolerate (or remove) 60-Hz hum from the data, a process generally referred to as "humbucking". This approach has the advantage that it might be used on tapes from other launches which have been recorded with hum (such as Nike Tomahawk 18.1006 and 18.1008). Two humbucking algorithms were developed and tested on the Nike Apache 14.534 tapes.

The first technique used the idea that when the probe is strongly negative it should draw only positive ion-current. Furthermore, since the ion-random-current density is about 200 times smaller than the electron-random-current density, this portion of the characteristic may be taken as a rough baseline for electron current and as a 60-Hz hum reference. The following algorithm was used: subtract from each data point the point which occurred 50 ms earlier. This should yield a curve without hum since 50 ms is the duration of precisely 3 cycles at 60 Hz. And although the curve would be offset by a constant (the positive-ion current) the slope would be preserved. The improvement in data quality is shown in Figures 6.6 (a) and (b).

The above technique was used with confidence until an attempt was made later to quantify the positive-ion current to the probe for potentials less than plasma potential (i.e., at the beginning of the probe sweep) It was
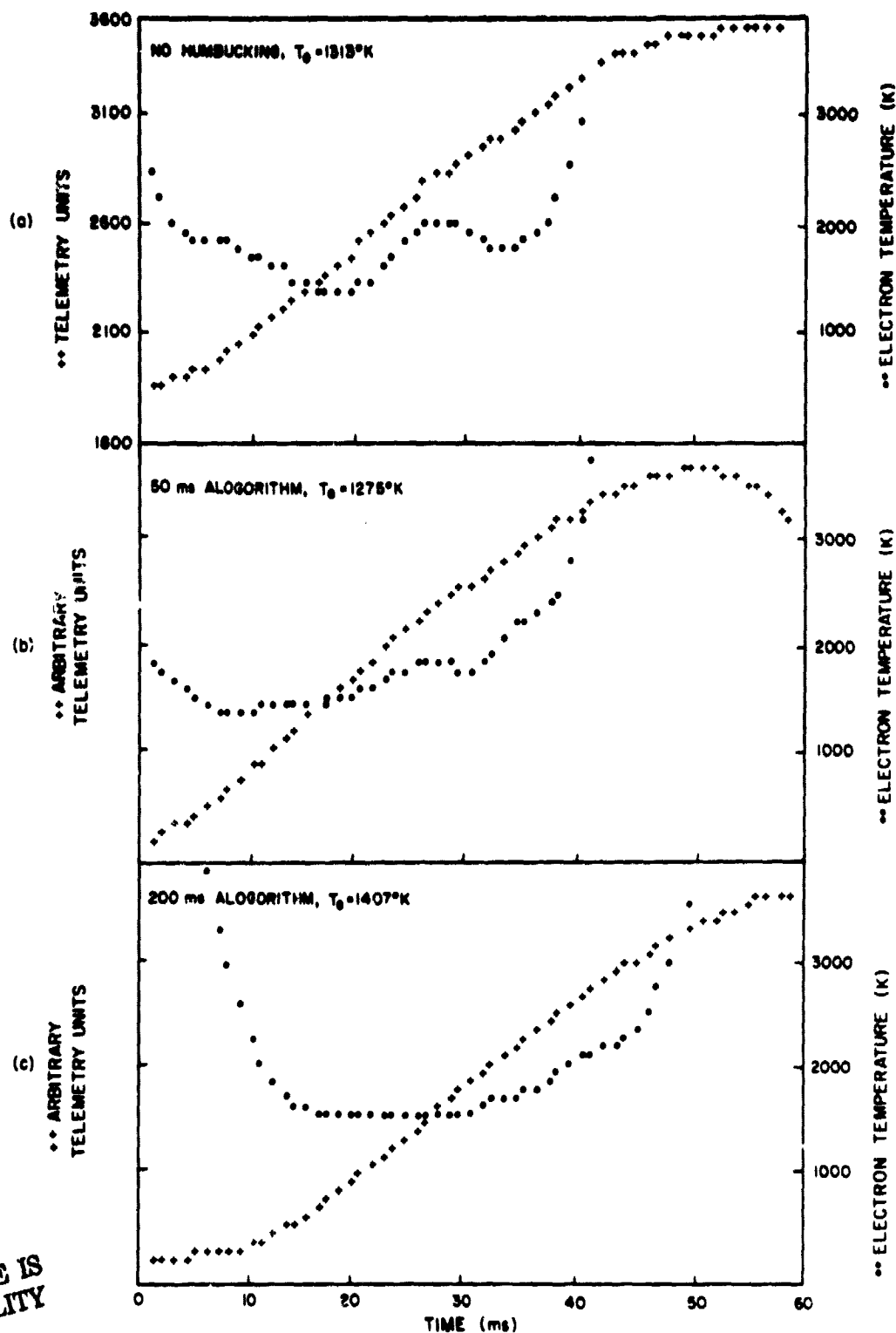
Figure 6.6 A comparison of two techniques for removing 60 Hz hum
from probe sweep data. (a) original data with a 60-Hz
component visible in the temperature curve (....); (b)
and (c) same data after processing with 50 ms and 200
ms, respectively, humbucking techniques described in
the text; (c) appears to be completely free of contam-
ination.

then discovered that the positive-ion current had a slight negative slope until the electron current became dominant further into the sweep. This slight negative slope, if subtracted from the electron-retarding portion of the characteristic, could artifically increase the slope there. The result would be to lower the apparent temperature.

In light of this a second humbucking technique was developed. Before the beginning of each probe sweep is a period when the probe is held at a positive potential (+4.05 V). This signal is constant over periods of time of interest here (~60 ms) except for 60 Hz hum. Therefore, this signal may be subtracted from the electron-retarding region to yield data relatively free of 60-Hz hum while preserving the slope. This was done in Figure 6.6 (c) where a 200-ms delay was used. The improvement in data quality is striking. The 200-ms humbucking routine resulted in temperatures averaging 135 K higher than the 50-ms routine. Note that T_e in Figure 6.6 (c) is 125 K greater than that in Figure 6.6 (b).

The 200-ms technique worked well and, it is felt, accurately recovered the electron-temperature information. The computer code for this algorithm is documented in Appendix II.

A simpler technique was used with the data from Nike Apache 14.533. There the electron temperature was so high that the constant slope persisted for over 80 ms. Thus it was reasonable to average 17 points at a time to produce data free of 60-Hz hum. The coding for this was incorporated within subroutine CRUNCH and is documented in Appendix V.

6.3 *Low-Pass Filtering*

The signal from the Langmuir probe is low-pass filtered several times prior to and during data reduction. Low-pass filtering at intermediate stages restricts high-frequency noise (>450 Hz) and permits the time derivatives necessary for temperature determination to be made. If the frequency response of any filtering stage is so low as to reduce the slope of the $\log(di/dv)$ signal, the result will be an apparent increase in the electron temperature. This effect might be important in the lower portion of the E region (~100 km) where the electron temperature is about 300 K. Figure 6.7 indicates the various stages in which low-pass filtering occurs.

It is important to understand the distortion of the probe signal that occurs in the electrometer circuitry and telemetry system. For the following
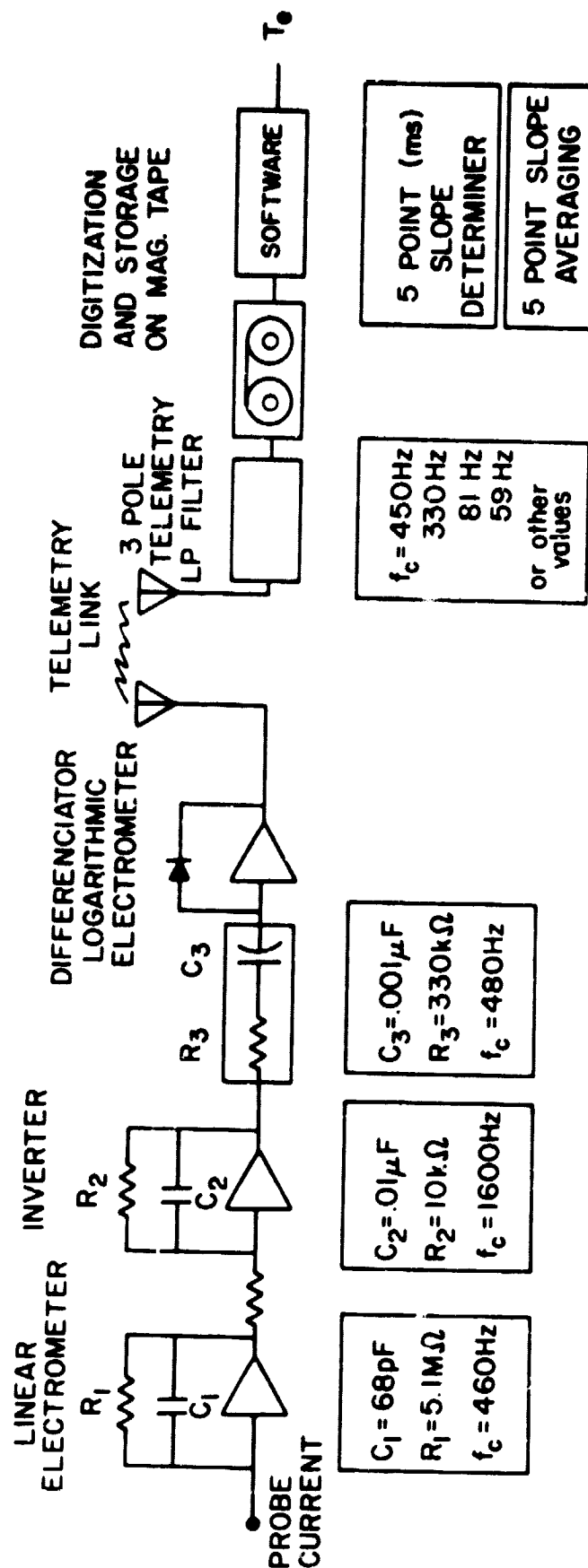
Figure 6.7 In the electron-temperature measurement experiment there are at least six stages where low-pass filtering occurs.

development refer to Figure 6.8, a simplified schematic of the probe electrometer circuit. For this discussion we assume that the current from the probe is strictly electron current, given by

$$i_o(t) = A \; j_{eo} \; \exp\left[\frac{e(v_s t - v_f)}{kT_e}\right] \tag{6.2}$$

where

A = effective probe area

j_{eo} = electron random current density

v_f = rocket floating potential

v_s = probe voltage sweep rate

e = electronic charge

k = Boltzmann's constant

T_e = electron temperature

Let $\alpha = (ev_s/kT_e)$. The probe current flows into the first linear electrometer, which has feedback elements R_1 and C_1. The resultant output voltage is:

$$V_1(t^+) = \frac{A \; j_{eo} \; \exp\left[\frac{e(v_s t - v_f)}{kT_e}\right]}{C_1(\alpha + 1/R_1 C_1)} + V_1(0^-) \; e^{-t/R_1 C_1} \tag{6.3}$$

The electrometer is actually an inverting op amp, although the sign is not displayed explicitly. This voltage causes a current i_1 to pass through R_0 into the second linear electrometer. The output voltage from it is:

$$V_2(t^+) = \frac{A \; j_{eo} \; \exp\left[\frac{e(v_s t - v_f)}{kT_e}\right]}{R_0 C_1 \left(\alpha + \frac{1}{R_1 C_1}\right) C_2 \left(\alpha + \frac{1}{R_2 C_2}\right)} + \frac{V_1(0^-) \; e^{-t/R_1 C_1}}{R_0 C_2 \left(\frac{1}{R_2 C_2} - \frac{1}{R_1 C_1}\right)}$$

$$+ V_2(0^-) \; e^{-t/R_2 C_2}$$
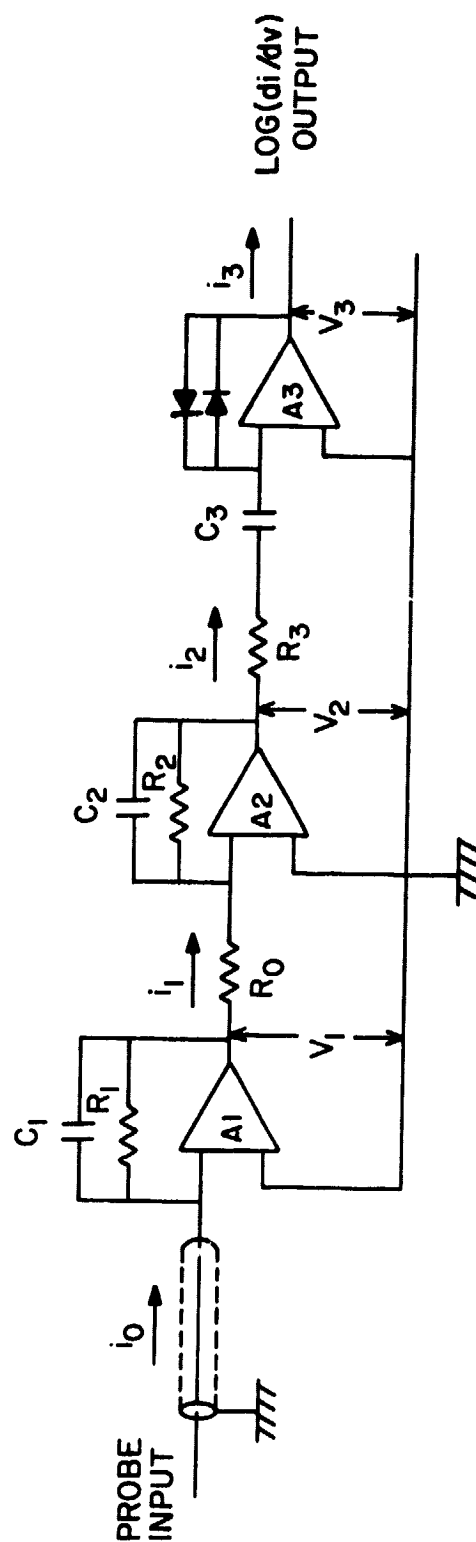
Figure 6.8 Simplified Langmuir probe electrometer circuitry. A1 and A3 are Keithley Model 302 operational amplifiers; A2 is a 741 operational amplifier.

Typical values for the constants in the above expression are

$$R_0 = 10 \text{ K}\Omega \qquad \alpha = 156717 \text{ K}\cdot\text{S}^{-1}/T_e \qquad 1/R_1 C_1 = 2884 \text{ s}^{-1}$$

$$R_1 = 5.1 \text{ M}\Omega \qquad C_1 = 68 \text{ pF} \qquad 1/R_2 C_2 = 10000 \text{ s}^{-1}$$

$$R_2 = 10 \text{ K}\Omega \qquad C_2 = .01 \text{ mF}$$

Substitution of these values in equation (6.3) shows that the second and third terms in the RHS are negligible compared with the first term.

The probe is 0 V for 20 ms before the sweep begins. This permits transients to die away and establishes initial conditions $V_1(0^-)$ and $V_2(0^-)$. During this period the only current to the probe is a very small constant positive-ion current of about 5×10^{-9} A. This sets $V_1(0^-)$ and $V_2(0^-)$ at 25 mV. $A j_{eo}$ is about 1×10^{-7} A. If $T_e = 400$ K, $v_s = 13.5$ V s^{-1}, and $v_f = 1.5$ V, say, equation (6.3) becomes

$$V_2(t^+) = -0.43 \exp[29(13.5t - 1.5)] + 0.035 \exp(-2884t)$$
$$+ 0.025 \exp(-10^4 t) \tag{6.4}$$

The first term is the response to the electron current and becomes significant at about $t = 70$ ms ($V_2 = -4 \times 10^{-8}$ V). The other terms are less than this at $t = 5$ ms and are completely insignificant during the time period of interest here.

Voltage V_2 is differentiated by resistor R_3 in series with capacitor C_3. The purpose of the differentiation is to ensure that the current i_2 into the logarithmic electrometer does not pass through zero during the sweep. (This would otherwise occur for, as mentioned earlier, at the beginning of the probe sweep there is some positive ion current.) Now, ignoring the transient terms in equation (6.3), current i_2 is

$$i_2(t) = \frac{A j_{eo} \alpha \exp \dfrac{e(v_s t - v_f)}{kT_e}}{R_0 R_3 C_1 \left(\alpha + \dfrac{1}{R_1 C_1}\right) C_2 \left(\alpha + \dfrac{1}{R_2 C_2}\right)\left(\alpha + \dfrac{1}{R_3 C_3}\right)}$$
$$+ \frac{V_3(0^-) e^{-t/R_3 C_3}}{R_3} \tag{6.5}$$

where $V_3(0^-)$ is the voltage across C_3 at $t = 0$. Again, the transient term is unimportant because $1/R_3 C_3 = [330 \text{ K}\Omega \times 0.001 \text{ }\mu\text{F}]^{-1} = 3030 \text{ s}^{-1}$.

Current i_2 enters the logarithmic electrometer formed by an operational amplifier with diode feedback elements. The output voltage is a ramp containing the temperature information, with another term:

$$V_3(t) = V_e \frac{e\left(v_8 t - v_f\right)}{kT_e}$$

$$+ V_e \ln \frac{A \, j_{eo} \, \alpha}{I_0 R_0 R_3 C_1 C_2 \left(\alpha + \frac{1}{R_1 C_1}\right)\left(\alpha + \frac{1}{R_2 C_2}\right)\left(\alpha + \frac{1}{R_3 C_3}\right)} \qquad (6.6)$$

where V_e is the electrometer e-folding voltage and I_0 is the reverse saturation current of the diode used as a feedback element. The second term is temperature dependent (recall that $\alpha = ev_8/kT_e$) and will be considered later. The first term is a ramp with slope inversely proportional to T_e. V_3 is telemetered to ground, low-pass filtered, digitized, and recorded on digital magnetic tape for later analysis.

The error introduced by the low-pass filter may be significant, depending on T_e and ω_c (the filter cutoff frequency). The filter phase and amplitude response is given in Figure 6.9 in a plot provided by the manufacturer, Data-Control Systems, Inc.* DCS refers to the filter as a third-order "linear phase" output filter, a term used to signify a Bessel response filter. The transfer function for a third-order Bessel filter, normalized for a dc delay of 1s, is**

$$H(s) \Big|_{n=3} = \frac{15}{s^3 + 6s^2 + 15s + 15} = \frac{15}{(s^2 + 3.67782s + 6.45944)(s + 2.32219)} \qquad (6.7)$$

This may be renormalized for a cutoff frequency $\omega=1$ by substituting $1.753s$ in place of s in equation (6.7). This yields the actual transfer function for the response in Figure 6.9.

$$H(s) \Big|_{\omega=1} = \frac{2.78449}{(s^2 + 2.09801s + 2.10199)(s + 1.32469)} \qquad (6.8)$$

The response $Y(s)$ from such a filter (with cutoff frequency ω) upon the application of an input signal αt is,

---

*Data-Control Systems, Inc., P.O. Box 860, Commerce Drive, Danbury Connecticut.

**see, for example, Principles of Active Network Synethesis and Design, Gobind Daryanani, John Wiley and Sons, 1976, p.g. 119-120.
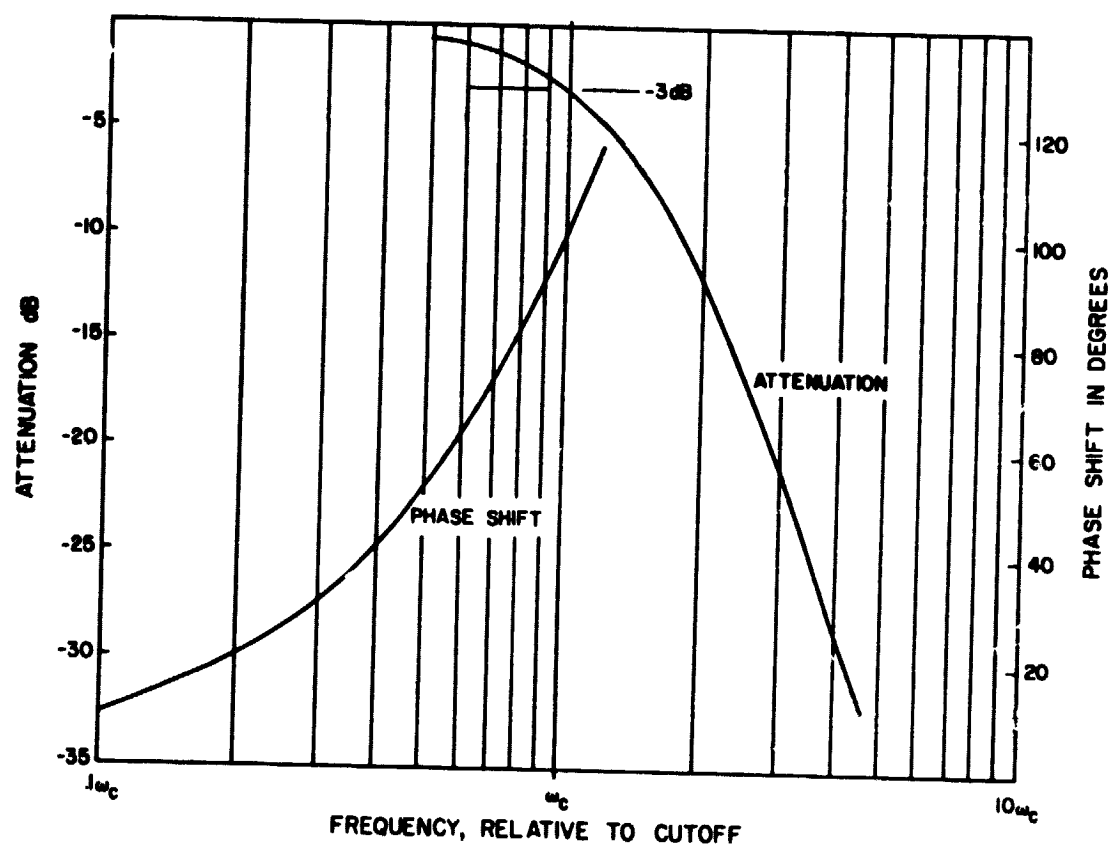
Figure 6.9   Normalized frequency response characteristics of linear phase
output filter for Data-Control Systems telemetry discriminator
type GFD-13.

$$Y(s) = \frac{\alpha}{s^2} \cdot \frac{2.78449\omega^3}{(s^2 + 2.09801\omega s + 2.10199\omega^2)(s + 1.32469\omega)} \qquad (6.9)$$

This may be written as a partial fraction expansion $\qquad (6.10)$

$$Y(s) = \frac{-1.753\ \alpha/\omega}{s} + \frac{\alpha}{s^2} + \frac{(.28046\ \alpha/\omega)s + 1.53907\alpha}{s^2 + 2.09801\omega s + 2.10199\omega^2} + \frac{1.47254\ \alpha/\omega}{s + 1.32469\omega}$$

The time domain response can then be determined from a table of Laplace transforms. For an input signal $\alpha t\ u(t)$ the output is (omitting $u(t)$),

$$Y(t) = -1.753\ \alpha/\omega + \alpha t + 1.275511\ \alpha/\omega\ e^{-1.04900\omega t} \qquad (6.11)$$

$$\cos(-1.34902 + 1.00079\omega t) + 1.47254\ \alpha/\omega\ e^{-1.32469\omega t}$$

The input ramp comes through the low-pass filter with slope unchanged, but with three additional terms: a dc offset, an overdamped oscillation, and a decaying exponential. The magnitude of these terms is proportional to α/ω.

It is the slope of the response (albiet modified) which contains the temperature information. Taking the time derivative of equation (6.11) yields.

$$\dot{Y}(t) = \alpha[1 - 1.33760\ e^{-1.04900\omega t}\ \cos(-1.34902 + 1.00079\omega t)$$

$$- 1.27612\ e^{-1.04900\omega t}\ \sin(-1.34902 + 1.00079\omega t)$$

$$- 1.95066\ e^{-1.32469\omega t}] \qquad (6.12)$$

Here α is the desired slope, the remaining terms being error terms. It is interesting that the error terms depend only on the product ωt and display no dependence on temperature. Measuring the signal slope at $t = 15$ ms from a 100 Hz low-pass filter should incur the same error as measuring the slope at 30 ms from a 50 Hz low-pass filter.

More important and more subtle is this point: the output of the logarithmic electrometer is fairly constant for the initial portion of each sweep, then changes to a ramp (slope proportional to $1/T_e$) when electron current dominates, and finally saturate in the electron-accelerating portion of the sweep. The transition from constant output to ramp occurs fairly abruptly for low temperatures (<15 ms for $T_e = 400$ K) with saturation occurring shortly thereafter. For higher temperatures the transition occurs much more slowly, the ramp continues for a longer time, and saturation occurs later. For example, when $T_e = 2000$ K the ramp output continues for more than 90 ms, whereas for $T_e = 400$ K the ramp output lasts about 20 ms. This effect is demonstrated in Figure 6.10. Therefore, lower temperatures imply a shorter period of time between the transition to ramp output and the
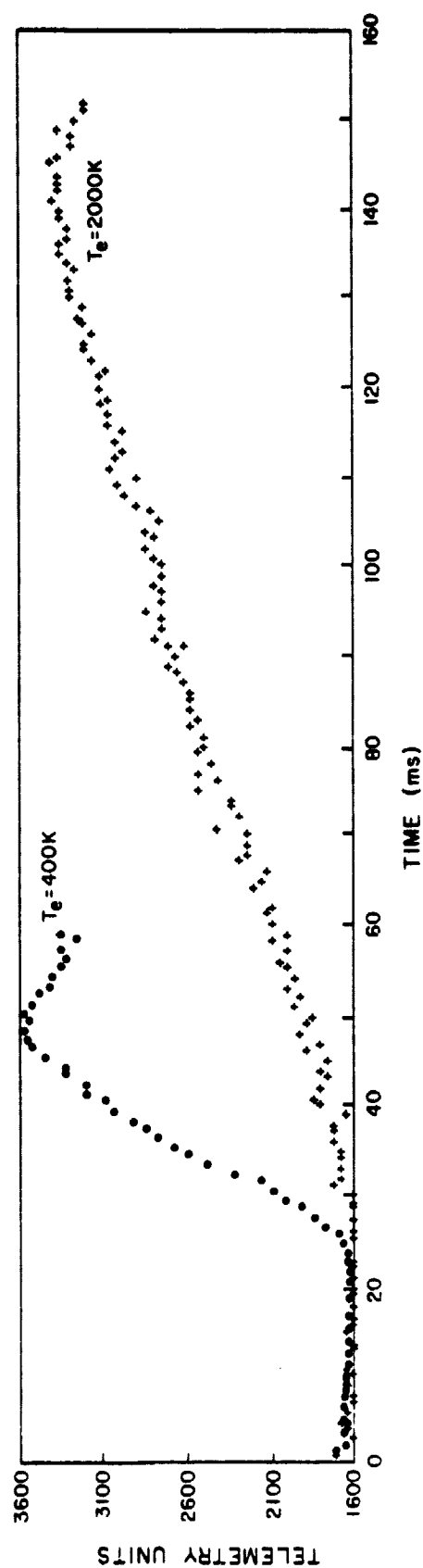
Figure 6.10. A comparison of probe response for T_e = 400 K and T_e = 2000 K from Nike Apache 14.533. Because the duration of the ramp response is longer for high temperatures, it is possible to reduce slope measurement errors due to low-pass filtering.

center of the ramp (where the slope must be measured). The shorter time
will cause more error for a given low-pass filter.

As an example of error that might occur due to using a low-pass filter
consider the case T_e = 400 K with a 450-Hz filter and then again for a 50-Hz
filter. Suppose the slope is measured from the output signal at t = 10 ms,
that is, in the center of the 20-ms ramp output. For the 450-Hz filter
ωt = 450 × 2π × 0.01 = 28. Using equation (6.12) the slope is Y(0.01) = α
and the recovered temperature is 400 K. But for the 50-Hz filter
ωt = 50 × 2π × 0.01 = 3. The recovered slope now is 0.91 and the apparent
temperature is 400(1/0.91) = 440 K, an error of 10 percent. Both filters
give neglible error if t = 45 ms, as would be the case for T_e = 2000 K.

The above error analysis is in general quantitative agreement with an
experimental assessment of error due to filtering done in 1967 by L. G. Smith
(previously unpublished). In the laboratory a 500 K space plasma was
simulated by using a diode and resistor combination as shown in Figure 6.11.
The output of the probe circuit was passed through low-pass filters with
cutoff frequencies between 450 Hz and 20 Hz. The apparent temperature was
determined, with the error using the 450-Hz filter taken to be zero. The
results are shown in Table 6.1. Note that the error attributed to using
a 59-Hz filter is 8.6 percent and that due to a 35-Hz filter is 11.5 percent,
for this temperature (500 K).

Figure 6.12 is a plot of $\dot{Y}$ as a function of ωt, as well as $[(\alpha/\dot{Y}) - 1]100$
as a function of ωt. The latter quantity is the percentage error in
temperature measurement due to low-pass filtering.

This concludes the examination of experimental error incurred by
low-pass filtering in the hardware, both in the payload and at the telemetry
station. Errors due to low-pass filtering in the rocket payload appear to
be neglibible under all circumstances. It seems that the telemetry low-pass
filter might contribute an error of 10 percent under what may be considered
a 'worst case' condition (T = 400 K, ω = 50 Hz). The lowest frequency filter
used on data in this report is 81 Hz; taking Table 6.1 as a guide, it is
conservative to assume the temperature error in this case is always less
than 8.6 percent.

There remain two additional stages of low-pass filtering, these occur
in computer processing of the data in program ELTEMP. Within subroutine

TO PROBE

100kΩ

IN483B   10MΩ
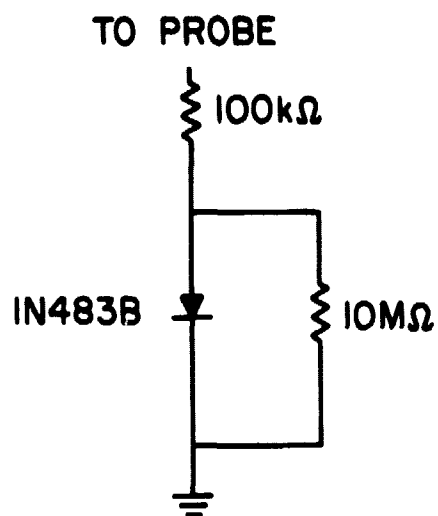
Figure 6.11   Diode and resistor combination used to
experimentally model 500 K space plasma.

Table 6.1 Experimentally measured error
due to low-pass filtering.

Frequency (Hz)	θ	tan θ	Relative tan θ	Percentage error
450	1b.5	0.335	1.000	0
220	19.0	0.344	1.027	2.7
110	19.5	0.354	1.056	5.6
59	20.0	0.364	1.086	8.6
35	20.5	0.374	1.115	11.5
20	24	0.445	1.328	32.8
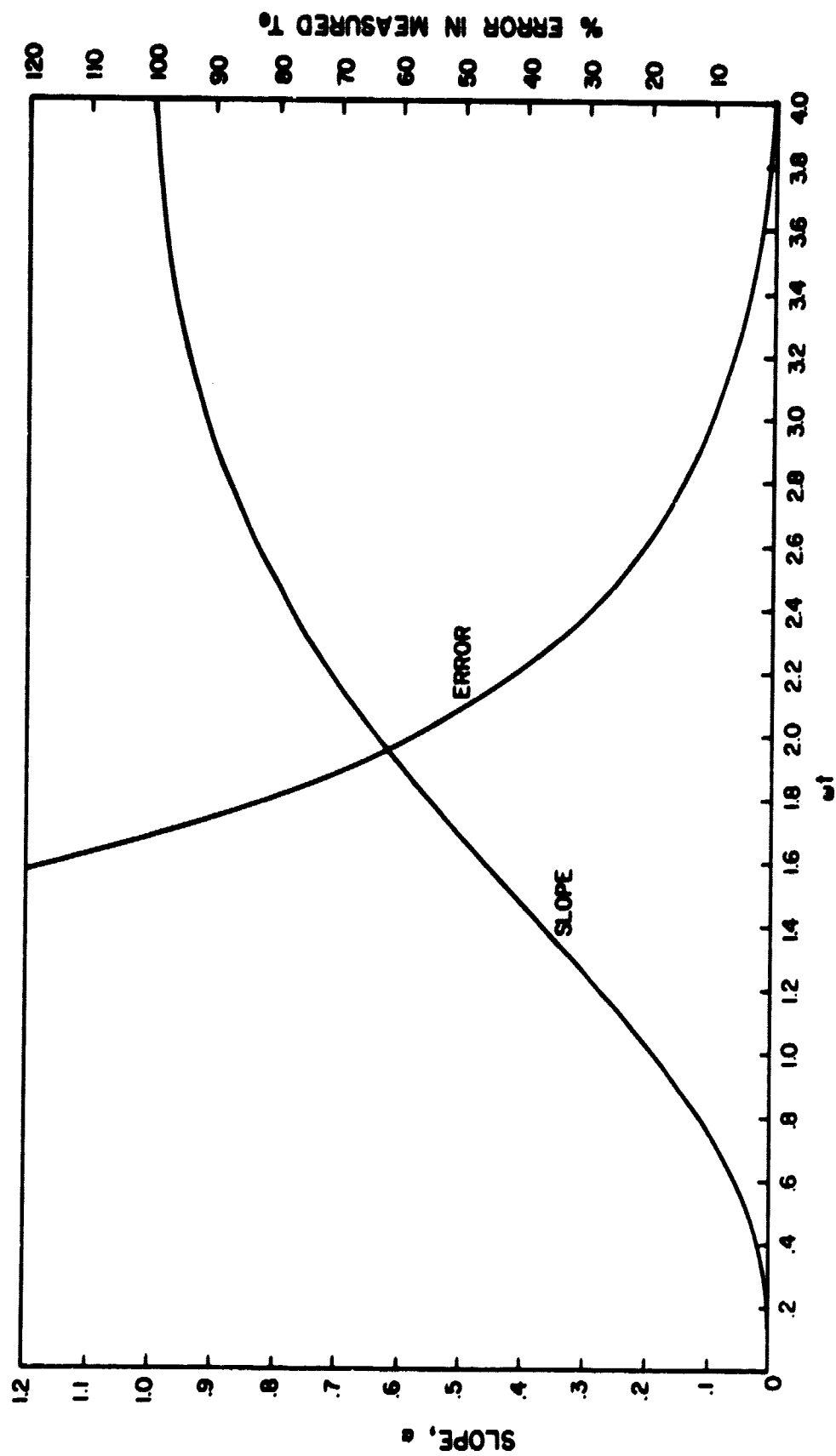
Figure 6.12 Apparent slope and measurement error as a function of ωt due to low-pass filtering.

CRUNCH the signal slope is determined by a five-point least-squares line fit. This technique was implemented because of scatter on the data points. The resultant slopes still showed significant amounts of variation; to reduce the scatter even further the present program averages five consecutive slopes to produce a smoothed slope. Both of these operations are low-pass filtering operations. However, no error should occur due to this technique because even at 400 K the ramp output from the telemetry filter lasts for 20 ms (i.e., 20 points) before saturation occurs, whereas only nine points are needed to determine the slope.

Clearly, if too long a period is used to determine the slope (namely, a period longer than the duration of the ramp), the effect will be to artifically decrease the slope and elevate the temperature. The nine-point slope determination period is short enough to avert any problem in this respect. Furthermore, the routine of taking five-point line fits and then averaging five slopes yields a smoothed slope equal to

$$
\text{slope}_1 = \frac{2a_9 + 3a_8 + 3a_7 + 2a_6 - 2a_4 - 3a_3 - 3a_2 - 2a_1}{50} \qquad (6.13)
$$

where a_1, a_2,..., a_9 are equally spaced data points. This weights the points near the center of the interval more than a regular nine-point least-squares fit would.

$$
\text{slope}_2 = \frac{4a_9 + 3a_8 + 2a_7 + 1a_6 - 1a_4 - 2a_3 - 3a_2 - 4a_1}{60} \qquad (6.14)
$$

This could be advantageous at temperatures below 400 K. Of course, if a ramp continues for 9 ms or longer, slope_1 is equal to slope_2.

6.4 *Probe Surface Contamination*

Rocket and laboratory experiments have shown that Langmuir probes may indicate electron energies much higher than present in the ambient plasma if the probe has a contaminated surface [*Wehner and Medicus*, 1952; *Hirao and Oyama*, 1972]. In laboratory studies carried out by *Szuszczewicz and Holmes* [1975] they found the electron temperature may be overestimated by as much as 100 percent.

A phenomenological model for the error due to surface contamination has been proposed by *Hirao and Oyama* [1972] and critically tested by Hirao and Oyama in Japan and Szuszczewicz and Holmes in the United States. The contamination layer is modeled as a 'leaky' capacitor in series with the probe,

as in Figure 6.13. Hirao and Oyama estimate the effective values of the contamination capacitance C_c and resistance R_c (for small probes in the E region) to be on the order of 1 µF and 400 KΩ. Current to the probe acts to charge the contamination layer, so that the potential applied to the probe is not the potential seen by the plasma. The first effect of this contact potential difference (c.p.d.) is to displace the probe I-V characteristic by an offset voltage. A secondary effect is present for Langmuir probes of the type used here. Namely, since the probe draws positive-ion current early in the sweep and later draws considerable electron current, the voltage to which the contamination layer is charged (c.p.d.) will vary during the period of a single sweep and distort the I-V characteristic. Evidently it is this temporal variation that causes error in electron temperature measurement. The polarity of the c.p.d. is always such as to effectively reduce the probe sweep rate. The resultant I-V characteristic is that for a sweep rate less than that actually applied to the probe. The calibration constant is calculated with the actual sweep rate (either 13.5 or 10.8 V s^{-1}) which results in an overestimation of the electron temperature.

The contamination layer suggested by Szuszczewicz and Holmes is nothing more than adsorption of neutral atmospheric gas by the probe surface. They provide the following illustration: consider an initially clean probe immersed in a neutral gas with a mean molecular weight of 28 amu at 10^{-4} mm Hg pressure and a temperature of 300 K. These are values typical of the E region at an altitude of 120 km. With unity sticking probability and a monolayer defined by approximately 5×10^{14} molecules per square cm, the first monolayer of contamination develops in approximately 0.13 ms. The next monolayer forms in some tens of seconds (due to the decreased probability of sticking) with an equilibrium surface condition resulting in several minutes. This contamination is in addition to any terrestrial contamination, such as water vapor or finger prints. It is obvious that an atomically clean probe is a short-lived phenomena, and that attention must be paid to the surface physics of the probe.

A convenient method of determining when the probe characteristic is being adversely affected by surface contamination is to sweep the probe using both positive and negative gradients, i.e., $+dV/dt$ and $-dV/dt$. If the characteristic is duplicated, then the effect of contamination is small and the electron
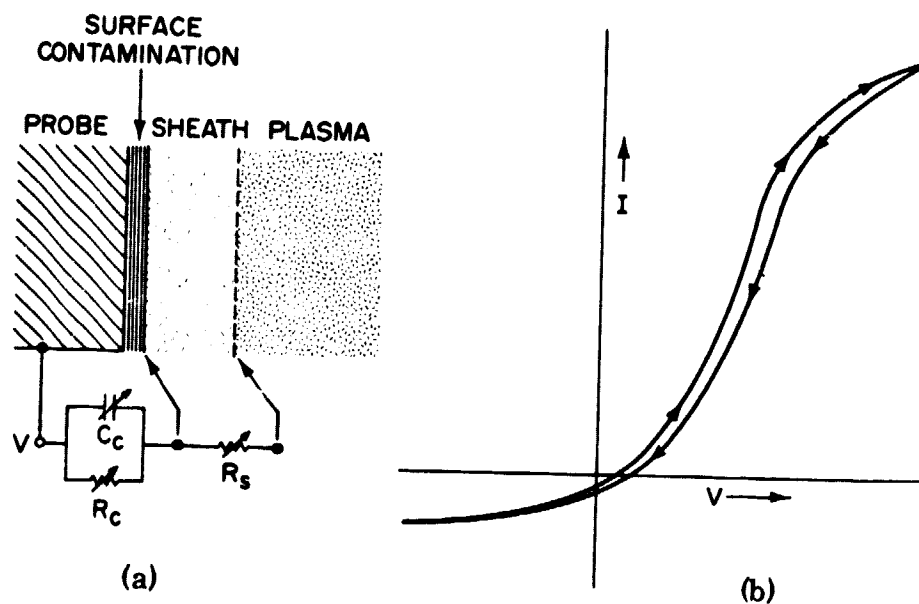
Figure 6.13 (a) Effective circuit model for contamination layer as proposed by Hirao and Oyama. (b) Hysteresis in conventional Langmuir probe I-V characteristic resulting from probe surface contamination [*Szuszczewicz and Holmes*, 1975].

temperature is correct. If hysteresis is present as in Figure 6.13b the characteristic is not usable for temperature determination.

Hirao and Oyama have suggested a technique for avoiding error due to varying c.p.d. They sweep the probe at a rate fast enough that the sweep period is considerably less than the time constant of the contamination layer, $R_c C_c$ =0.4 s. Physically, the sweep occurs so quickly that the contamination layer does not have time for its voltage to change significantly. In this sweeping mode the effective impedance of the contamination capacitance is much smaller than the plasma sheath impedance and can be overlooked. Experimentally, a sweep repetition rate of 10 Hz was found to do away with surface contamination error. Properly, the sweep rate should be given in $V\ s^{-1}$, this being the important factor.

Szuszczewicz and Holmes have adopted a variation of the above technique in their development of the pulsed plasma probe. They keep the probe at a constant voltage in order to maintain the c.p.d. at a constant value. The Langmuir probe characteristic is generated in a point-by-point fashion by applying digital voltage pulses to the probe, as shown in Figure 6.14. While the voltage pulse is applied to the probe the resultant current is sampled. Two conditions must be met for this technique to be effective: the pulse period must be much shorter than the layer time constant, and much shorter than the interpulse period. A variation of this technique would allow the probe to float (drawing no net current) between voltage pulses.

The instrumentation described in this report uses an analog positive-going ramp to voltage sweep the probe. Accordingly, there is no hysteresis or other effects to indicate if surface contamination is a significant error source. With effective repetition rates of only 2 Hz (for the boom probe) and 3.3 Hz (for the nose-tip probe), it seems likely that surface contamination and the resultant varying contact potential difference could be important. In future instrumentation the probe should be alternately swept with positive- and negative-going ramps.
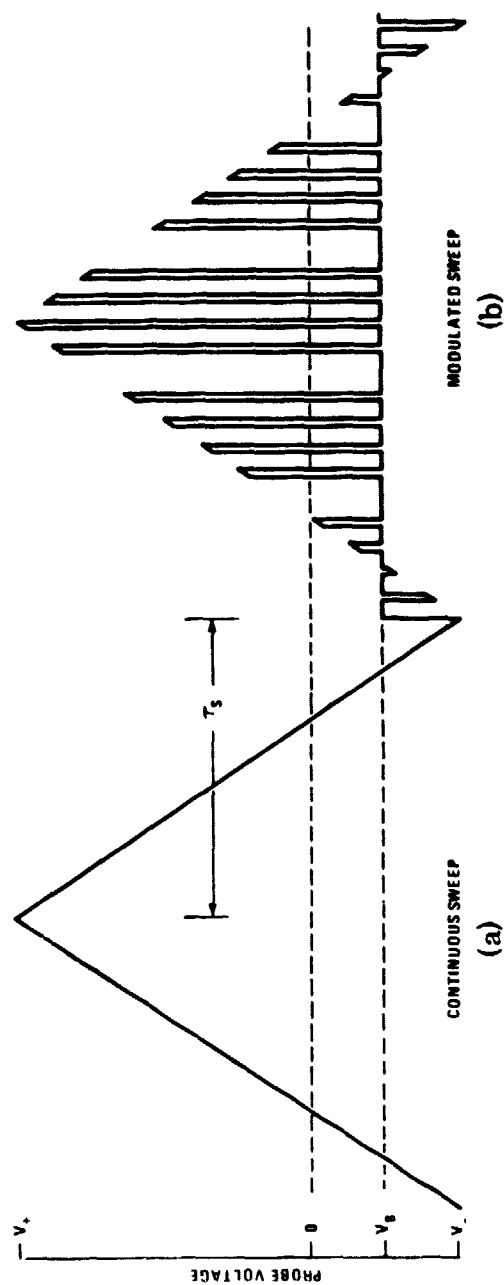
Figure 6.14 Continuous and pulsed modes of Langmuir probe operation.
(a) Conventional sweep using positive- and negative-going
ramp signals. (b) Schematic representation of the sweeping
technique used in the pulsed plasma probe of *Szuszczewicz
and Holmes* [1975].

7. ELECTRON TEMPERATURE IN THE EQUATORIAL E REGION MEASURED BY TWO ROCKET EXPERIMENTS AND BY INCOHERENT SCATTER*

A Nike Apache rocket, 14.532, instrumented with two independent electron-temperature probes was launched at 1526 LST into the daytime equatorial ionosphere on 28 May 1975 from the Chilca rocket range (12° 30.3' S, 76° 47.4' W), Peru, as part of the NASA operation Project Antarqui. These probes were a differential Langmuir probe described by *Smith et al.* [1968], and an ac rectification probe described by *Hirao and Oyama* [1970]. Personnel at Jicamarca Observatory (11° 57' S, 76° 52' W), as co-participants in Project Antarqui, simultaneously measured the electron temperatures above 150 km by incoherent-scatter radar. The ionosphere was quite, with the three-hour geomagnetic planetary index (Kp) being equal to 2-. Figure 7.1 shows the location of the launch site relative to the city of Lima; Jicamarca Observatory is northeast from the Lima metropolitan area.

The operation of the differential Langmuir probe is presented in Figure 7.2. The upper curve is the typical I-V characteristic for a voltage-swept Langmuir probe in the ionosphere. On board differentiation of the I-V curve results in the lower curve which is telemetered to ground by standard FM/FM telemetry. The electron temperature is recovered by digitally measuring the slope of the lower curve between the floating potential and the plasma (space) potential. The reciprocal slope in this interval is proportional to the electron temperature.

The operation of the rectification probe is indicated in Figure 7.3. The floating potential is a nonlinear function of the amplitude of a superposed ac signal and the electron temperature of the ambient plasma. The depression of the floating potential is measured for two levels of ac voltage which are successively applied to the probe. It is usual to apply an ac voltage of a and $2a$, the ratio of the floating potential depressions being,

$$\gamma = \frac{\Delta V_{fl}(2a)}{\Delta V_{fl}(a)} = \frac{\ln\left[I_o \frac{2ae}{kT_e}\right]}{\ln\left[I_o \frac{ae}{kT_e}\right]} \tag{7.1}$$
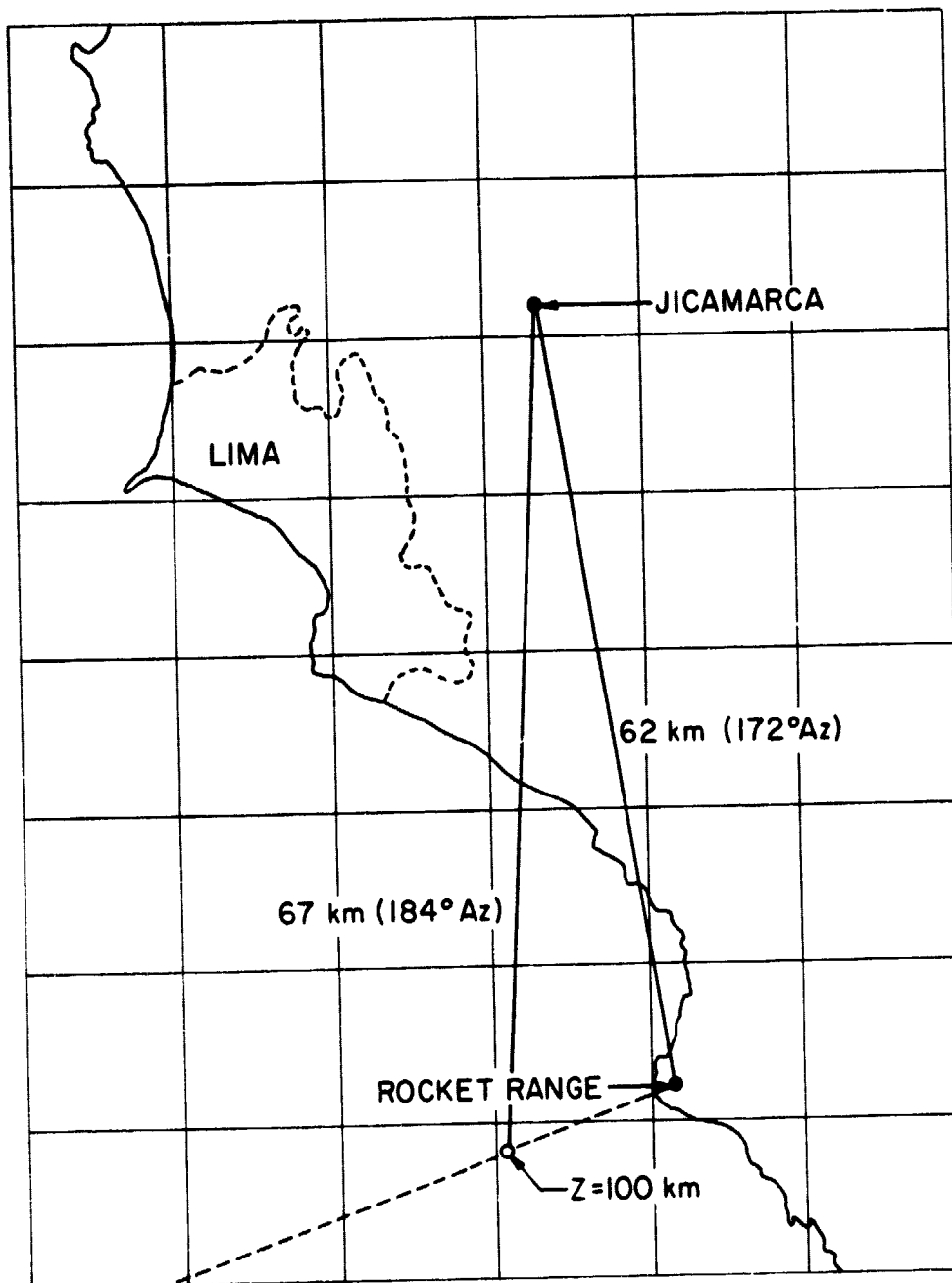
Figure 7.1   The location of the rocket range at Chilca and the
Jicamarca Observatory are shown relative to Lima,
Peru.   The initial trajectory of Nike Apache 14.532
is indicated by the dashed line.
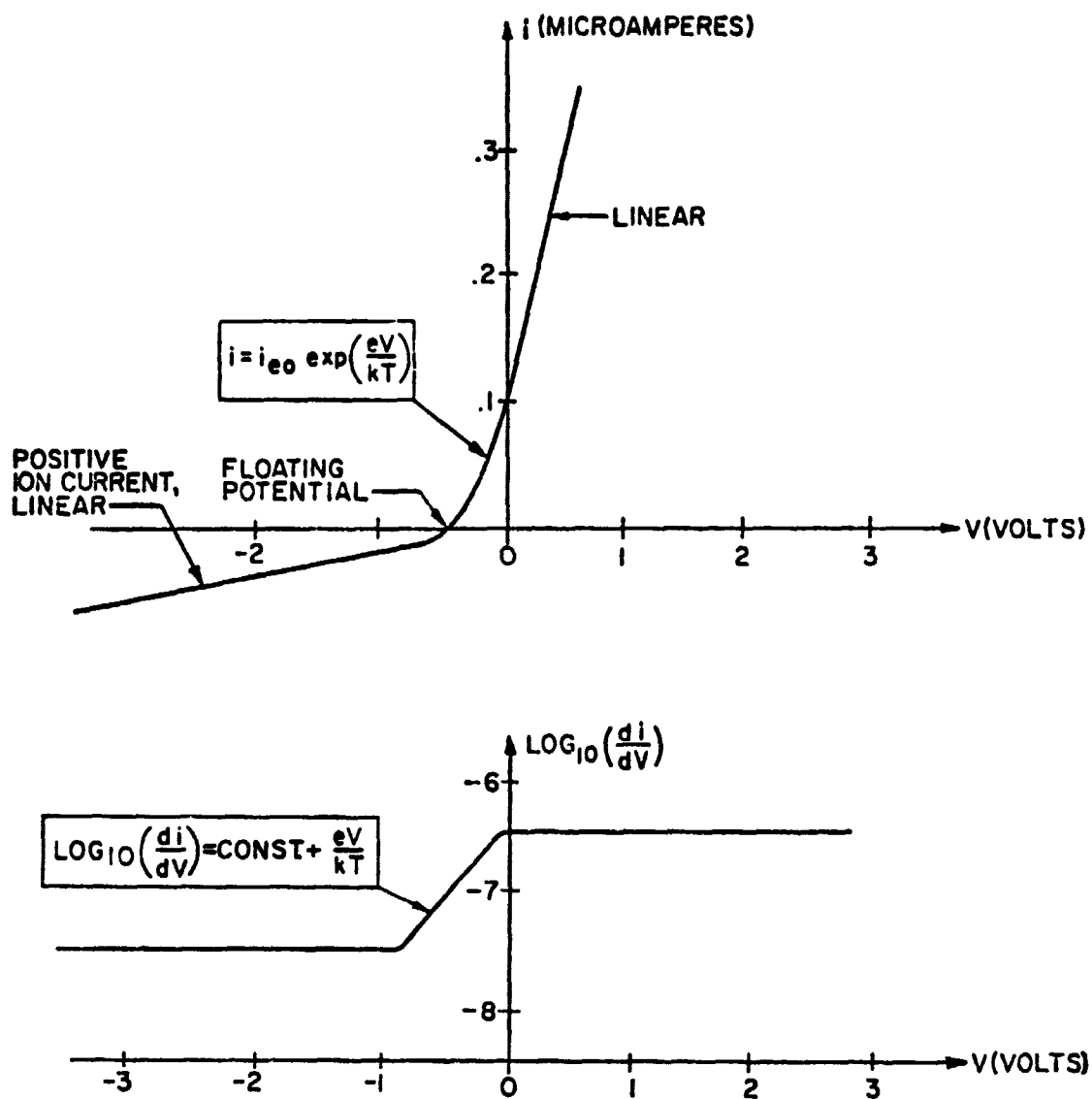
Figure 7.2 The upper curve is the I-V characteristic for a Langmuir
probe in the ionosphere. The lower curve, derived from
the first by on-board differentiation, is used to cal-
culate T_e.
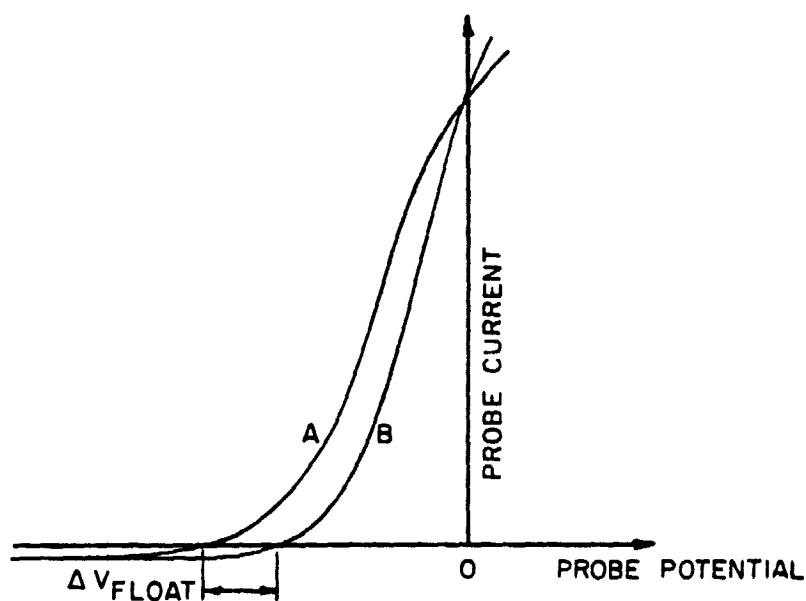
Figure 7.3   Curve B is the I-V characteristic of the
rectification probe with no ac voltage
applied.   Curve A is the displaced curve
due to partial rectification of an applied
ac voltage; the effect is to depress the
floating potential.   The temperature may
be determined by measuring the ratio of
floating potential depressions for two
levels of applied ac voltage.

which may be solved for T_e. The frequency (20 kHz) of the superposed signal is chosen to be lower than the electron-plasma frequency and higher than the ion plasma frequency of the ambient plasma.

The ascending electron-temperature data from both probes are displayed in Figure 7.4. The difference, generally being less than 100 K, is attributed to experimental error. There is a generally linear increase of electron temperature from 300 K at 110 km to 1200°K at 180 km.

Using these data and the experimentally measured electron concentration, Figure 7.5, we have made a study of electron heating and cooling in the equatorial ionosphere. We used the 1972 COSPAR International Reference Atmosphere, with T_∞ = 800 K corresponding to $S_{10.7}$ = 70.6 × 10^{-22} W m^{-2} Hz^{-1} for neutral temperature (also shown in Figure 7.4) and composition, and the discrete cooling formulas given by *Dalgarno* [1969] and *Lane and Dalgarno* [1969]. These formulae account for electron cooling due to excitation of the atomic oxygen fine structure states, and vibrational and rotational states of N_2 and O_2. We used an oxygen fine structure cooling rate coefficient equal to 60% of that suggested by Dalgarno; this is in better agreement with a recent cross section calculation by *Hoegy* [1976].

Curves 1 and 2 in Figure 7.6 are the derived cooling rates using T_e data from the rectification probe and the differential Langmuir probe, respectively. Curves 3 and 4 are heating rate curves from a numerical model by *Dalgarno et al.* [1968] for solar zenith angles χ = 72.1° and 50.2°, respectively. The solar zenith angle was 60° at the launch time of Nike Apache 14.532. Above 140 km the electron heating and cooling rates are in agreement considering the uncertainties in the model. Below 130 km the rocket data show cooling rates considerably greater than expected on the basis of solar heating, suggesting another source of heating.

As an estimate of the Joule heating at 110 km that might result from equatorial electrojet, let us take the current density in the east-west direction to be 10 A km^{-2} as suggested by *Davis et al.* [1967] and the conductivity in the east-west direction to be σ_{yy} = 6 × 10^{-3} ms m^{-1} from the model by *Sugiura and Cain* [1966]. The Joule heating by the electrojet at 110 km is thus of the order of 1 × 10^5 eV cm^{-3} s^{-1}, in agreement with the values shown in Figure 7.6. Heating of this magnitude may account for the additional source of heating at low altitudes. However, *Schutz et al.* [1975] using identical instrumentation have observed a similar effect at Wallops
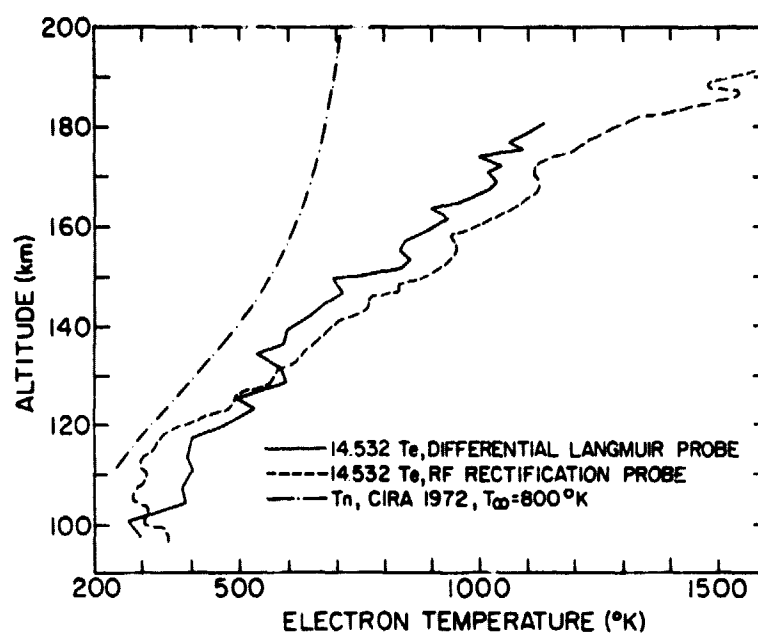
Figure 7.4 Electron temperature measured by two rocket-borne probes on Nike Apache 14.532. Also shown is the neutral temperature model appropriate to the 2800 MHz solar flux and time of day.
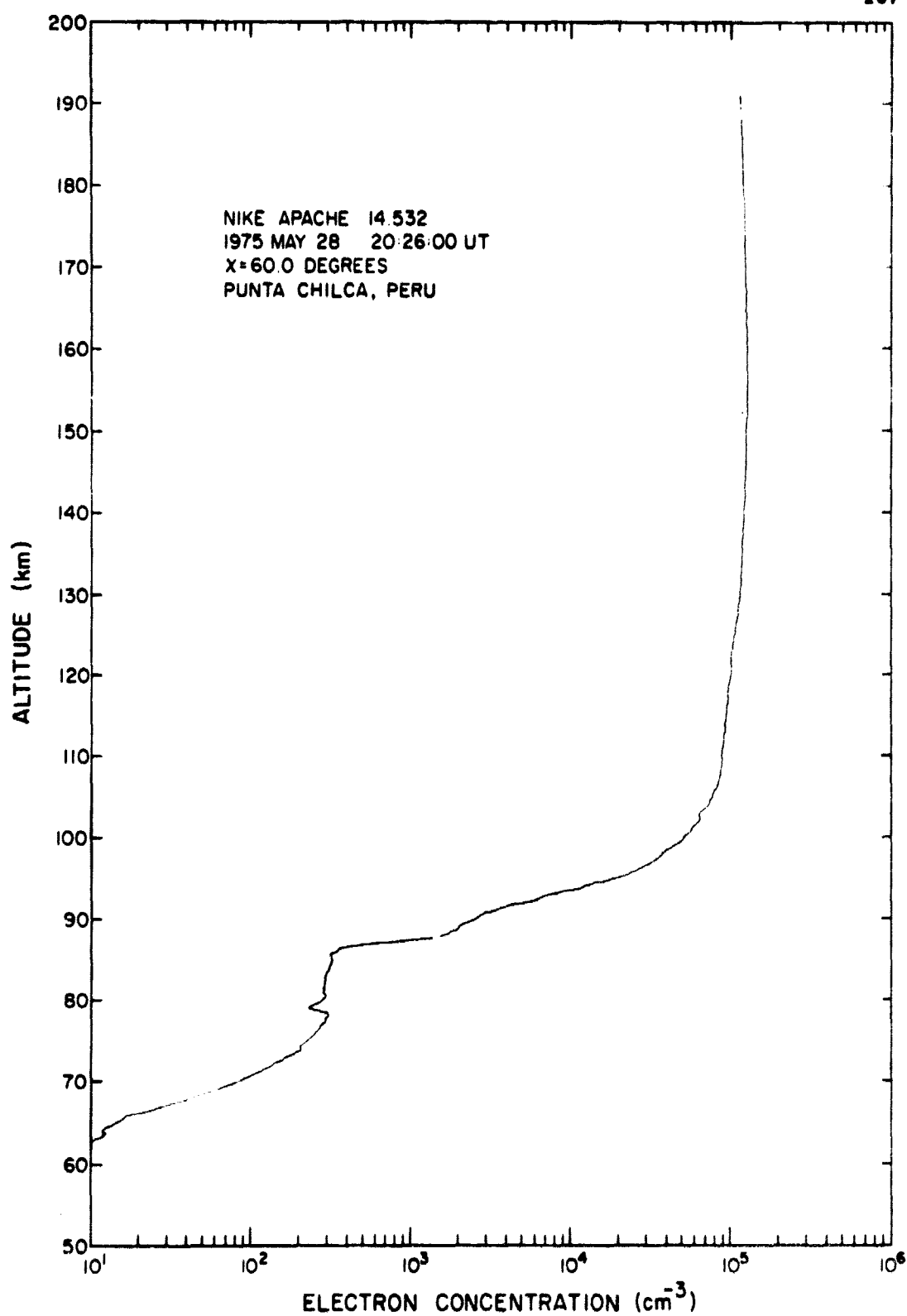
Figure 7.5   Electron-concentration profile in the daytime
             equatorial ionosphere.
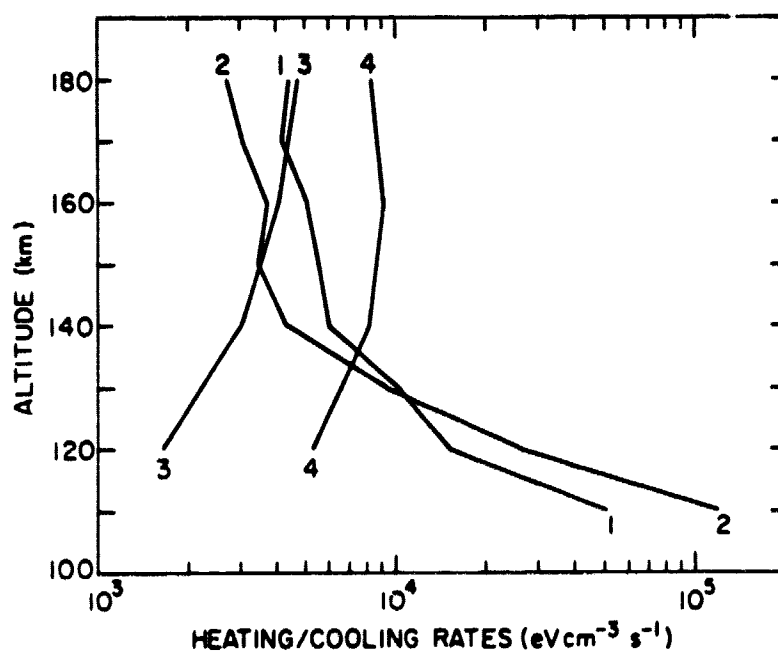
Figure 7.6 A comparison of the calculated electron heating and
cooling rates. Curve 1 is the cooling rate calculated
from electron temperature data measured with a recti-
fication probe. Curve 2 is the cooling rate from
data taken with a differential Langmuir probe. Curve
3 is the heating rate from a numerical model by Dalgarno
for $\chi = 72.1°$ and $T_\infty = 734$ K. Curve 4 is the same
heating model with $\chi = 50.2°$ and $T_\infty = 766$ K.

Island. They suggest an additional source of heat below 150 km due to a local aerodynamic effect. It is clear that if the Joule heating by the equatorial electrojet is to be measured it is necessary to better understand the aerodynamic effects of a supersonic probe and to have a simultaneous measurement of the neutral temperature.

During the flight of Nike Apache 14.532, Jicamarca Observatory obtained electron temperature data down to 150 km. These data are displayed in Figure 7.7 together with the electron temperature measured by the two rocket-borne probes. In the region of overlap (150 to 180 km) the data are in good agreement.
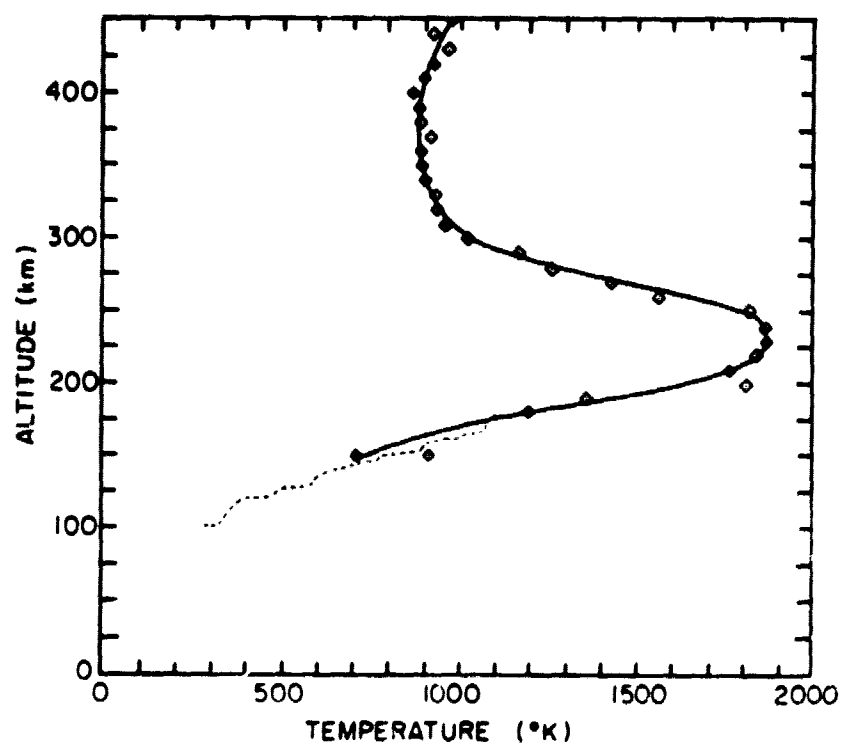
Figure 7.7   The average of the electron temperatures from
the two rocket-borne probes is shown here
with electron temperature data obtained
simultaneously by incoherent scatter at
Jicamarca Observatory.

8. OBSERVATIONS AND DISCUSSIONS

Electron-temperature profiles for Nike Apache 14.532, 14.534, and 14.533 are presented in Figures 8.1 through 8.4. There are two profiles for 14.534, Figures 8.2 and 8.3, since data were available using two low-pass filters, 81 Hz and 450 Hz, respectively. These profiles are plotted on the same axes in Figure 8.5 for comparison.

On the afternoon of 14.532 there was a constant temperature gradient of $11°K\ km^{-1}$ between 100 and 183 km. These data have been used as the basis for a heating/cooling study of the equatorial E region as explained in chapter 7.

On the night of 14.534 the temperature was nearly constant during the ascent at about 1350 K or 1300 K, depending on whether Figure 8.2 or 8.3 is taken as correct. This temperature difference is due strictly to the use of different low-pass filters in the telemetry station. The 81-Hz filter causes the recovered temperature to be elevated by 50 to 100 degrees over the 450-Hz data.

The descent data are between 200 and 300 degrees cooler in both cases. This is due to a combination of rocket wake effects and, to a lesser degree, probe surface contaminants (probe aging). That the wake effect is the major error contribution is verified by the temperature drop occurring rather abruptly at apogee and early in the descent leg. A more complete verification of this would be to fly a probe which is not sensitive to probe surface effects, such as that described by *Holmes and Szuszozewicz* [1975].

The ascent data are considered valid and representative of conditions during a moderately disturbed night. *Smith et al.* [1974] have considered incoherent-scatter data from *Evans* [1973] and developed the following relation for the electron temperature as a function of altitude and Kp.

$$T_e(z) = (z - 120) \times (1.40\ Kp + 2.91) + 335°K \qquad (8.1)$$

This would yield a temperature of 1035 K for an altitude of 200 km and Kp = 4. A value of Kp of 6.5 is required in this formula to cause temperatures close to 1300 K as observed. It is roughly 300° warmer than would be anticipated due to energetic-particle precipitation associated with the magnetic disturbance. This is probably due to lessened efficiency in one of the electron cooling processes, which would allow a higher final temperature to be attained for a given energy flux to the upper atmosphere.
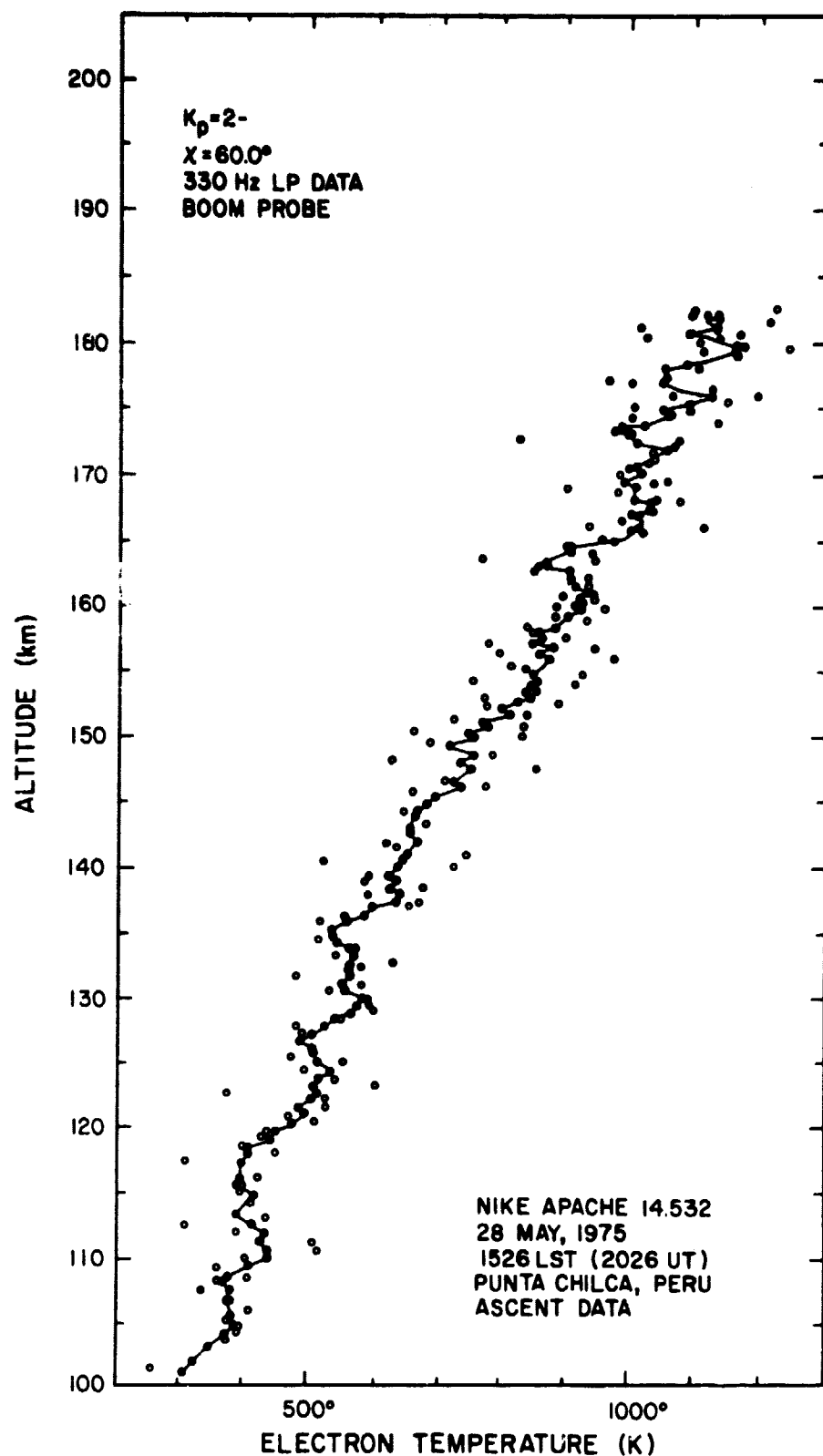
Figure 8.1 Recovered electron-temperature profile for Nike Apache 14.532. Points connected by the broken line are five-point average values. Generally, there is a linear temperature gradient with height of about 11 K/km.
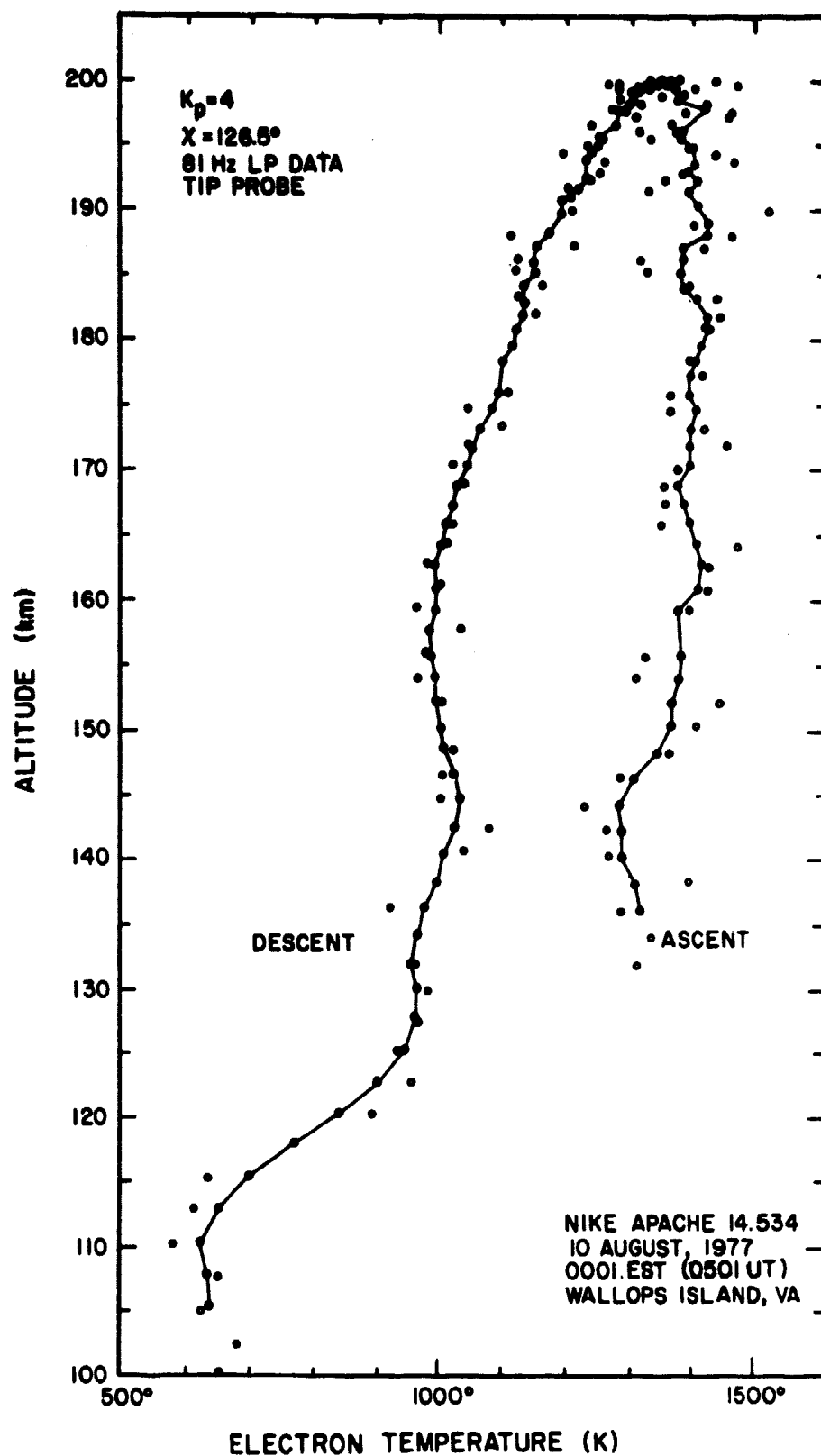
Figure 8.2 Recovered electron-temperature profile for Nike Apache
14.534 using an 81-Hz low-pass filter at the telemetry
station. The points connected by the broken line are
five-point average values.
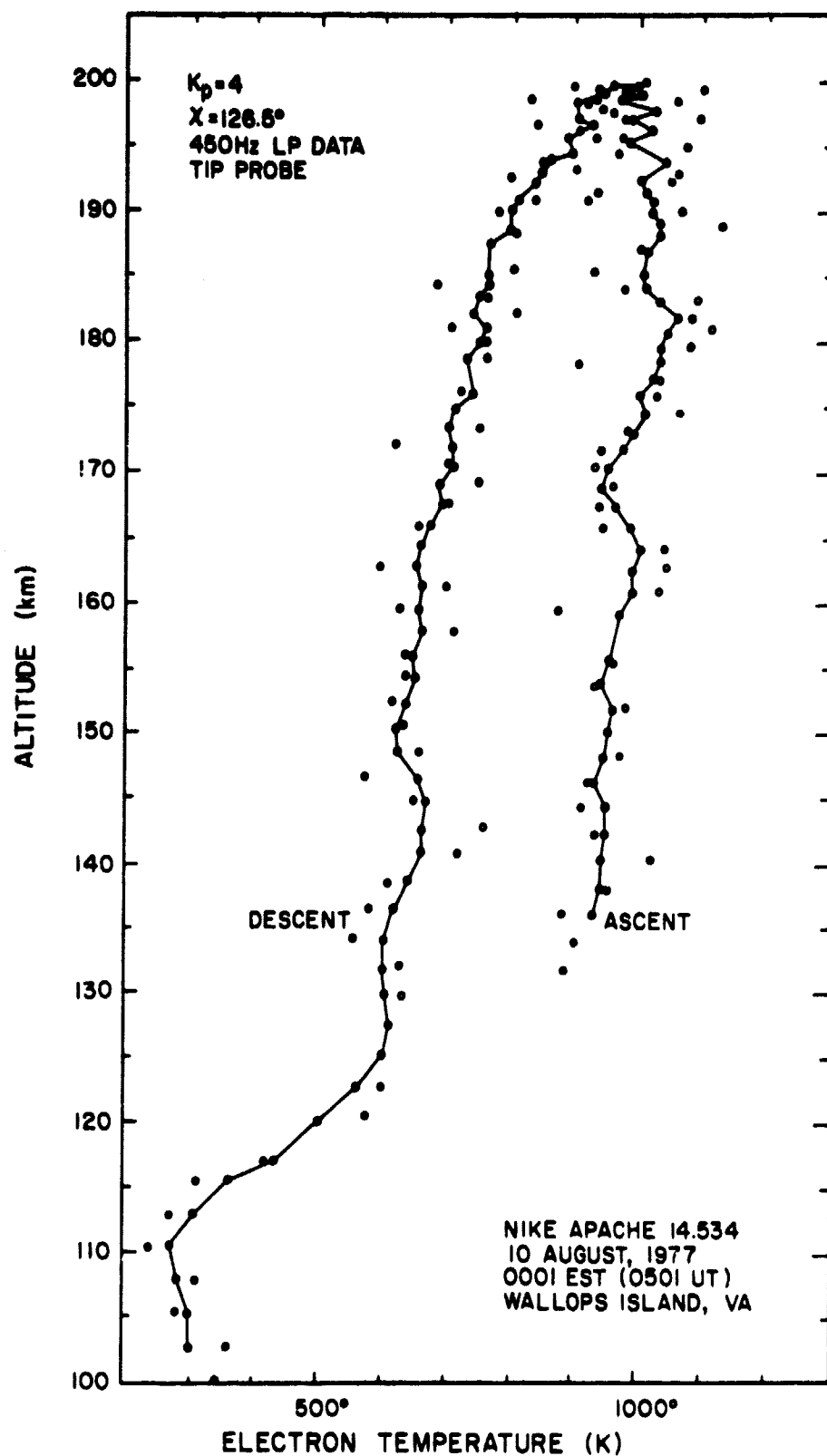
Figure 8.3 Recovered electron-temperature profile for Nike Apache
14.534 using a 450-Hz low-pass filter at the telemetry
station. Points connected by the broken line are five-
point average values.

ELECTRON TEMPERATURE (K)

ALTITUDE (km)

$K_p=5$
$X=164.8°$
450Hz LP DATA
TIP PROBE

NIKE APACHE 14.533
5 JANUARY, 1978
0001 EST (0501 UT)
WALLOPS ISLAND, VA
ASCENT DATA
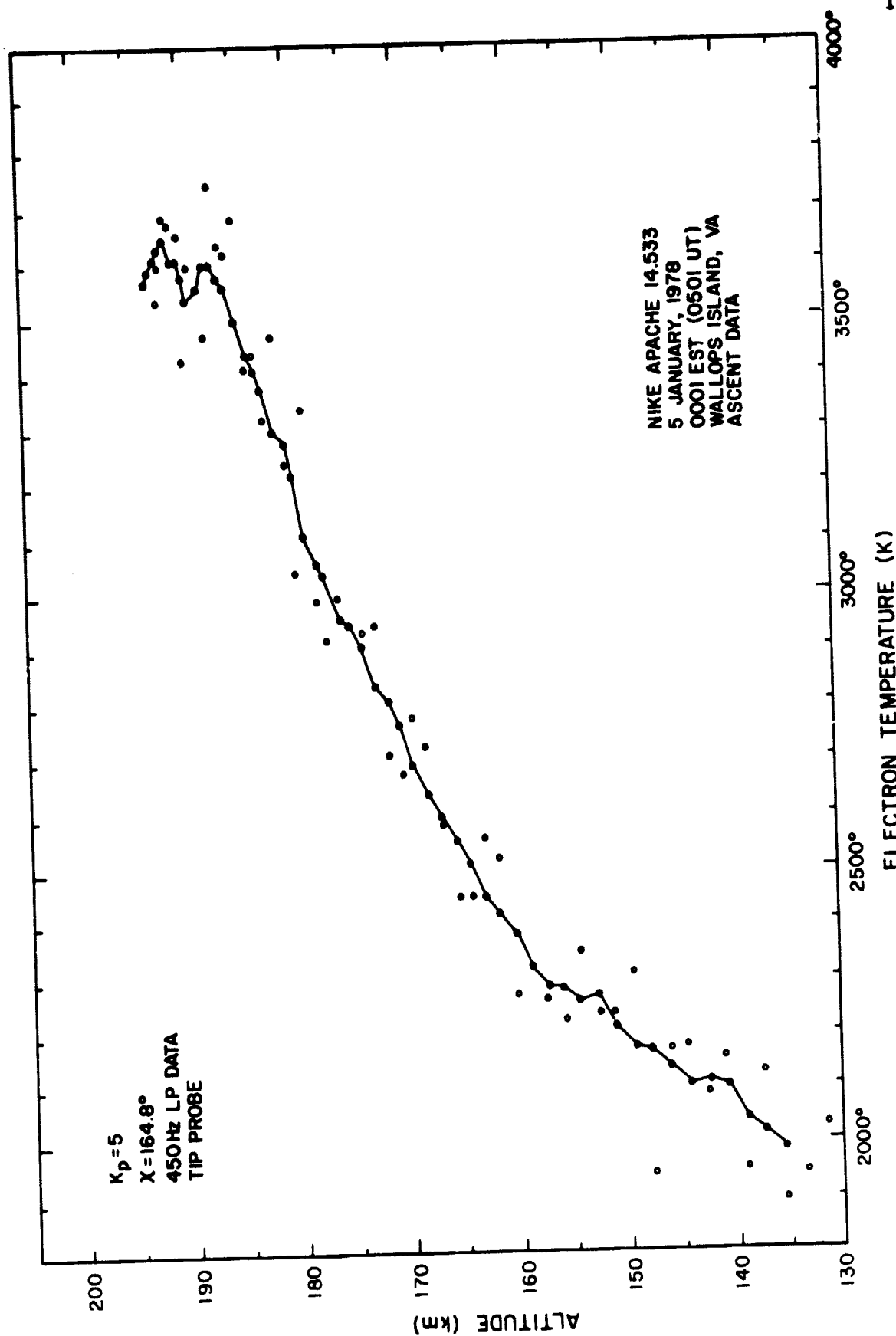
Figure 8.4   Recovered electron-temperature profile for Nike Apache 14.533.   Points connected by the broken
line are five-point average values.   The extremely high temperature encountered during this
flight cannot be accounted for in terms of normal nighttime heating processes.
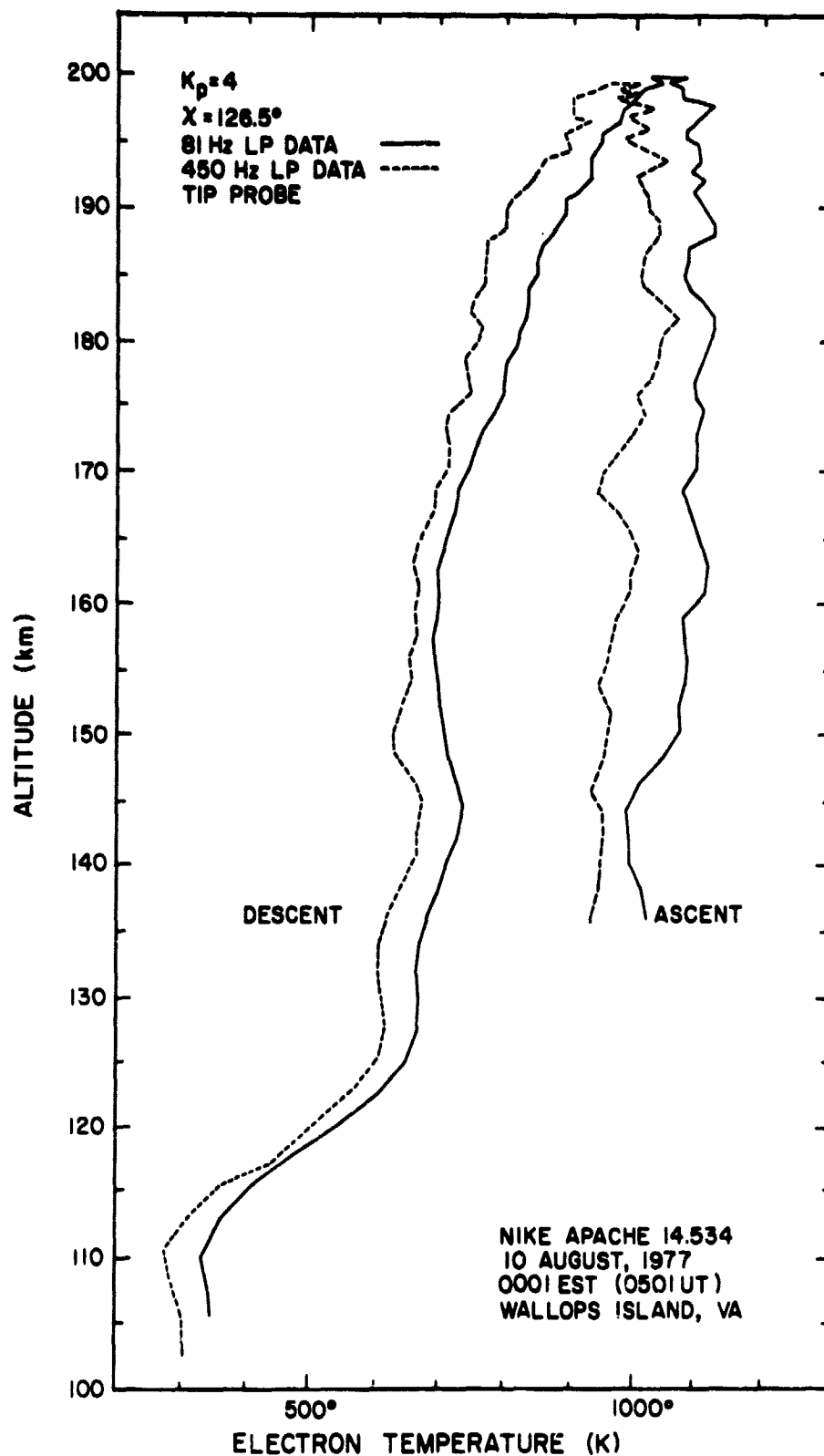
Figure 8.5   Comparison of temperature profiles obtained from Nike Apache
14.534 using different low-pass filters at the telemetry
station.   Heavy low-pass filtering elevates the recovered
electron temperatures as examined in section 6.3.

The temperature profile from Nike Apache 14.533 is much higher than can be explained by normal nighttime particle precipitation. Using equation (8.1) again, a temperature of 1150 K would be expected for Kp = 5 at an altitude of 200 km. Although temperature data are not available for altitudes above 193 km (or on descent) due to an instrumentation failure, it seems reasonable to assume the temperature at 200 km was in excess of 3500 K. The only explanation presently able to account for the observed high temperatures is that Nike Apache 14.533 passed beneath an SAR arc.

Battelle-Northwest Laboratory operates a network of computer-controlled spectrophotometers which moniter the 6300 Å radiation characteristic of SAR arcs. On the night of the launch of Nike Apache 14.533 their Michigan observatory was inoperative due to hardware problems, and both the Washington and Montana observatories were obscured by cloud cover.* Their observatory in New York was not yet in operation. There remains some possibility that independent verification will come from another ground-based observatory or from satellite photographs (although satellite confirmation would be questionable unless a 6300 Å filter were used, such as on the read line photometer aboard the ISIS 2 spacecraft). Presently, the strongest evidence for the existence of an arc that night are the extremely high temperatures recorded by Nike Apache 14.533 and the simultaneous observation of a broad depression in the F-region electron concentration (density) by the Wallops Island ionospheric sounding station. This was noted as characteristic of SAR arcs by *King and Roach* [1961] using bottomside ionograms and later using the topside sounder aboard the Alouette II satellite [*Clark et al.*, 1969; *Norton and Marovich*, 1969; *Norton and Findlay*, 1969].

Wallops Island has a magnetic L-shell value (at 100 km) of 2.6. SAR arcs are generally observed between L = 2 and 4 [*Roach and Roach*, 1963]. The mean L-shell value for arcs during the last solar cycle maximum period was L = 2.98 [*Marovich and Roach*, 1963].

The thermal gradient between 158 and 187 km is nearly constant at 41 K km^{-1}. If this is due to downward heat conduction from the base of an SAR arc it cannot continue far above 200 km. For example, from visual sightings of Sar arcs it has been determined SAR arcs have a well-defined base between 300 and 400 km. [*Tohmatsu and Roach*, 1962; *Clark et al.*, 1969;

---

*Personal communication with D. Slatter, Rattlesnake Mountain Observatory, Battelle-Northwest Laboratory.

Roble et al., 1971]. If the gradient continued to a height of 300 km the temperature within the arc would be about 8200 K, whereas temperatures measured above arcs by satellites at approximately 1000 km usually peak between 4000 and 5000 K [*Norton and Findlay*, 1969; *Chandra et al.*, 1971; *Roble et al.*, 1971; *Nagy et al.*, 1972]. If we take the electron temperature in the arc to be 4000 K, the observed gradient could continue for only 10 km above 187 km. The gradient would then be constrained to remain close to zero by the markedly higher thermal conductivity above 200 km. Some evidence to this effect might be seen at the top of the profile in Figure 8.4 although not enough to substantiate this point.

9. RECOMMENDATIONS FOR FUTURE WORK

The Langmuir probe as used here has an absolute accuracy of ±50 K under optimal experimental conditions. There are many sources of error and from internal evidence, such as the difference between data obtained on ascent and descent of a particular rocket, the error may be ±100 K or more. Some improvements seem desirable.

One possibility is to change the probe sweep to a sawtooth waveform. This may allow error due to probe surface contamination to be detected and quantified by observing hysteresis effects.

If surface effects are found to be compromising experimental accuracy two routes may be taken: substitution of a faster sweeping rate as suggested by *Hirao and Oyama* [1972], or use of the pulsed-plasma-probe technique developed by *Holmes and Szuszczewicz* [1975]. The latter method appears to have three advantages. First, the pulse period can always be made shorter than the analog sweep period, making the system immune to surface effects over a wider range of ionospheric conditions. Secondly, data are generated at a more reasonable rate than with fast sweeping, so that data buffering is not necessary prior to transmission. And third, the pulsed-plasma probe readily interfaces with digital-data transmission.

Digital-data transmission should be substituted for the analog FM/FM telemetry system presently used. This would eliminate telemetry channel noise, power line noise, and filtering error. Digital data should be directly recorded at the telemetry station with no conversion of any type. For a given data rate digital FM transmission will result in a broader channel spectrum than analog FM transmission. It will be advantageous and reasonable to change the telemetry transmitter modulation index from 5 to 1 when digital data are being transmitted.

We suspect the statistical nature of the present electron-temperature data (for the nose-tip probe data, anyway) is due to probe surface contamination rather than to actual plasma oscillations or plasma instabilities due to the vehicle. This was true in *Hirao and Oyama's* study [1972]. This should be remedied by a faster sweeping rate of the pulsed-probe technique. If the data are still statistical after implementation of either of these techniques it would be desirable to generate more data to give a higher level of confidence to the data. Accordingly, it might be

desirable to separate the electron-concentration function of the probe from the electron-temperature function.

The importance of positive-ion current in electron-temperature determination has still not been determined, or proper corrections made. Implementation of techniques to do away with surface effects (as recommended above) should, at the same time, permit an assessment of the importance of positive-ion current.

APPENDIX I. Frequency response of a logarithmic electrometer

Consider the log electrometer circuit shown in Figure AI.1. A is an ideal operational amplifier characterized by infinite input impedance (between the + and - terminals), by zero output impedance and a voltage gain A such that

$$v = -Av_-\qquad\text{(I.1)}$$

The feedback network consists of a diode D, whose properties are represented, for forward bias, by

$$i_D = i_S \exp\{(v-v_-)/v_T\}\qquad\text{(I.2)}$$

where i_S is the leakage current (for reverse bias) and $v_T(=kT/e)$ is a constant with a value of about 25 mV. This formula is valid for $i_D < 10^{-5}$ A, by experiment.

The frequency response of the circuit is limited by capacitance C in parallel with the diode. This combines the capacitance of the diode itself with stray capacitance present in a practical circuit.

We assume that a current i is applied to the electrometer at $t = 0$, with $v = 0$. Then

$$i = i_D + i_C\qquad\text{(I.3)}$$

where i_C is the displacement current in the capacitor and is given by

$$i_C = C\frac{d}{dt}(v-v_-)\qquad\text{(I.4)}$$

Using equation (I.1) to eliminate v_- in equations (I.2) and (I 4), equation (I.3) becomes

$$i = i_S \exp\left[\frac{v}{v_T}\left(1 + \frac{1}{A}\right)\right] + C\frac{dv}{dt}\left(1 + \frac{1}{A}\right)\qquad\text{(I.5)}$$

The solution, for $v = 0$ at $t = 0$, is

$$-\frac{v}{v_T}\left(1 + \frac{1}{A}\right) = \ln\left[\frac{i_S}{i} + \left(1 - \frac{i_S}{i}\right)\exp\left(-\frac{it}{Cv_T}\right)\right]\qquad\text{(I.6)}$$
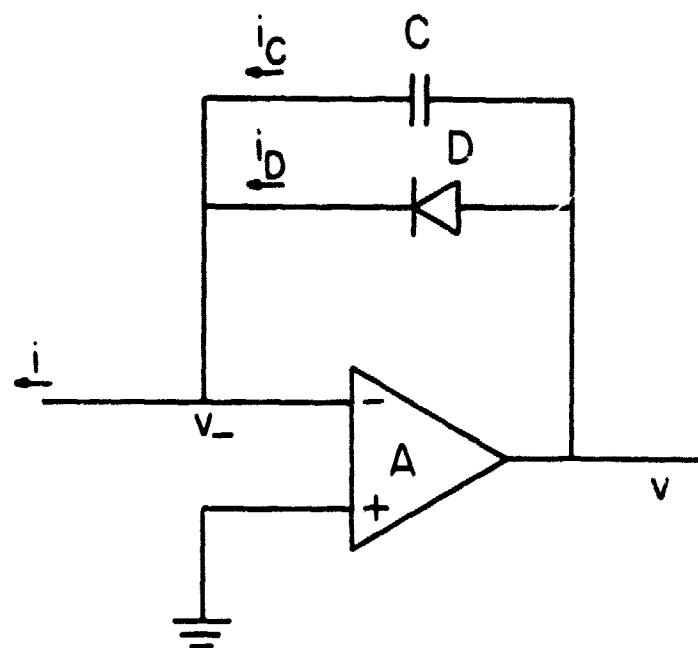
Figure AI.1 Circuit of a log electrometer.

Noting that $A \gg 1$ and that, as $t \to \infty$, $v \to v_T \ln(i/i_S) = v_o$, say, the equation becomes

$$v = -v_T \ln\left\{\exp(-v_o/v_T) + [1 - \exp(-v_c/v_T)] \exp\left(-\frac{it}{Cv_T}\right)\right\} \qquad (I.7)$$

This equation can be put in the parametric form

$$e^{-y} = e^{-y_O} + (1 - e^{-y_O}) e^{-x} \qquad (I.8)$$

where $y = v/v_T$ and $x = (i/Cv_T)t$. The equation is shown in Figure AI.2 for $y_o = 10$ and $y_o = 20$.

We note that, for $x = y_o$

$$e^{-y} = e^{-y_O}(2 - e^{-y_O}) \simeq 2e^{-y_O} \text{ or } y = y_o - \ln 2 \qquad (I.9)$$

It can be seen in the figure the curves are simply displaced along the line $y = x$, in agreement with equation (I.9).

Again, from Figure AI.2, the response time may conveniently be specified as the time τ at which $x = y_o$, that is

$$\tau = Cv_o/i \qquad (I.10)$$

From equation (I.1) $|v| \gg |v_-|$, since $A \gg 1$ and

$$v_o = v_T \ln(i/i_S) \qquad (I.11)$$

so that equation (I.10) can be written

$$\tau = Cv_T \frac{\ln(i/i_S)}{i} \qquad (I.12)$$

Thus the response time varies essentially inversely as i. Stated another way the frequency response is proportional to i.

The increase in frequency response as the input current increases is illustrated in Figure AI.3. Here the scaled output voltage $y = v/v_T$ is plotted as a function of scaled time $xi_S/i = (i_S/Cv_T)$ for eight values of the input current, expressed by $N = i/i_S$. Larger input currents cause a proportionally faster change in the output voltage, consistant with the conclusion that the frequency response is proportional to input current.
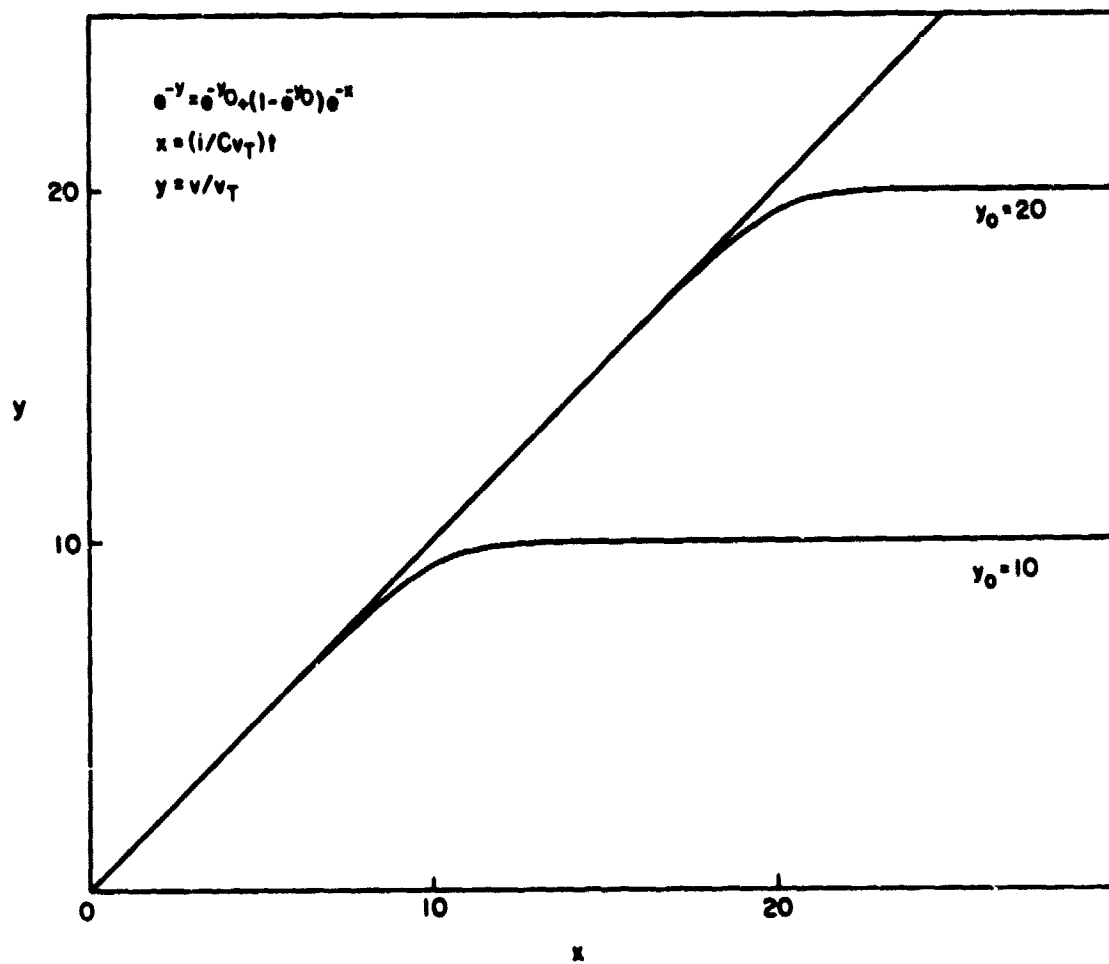
Figure AI.2 Parametric representation of the response of a logarithmic
electrometer to a current applied at $t = 0$.
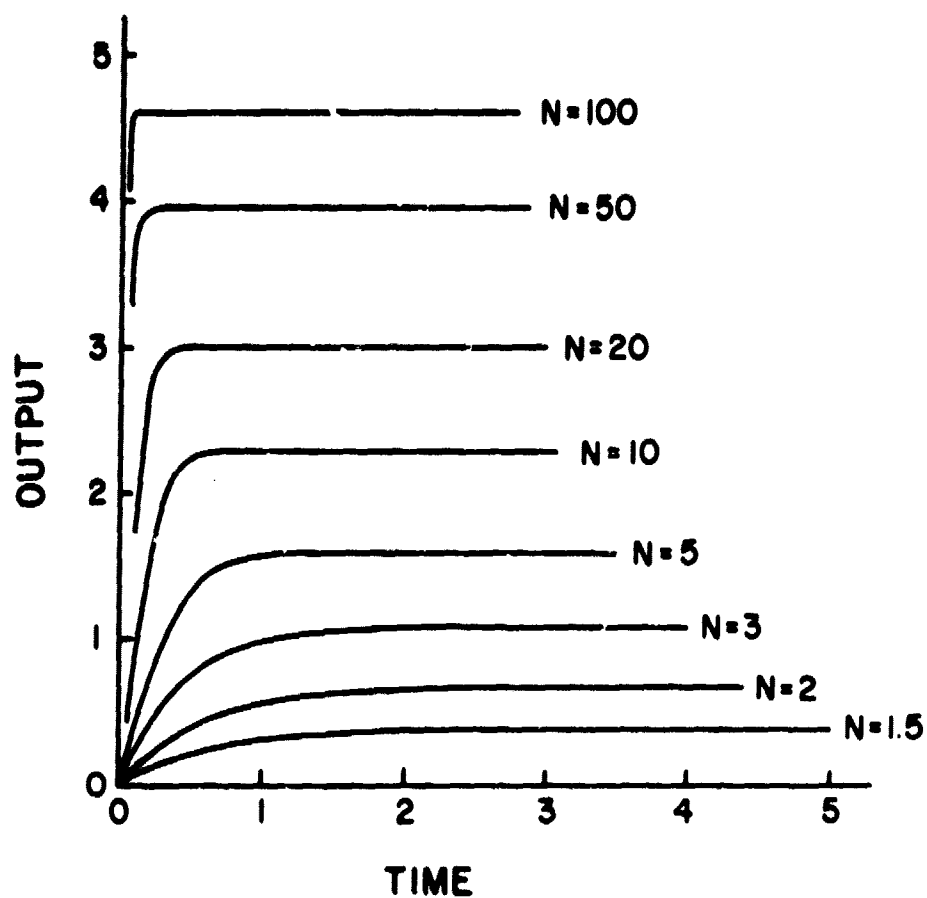
Figure AI.3 Plot of the output voltage (scaled) of the
logarithmic electrometer against time (scaled)
for nine values of input current. The scaled
time parameter is $xi_S/i = (i_S/Cv_T)t$, where i_S
is the diode reverse saturation current, C is
the feedback capacitance, v_T is a constant (25
mV) and t is the time since the current was
applied.

It is both interesting and instructive to compare the preceding analysis, which considers a step-function increase of current from zero to some value i, with the quite-different situation of small changes in current about the value i. This is accomplished by considering the dynamic resistance of the diode.

From equation (I.2), by differentiation, the dynamic resistance of the diode is, with $|v| \gg |v_-|$ (since $A \gg 1$)

$$R_D = \frac{dv}{di_D} = \frac{v_T}{\overline{i_D}} \tag{I.13}$$

where $\overline{i_D}$ is the average current in the diode. The time constants determining the frequency response of the log electrometer for the average current $\overline{i_D}$ is thus

$$\tau = CR_D = \frac{Cv_T}{\overline{i_D}} \tag{I.14}$$

The upper 3-dB frequency for the frequency response is

$$f_H = \frac{\overline{i_D}}{2\pi Cv_T} \tag{I.15}$$

The frequency response of a log electrometer has been investigated by *Klaus and Smith* [1978]. For an average current $(\overline{i_D})$ of 1×10^{-8} A they found that the response to a superimposed square wave variation of current was a rise time (to 90% of the final value) of 150 μs. This corresponds to an upper 3-dB frequency (f_H) of 2.5 kHz.

Using equation (I.14), which $v_T = 25$ mV we find $C = 25$ pF. This, then is the effective value of the capacitance of the feedback circuit which consists of two diodes in parallel, opposed, and stray capacitance.

The experimental measurements of *Klaus and Smith* [1978] also show that $v_o = 0.24$ V for $i = 1 \times 10^{-8}$ A. From equation (I.11), therefore, $i_S = 1 \times 10^{-12}$ A. Substituting values for C and i_S in equation (I.12) gives the response time for a step-function increase of current from zero.

$$\tau = 6.25 \times 10^{-13} [\ln(10^{12}i)]/i \tag{I.16}$$

This can be interpreted as a frequency response

$$f = \frac{1}{2\pi\tau} = 2.5 \times 10^{11} i / \ln(10^{12} i)$$

This shows, for example, that $f = 500$ Hz for $i = 2 \times 10^{-8}$ A.

APPENDIX II. Complete listing of Program ELTEMP. Subroutine CRUNCH contains a
200 ms humbucking algorithm as used in the analysis of Nike Apache
14.534 (described in section 5.2).

```
/JOB
JOBRKZ.
SIGNON(355469629).
ZIMMO.
CHARGE,ELEC,PS6899.
SETTL,20.
PRINT/RJE=EE.
/NOSEQ
FTN,ER,T,A,L=0.
LABEL(TAPE3,NT,LB=KU,PO=R,VSN=WI534L-F008,F=L).
ATTACH,IMSLIB,UOILIB/UN=LIBRARY.
$LIBRARY,IMSLIB,JOILIB.
LGO.
SKIPTO,X.
EXIT.
ENDSKIP,X.
DAYFILE.
/EOR
      PROGRAM ELTEMP(INPUT,OUTPUT,TAPE1=INPUT,TAPE2=OUTPUT,TAPE3)
      INTEGER LOG,ARRAY,RECNUM,START,STOP,WORD,OFFSET
      DIMENSION TEMP(400),D(8)
      LOGICAL FLAG
      COMMON LOG(3,400),RECNUM(3),RECTIM(3),OFFSET,CALIB,KMAX,KMIN
      COMMON/ZIM/ ARRAY(2008),NBLOCK,ICHAN
      COMMON/Q/T(50),ALT(50),TIME(400),AALT(400),IJK,NUM
      COMMON/P/TMLNCH
      DATA (NBLOCK=0),(SPREAD=250.0)
      REWIND 3
* THE CARD DECK SUPPLIED WITH THIS PROGRAM MUST USE THIS FORMAT.
*    CARD 1    ROCKET TYPE AND NUMBER.              3A10
*    CARD 2    LAUNCH DATE AND TIME INFORMATION.    3A10
*    CARD 3    SOLAR ZENITH ANGLE.                  2A10
*    CARD 4    LAUNCH LOCATION.                     3A10
*    CARD 5    DIGITAL TAPE NAME.                   1A10
*    CARD 6    DIGITAL TAPE RACK NUMBER.            1A10
*    CARD 7    TAPE CHANNEL TO BE EXAMINED, I1 (1,2,3,4,OR 5)
*    CARD 8    RECORD NUMBER TO START DATA REDUCTION, I4
*    CARD 9    RECORD NUMBER TO STOP  DATA REDUCTION, I4
*    CARD 10   CALIBRATION CONSTANT, F6.0
*    CARD 11   OFFSET PARAMETER, I3  (POSITIVE NUMBER).
*    CARD 12   KMAX, I4
*    CARD 13   KMIN, I4
*    CARD 14   LAUNCH TIME  DDD:HH:MM:SS
*    CARD 15   AND ON SHOULD BE TRAJECTORY DATA SUPPLIED EVERY TEN SECONDS
*              THROUGHOUT THE FLIGHT.  FORMAT(F5.1,F11.3)

* INPUT THE CARD INFORMATION.
      READ(1,2)A1,A2,A3,B1,B2,B3,C1,C2,D1,D2,D3,E1,F1
```

```
    2 FORMAT(3A10/3A10/2A10/3A10/1A10/1A10)
      READ(1,4)ICHAN,START,STOP,CALIB,OFFSET,KMAX,KMIN,LD,LH,LM,LS
    4 FORMAT(I1/I4/I4/F5.0/I3/I4/I4/I3,1X,I2,1X,I2,1X,I2)
      TMLNCH=LD*86400.+LH*3600.+LM*60.+LS*1.
      DO 8 J=1,50
      READ(1,6) T(J),ALT(J)
    6 FORMAT(F5.1,F11.3)
      IF(EOF(1)) 10,8
    8 CONTINUE
   10 NUM=J-1
*  OUTPUT THE CARD INFORMATION.
      WRITE(2,12)
   12 FORMAT("0"/"0",6X,"EEEEEE  L",5X,"TTTTTTT  EEEEEE  M",5X,"M  PPPPP
     J",12X,"AERONOMY"/" ",6X,"E",7X,"L",8X,"T",5X,"E",7X,"MM   MM  P
     J P"/" ",6X,"E",7X,"L",8X,"T",5X,"E",7X,"M M M M  P    P",9X,"LABOR
     JATORY"/" ",6X,"EEEEEE  L",8X,"T",5X,"EEEEEE  M M M  PPPPP"/" ",
     J6X,"E",7X,"L",8X,"T",5X,"E",7X,"M    M  P",18X,"ROCKET"/" ",6X,"E
     J",7X,"L",8X,"T",5X,"E",7X,"M    M  P"/" ",6X,"EEEEEE  LLLLLL   T
     J    EEEEEE  M    M  P",17X,"PROGRAM"/"0")
      WRITE(2,14)A1,A2,A3,B1,B2,B3,C1,C2,D1,D2,D3,E1,F1
   14 FORMAT(" ",10X,3A10/" ",10X,3A10/" ",10X,2A10/" ",10X,3A10/" ",10X
     J,"DIGITAL TAPE NAME: ",1A10/" ",10X,"DIGITAL TAPE RACK NUMBER: ",
     J1A10)
      WRITE(2,16) ICHAN,START,STOP,CALIB,OFFSET,KMAX,KMIN
   16 FORMAT(" ",10X,"TAPE CHANNEL: ",1I1/" ",10X,"START RECORD: ",1I4/
     J" ",10X,"STOP RECORD: ",1I4/" ",10X,"CALIBRATION CONSTANT: ",F6.0
     J/" ",10X,"OFFSET PARAMETER: ",I3/" ",10X,"KMAX: ",I4/" ",10X,"KMIN
     J: ",I4/" ")
      CALL DATE(W)
      CALL GBYTES(W,D(1),6,6,0,8)
      WRITE(2,18)D(4),D(5),D(7),D(8),D(1),D(2)
   18 FORMAT(" ",10X,"TODAYS DATE: ",2R1,"/",2R1,"/",2R1/" ")
      WRITE(2,20)(T(J),ALT(J),J=1,NUM)
   20 FORMAT(" ",10X,"TRAJECTORY DATA"/" ",13X,"TIME",5X,"HEIGHT",
     J 70(/" ",12X,F5.1,F11.3) )
*  START UP ROUTINE.
      IC=START-2
      DO 22 J=1,IC
   22 CALL FORWRD(3,NBLOCK)
      DO 30 N=1,3
   30 CALL LOAD(N)
*   START UP ROUTINE IS COMPLETE. BEGIN DATA PROCESSING.
      IJK=0
      M=2
      WORD=1
   35 CALL TRSHLD(M,FLAG,WORD)
      IF(FLAG) GO TO 40
      IF(RECNUM(M).GE.STOP) GO TO 50
      CALL LOAD(LAST(M))
      M=NEXT(M)
      WORD=1
      GO TO 35
   40 IJK=IJK+1
      CALL CRUNCH(M,WORD,SPREAD,TIME(IJK),TEMP(IJK))
```

```
      WRITE(2,45) TIME(IJK),TEMP(IJK)
   45 FORMAT(" ","** TIME=",F9.4," TEMP=",F8.0," DEGREES K."/" ")
      IF(RECNUM(M).GE.STOP) GO TO 50
      CALL LOAD(LAST(M))
      M=NEXT(M)
      GO TO 35
*  PROBLEM TERMINATION AND DATA OUTPUT.
   50 CONTINUE
*  PARABOLIC ALTITUDE INTERPOLATION
*  RETURNS INTERPOLATED ALTITUDE IN ARRAY AALT(400)
*  FOR EACH TIME IN ARRAY TIME(400)
      CALL TRAJ
*  DATA OUTPUT.
      WRITE(2,55)
   55 FORMAT("0")
      WRITE(2,12)
      WRITE(2,14)A1,A2,A3,B1,B2,B3,C1,C2,D1,D2,D3,E1,F1
      WRITE(2,16)ICHAN,START,STOP,CALIB,OFFSET,KMAX,KMIN
      WRITE(2,80)
   80 FORMAT("0",T8,"TIME AFTER NOMINAL LAUNCH",T37,
     *"ALTITUDE",T51,"ELECTRON TEMPERATURE"/" ",T15,"(SECONDS)",
     *T35,"(KILOMETERS)",T55,"(DEGREES K)"/" ")
      DO 90  J=1,IJK
   90 WRITE(2,100) TIME(J),AALT(J),TEMP(J)
  100 FORMAT(" ",T14,F9.4,T37,F7.3,T59,F5.0)
      STOP 5
      END

      SUBROUTINE LOAD(M)
      INTEGER LOG,ARRAY,RECNUM,OFFSET
      COMMON LOG(3,400),RECNUM(3),RECTIM(3),OFFSET,CALIB,KMAX,KMIN
      COMMON/ZIM/ARRAY(2008),NBLOCK,ICHAN

*  SUBROUTINE LOAD IS USED TO PLACE ROCKET DATA IN THE
*  CIRCULAR DATA PROCESSING FILE FROM THE TAPE. THE EFFECT
*  OF A CALL TO LOAD(M) IS TO :
*    FILL ARRAY LOG(M,1-400) WITH LOG ELECTROMETER DATA.
*    SET RECNUM(M) TO THE RECORD NUMBER OF DATA TRANSFERRED.
*    SET RECTIM TO THE NOMINAL TIME OF RECORD (SECONDS).

      CALL TPGET(3,ARRAY,1,NWORDS,NBLOCK)
      IF(NWORDS.EQ.2008) GOTO 20
      WRITE(2,10) NBLOCK,NWORDS
   10 FORMAT("0","RECORD ",I3," CONTAINS ",I4," WORDS.")
      STOP 6
   20 RECNUM(M)=NBLOCK
      DO 30 N=1,400
      I=ICHAN+N*5
   30 LOG(M,N)=ARRAY(I)
      CALL CALTIM(ARRAY(2006),ARRAY(2007),ARRAY(2008),RECTIM(M))
      RETURN
      END

      SUBROUTINE CALTIM(T2006,T2007,T2008,TIME)
```

```
         INTEGER DAY,HOUR,MIN,SEC,FRCSEC,T2006,T2007,T2008,I(16)
         COMMON/P/TMLNCH
*   SUBROUTINE CALTIM (CALCULATE TIME) CALCULATES TIMES
*   BY DECODING THE NASA DIGITAL TIME DATA IN THE LAST
*   THREE WORDS OF A TAPE RECORD.   THIS IS UNIVERSAL
*   COORDINATED TIME IN DAYS, HOURS, MINUTES, SECONDS,
*   AND DECIMAL FRACTIONAL SECONDS. THE NOMINAL LAUNCH
*   TIME IS INPUT TO THE PROGRAM IN THE DECK OF DATA
*   CARDS. THE TIME AFTER NOMINAL LAUNCH  [IN SECONDS]
*   IS CALCULATED BY TAKING THE DIFFERENCE BETWEEN THE
*   TAPE TIME AND THE LAUNCH TIME.

*   CONVERT T2006 INTO FRACTIONAL SECONDS.
         CALL BINARY(T2006,I)
         FRCSEC=(8*I(16)+4*I(15)+2*I(14)+I(13))*1000
        1+(8*I(12)+4*I(11)+2*I(10)+I(9))*100
        2+(8*I(8)+4*I(7)+2*I(6)+I(5))*10
        3+(8*I(4)+4*I(3)+2*I(2)+I(1))

*   CONVERT T2007 INTO MINUTES AND SECONDS.
         CALL BINARY(T2007,I)
         MIN=(4*I(15)+2*I(14)+I(13))*10
        1+(8*I(12)+4*I(11)+2*I(10)+I(9))
         SEC=(4*I(7)+2*I(6)+I(5))*10
        1+(8*I(4)+4*I(3)+2*I(2)+I(1))

*   CONVERT T2008 INTO DAYS AND HOURS
         CALL BINARY(T2008,I)
         DAY=(2*I(16)+I(15))*100
        1+(8*I(14)+4*I(13)+2*I(12)+I(11))*10
        2+(8*I(10)+4*I(9)+2*I(8)+I(7))
         HOUR=(2*I(6)+I(5))*10
        1+(8*I(4)+4*I(3)+2*I(2)+I(1))

*   CALCULATE THE NOMINAL TIME AFTER LAUNCH.
         TMTAPE=DAY*86400.+HOUR*3600.+MIN*60.+SEC*1.+FRCSEC*.0001
         TIME=TMTAPE-TMLNCH
         RETURN
         END

         SUBROUTINE BINARY(IINTGR,I)
         INTEGER I(16)
         INTGR=IINTGR
*   SUBROUTINE BINARY GENERATES THE BINARY REPRESENTATION
*   OF THE NUMBER INTGR, FOR USE IN SUBROUTINE CALTIM.

         DO 1 N=1,16
        1  I(N)=0
         DO 2 N=1,16
         J=17-N
         L=2**(J-1)
         IF(INTGR.GE.L) I(J)=1
         IF(INTGR.GE.L) INTGR=INTGR-L
        2  CONTINUE
```

```
*  THE ARRAY I(1-16) IS THE BINARY REPRESENTATION OF
*  THE NUMBER INTGR, WITH I(16) BEING THE MOST SIGNI-
*  FICANT BIT,2**15, AND I(1) THE LEAST SIGNIFICANT
*  BIT,2**0.
      RETURN
      END


      SUBROUTINE TRSHLD(M,FLAG,WORD)
*  SUBROUTINE TRSHLD(THRESHOLD) EXAMINES THE LOG ELECTROMETER
*  DATA TO LOCATE THE POSITION WHERE SUBROUTINE CRUNCH SHOULD
*  BE APPLIED. THE PARAMETERS ARE:
*   --M,INPUT. INDICATES WHICH FILE TO EXAMINE. M MAY EQUAL 1,2 OR 3.
*   --FLAG,LOGICAL OUTPUT. FLAG IS SET TO .TRUE. IF THE THRESHOLD
*     IS FOUND IN THE LOG DATA IN FILE M.
*   --WORD,INTEGER INPUT AND OUTPUT. ON INPUT WORD IS A POINTER
*     INDICATING WHICH WORD IN FILE M TO BEGIN THE THRESHOLD
*     SEARCH. ON OUTPUT WORD IS THE LOCATION OF A BONAFIDE THRES-
*     HOLD(IN WHICH CASE FLAG IS SET TO .TRUE.).

*  R. K. ZIMMERMAN, JR.               MARCH 1978
*  AERONOMY LABORATORY - UNIVERSITY OF ILLINOIS

      COMMON LOG(3,400),RECNUM(3),RECTIM(3),OFFSET,CALIB,KMAX,KMIN
      INTEGER LOG,RECNUM,OFFSET,WORD
      LOGICAL FLAG
      FLAG=.FALSE.
      DO 60 J=WORD,400
      MI=M
      JJ=J+5
      IF(JJ.GT.400) MI=NEXT(M)
      IF(JJ.GT.400) JJ=JJ-400
      IF((LOG(M,J).LT.KMAX).OR.(LOG(MI,JJ).GT.KMIN)) GOTO 60
      DO 55 IADD=6,14
      MI=M
      JJ=J+IADD
      IF(JJ.GT.400) MI=NEXT(M)
      IF(JJ.GT.400) JJ=JJ-400
      IF(LOG(MI,JJ).GT.KMIN) GOTO 60
   55 CONTINUE
*  THRESHOLD HAS BEEN FOUND.
      GOTO 70
   60 CONTINUE
*  THRESHOLD WAS NOT FOUND IN FILE M. RETURN.
      RETURN
*  THRESHOLD FOUND * RETURN TO CALLING PROGRAM.
   70 FLAG=.TRUE.
      WORD=J
      RETURN
      END


      SUBROUTINE CRUNCH(M,WORD,SPREAD,TIME,TEMP)
*  SUBROUTINE CRUNCH OPERATES ON THE LOG ELECTROMETER
*  DATA AT THE POSITION INDICATED BY THE POINTER WORD
*  FROM SUBROUTINE TRSHLD. CRUNCH EXAMINES 60 CONSECUTIVE
```

```
*   POINTS, FITTING A LINE TO THE POINTS BY A LEAST SQUARES
*   PROCEDURE (TAKING 5 CONSECUTIVE POINTS AT A TIME).

*   R. K. ZIMMERMAN, JR.                MARCH 1978
*   AERONOMY LABORATORY - UNIVERSITY OF ILLINOIS

        COMMON LOG(3,400),RECNUM(3),RECTIM(3),OFFSET,CALIB,KMAX,KMIN
        INTEGER LOG,RECNUM,OFFSET,WORD,LLOG(60)
        DIMENSION TE(52),SLOPEZ(56)

*   FIRST THE ARRAY LLOG(60) MUST BE FILLED WITH LOG
*   ELECTROMETER DATA.

        N =WORD+OFFSET+ 1
        NN=WORD+OFFSET+60
        L=1
        IF(N.GT.400)  GO TO 20
        IF(NN.GT.400) GO TO 40
        DO 10 J=N,NN
        JJ=J-200
        MM=M
        IF(JJ.LT.0) MM=LAST(M)
        IF(JJ.LT.0) JJ=JJ+400
        LLOG(L)=LOG(M,J)-LOG(MM,JJ)
     10 L=L+1
*  ARRAY LLOG(60) IS NOW FILLED WITH DATA FROM FILE M.
*  PROCEED TO LEAST SQUARE FIT.
        GO TO 80
     20 N =N -400
        NN=NN-400
        DO 30 J=N,NN
        JJ=J-200
        MM=NEXT(M)
        IF(JJ.LT.0) MM=M
        IF(JJ.LT.0) JJ=JJ+400
        LLOG(L)=LOG(NEXT(M),J)-LOG(MM,JJ)
     30 L=L+1
*  ARRAY LLOG(60) IS NOW FILLED WITH DATA FROM FILE NEXT(M).
*  PROCEED TO LEAST SQUARE FIT.
        GO TO 80
     40 DO 50 J=N,400
        JJ=J-200
        LLOG(L)=LOG(M,J)-LOG(M,JJ)
     50 L=L+1
        NN=NN-400
        DO 60 J=1,NN
        JJ=J-200
        MM=NEXT(M)
        IF(JJ.LT.0) MM=M
        IF(JJ.LT.0) JJ=JJ+400
        LLOG(L)=LOG(NEXT(M),J)-LOG(MM,JJ)
     60 L=L+1
*  ARRAY LLOG(60) IS NOW FILLED WITH DATA FROM FILE M AND FILE
*  NEXT(M). PROCEED TO LEAST SQUARE FIT.
```

```
 80 DO 170  J=1,56
    INDEX=65
    S1=0.
    ST=0.
    SY=0.
    ST2=0.
    SYT=0.
    JP=J+4
    IFLAG=0
 90 DO 100  I=J,JP
    RI=I
    RLOG=LLOG(I)
    S1=S1+1.
    ST=ST+RI
    SY=SY+RLOG
    ST2=ST2+RI*RI
    SYT=SYT+RLOG*RI
100 CONTINUE
    SLOPE=(S1*SYT-SY*ST)/(S1*ST2-ST*ST)
    B=(SY-SLOPE*ST)/S1
    DO 140  IDUM=1,2
    BADMAX=0.
110 DO 120  I=J,JP
    IF(I.EQ.IFLAG) GO TO 120
    RI=I
    RLOG=LLOG(I)
    THEO=SLOPE*RI+B
    DIFF=ABS(THEO-RLOG)
    IF(DIFF.GT.BADMAX) INDEX=I
    IF(DIFF.GT.BADMAX) BADMAX=DIFF
120 CONTINUE
    IF(BADMAX.LT.SPREAD) GO TO 160
    IWORD=WORD+OFFSET+INDEX
    IF(IWORD.GT.400) GO TO 122
    IF(IWORD.LT.1)   GO TO 124
    WRITE(2,126) J,INDEX,RECNUM(M),IWORD
    GO TO 130
122 MNXT=NEXT(M)
    IWD4=IWORD-400
    WRITE(2,126) J,INDEX,RECNUM(MNXT),IWD4
    GO TO 130
124 MLST=LAST(M)
    IWD4=IWORD-400
    WRITE(2,126) J,INDEX,RECNUM(MLST),IWD4
    GO TO 130
126 FORMAT("-",15X,"PASS NUMBER=",I2/
   *" ",15X,"DISCARD POINT(",I2,")"/
   *" ",15X,"RECORD NUMBER=",I4/
   *" ",15X,"WORD=",I3)
130 RI=INDEX
    RLOG=LLOG(INDEX)
    S1=S1-1.
    ST=ST-RI
    SY=SY-RLOG
```

```
      ST2=ST2-RI*RI
      SYT=SYT-RLOG*RI
      SLOPE=(S1*SYT-SY*ST)/(S1*ST2-ST*ST)
      B=(SY-SLOPE*ST)/S1
      IFLAG=INDEX
  140 CONTINUE
       WRITE(2,150)
  150 FORMAT("-",40X,"TWO BAD POINTS")
  160 CONTINUE
      IF(SLOPE.LE.1.) SLOPE=1.
      SLOPEZ(J)=SLOPE
  170 CONTINUE

*  BOXCAR AVERAGING OVER 5 CONSECUTIVE SLOPES.
*  COMPUTATION OF TEMPERATURES.

      DO 175  J=1,52
      JP=J+4
      SUM=0.0
      DO 173  K=J,JP
  173 SUM=SUM+SLOPEZ(K)
      SLOPEZ(J)=SUM/5.0
      TE(J)=CALIB/SLOPEZ(J)
      IF(TE(J).GT.3600.) TE(J)=3600.
  175 CONTINUE
       CALL PLOT(LLOG, TE, M, RECNUM)
      CALL MINI(TE,TEMP,JFLAG)
      CALL ITIME(JFLAG,WORD,M,TIME)
      RETURN
      END

      FUNCTION NEXT(M)
      IF(M.EQ.3) GO TO 10
      NEXT=M+1
      RETURN
   10 NEXT=1
      RETURN
      END

      FUNCTION LAST(M)
      IF(M.EQ.1) GO TO 10
      LAST=M-1
      RETURN
   10 LAST=3
      RETURN
      END

      SUBROUTINE PLOT(LLOG,TE,M,RECNUM)
*  THIS SUBROUTINE PLOTS THE CONTENTS OF ARRAY LLOG AND
*  ARRAY TE FOR EACH EXECUTION OF SUBROUTINE CRUNCH.
      DIMENSION TE(52),NSYM(2),NPTS(2),X(60),Y(60,2)
      INTEGER LLOG(60),RECNUM(3),IMAG4(5151)
      DIMENSION A(174),AA(16)
      DATA AA/16*" "/
```

```
      DATA (AA(I),I=1,8)/"LOG ELECTROMETER VALUE (+) AND TEMPERATURE (*)
     + VERSUS WORD NUMBER"/
      DATA (AA(I),I=9,12)/"WORD NUMBER"/
      DATA (AA(I),I=13,16)/"LOG VALUE/TEMPERATURE"/
      DATA (A(I),I=161,164)/0.0 , 60.0 , 0.0 , 3600.0/
      DATA (A(I),I=165,166)/"+" , "*"/
      DATA (NCALL=0)

      IF(NCALL .NE. 0) GOTO 15
      DECODE(160,1000,AA) (A(I),I=1,160)
      NCALL=1
15    CONTINUE
      WRITE(2,3) M,RECNUM(M)
    3 FORMAT("0"/"0"
     *             ,T32,"//////// RECNUM(",I1,")=",I4,". PLOT(+) IS LOG DAT
     *A, RANGE ZERO  ////////"/" ",T32,"//////// TO 1000.(DATA ARE SCALE
     *D TO FIT Y-AXIS). PLOT(*) ////////"/" ",T32,"//////// IS ELECTRON
     *TEMPERATURE, UNSCALED, 0.TO 3600.0 . ////////")
      XMIN=0.0
      XMAX=60.0
* SCALING OF LOG VALUES.
      DO 10  N=1,60
      Y(N,1)=(LLOG(N)-LLOG(1)+55)*3.6000
      IF(Y(N,1).GT.3600.0) Y(N,1)=3600.0
      IF(Y(N,1).LT.0.0) Y(N,1)=0.0
      X(N)=N
   10 CONTINUE
      DO 20  N=1,60
      Y(N,2)=TE(N)
      IF(Y(N,2).GT.3600.0) Y(N,2)=3600.0
      IF(Y(N,2).LT.0.0)  Y(N,2)=0.0
      X(N)=N
      IF(N.GT.52) Y(N,2)=0.0
   20 CONTINUE
      CALL USPLX(X,Y,60,2,1,60,A,IMAG4,IER)
      IF(IER.EQ.0) RETURN
      WRITE(2,30) IER
   30 FORMAT(" ","ERROR CODE IER = ",I3)
      STOP 7
 1000 FORMAT(160A1)
      END

      SUBROUTINE MINI(TE,TEMP,JFLAG)
      DIMENSION TE(56)
      DO 10  I=1,56
      IF(TE(I).LT.250.) TE(I)=50000.
   10 CONTINUE
   20 TEMP=999999.
      JFLAG=0
      DO 30  I=2,55
      IF(TE(I).LE.TEMP) JFLAG=I
      IF(TE(I).LE.TEMP) TEMP=TE(I)
   30 CONTINUE
      IF(TEMP.GE.49998.) GO TO 40
```

```
      DELTA=(TE(JFLAG+1)+TE(JFLAG-1))/2-TEMP
      IF(DELTA.GT.300) TE(JFLAG)=50000.
      IF(DELTA.GT.300) GO TO 20
   40 WRITE(2,45) JFLAG
   45 FORMAT(" ","** LOWEST TEMP I3 TE(",I2,")")
      RETURN
      END

      SUBROUTINE ITIME(JFLAG,WORD,M,TIME)
      COMMON LOG(3,400),RECNUM(3),RECTIM(3),OFFSET,CALIB,KMAX,KMIN
      INTEGER LOG,RECNUM,OFFSET,WORD
```

* R.K.ZIMMERMAN,JR.   MARCH 1978
* AERONOMY LABORATORY - UNIVERSITY OF ILLINOIS

```
      JWORD= WORD + OFFSET + JFLAG + 4
```
* IN THE ABOVE LINE:
* ---WORD IS THE WORD IN FILE M THAT QUALIFIED AS THRESHOLD.
* ---JFLAG IS THE LOCATION IN LLOG(56) THAT QUALIFIED AS HAVING
*   THE BEST TEMPERATURE WHEN EXAMINED BY MINI.
* ---OFFSET IS THE NUMBER OF WORDS BETWEEN THE THRESHOLD WORD
*   AND THE FIRST ENTRY IN ARRAY LLOG.
* ---INTEGER +4 IS TO ALLOW FOR THE FIVE POINT LINE FIT IN
*   CRUNCH. THAT IS, IF LLOG(1) IS INDICATED BY MINI AS
*   HAVING THE BEST TEMPERATURE, THE ACTUAL SLOPE WAS COMPUTED
*   FROM DATA IN LLOG(1), LLOG(2),....,LLOG(5). THE TIME
*   ASSOCIATED WITH THE BEST TEMPERATURE SHOULD THEREFORE BE
*   THE TIME OF LLOG(3), THE CENTER OF THE FIVE POINT FIT.
*   THE TIME OF LLOG(3) IS ACTUALLY THE TIME OF LOGG(5), SINCE
*   THERE IS A FIVE POINT BOXCAR AVERAGE OF THE SLOPES BEFORE
*   THE FIVE POINT LINE FIT.

      IF(JWORD.GT.400) GO TO 20
      FSEC=(401-JWORD)*.001
```
* NOTE:  THE STATEMENT ABOVE COMPUTES THE FRACTIONAL NUMBER OF SECONDS
*   TO BE SUBTRACTED FROM RECTIM(M) TO GENERATE THE PROPER TIME FOR
*   BEST TEMPERATURE. RECALL THAT THE TIME STORED IN RECTIM(M)
*   IS ACTUALLY THE TIME OF THE FIRST DATA ENTRY IN FILE (M+1). THAT
*   IS WHY WE SUBTRACT BELOW.
```
      TIME=RECTIM(M)-FSEC
      RETURN
   20 FSEC=(JWORD-401)*.001
      TIME=RECTIM(M)+FSEC
      RETURN
      END

      SUBROUTINE TRAJ
```
* SUBROUTINE TRAJ COMPUTES INTERPOLATED ALTITUDE VALUE FOR ANY
* TIME AFTER LAUNCH.  ALTITUDE AND TIME VALUES AT 10 SECOND
* INTERVALS MUST BE PROVIDED VIA ARRAYS T(50) AND ALT(50). THE
* ARRAY FTIME(400) CONTAINS THE TIMES FOR WHICH ALTITUDES ARE
* DESIRED. THESE ALTITUDES ARE CALCULATED AND RETURNED VIA
* ARRAY AALT(400). THE NUMBER OF ENTRIES IN FTIME IS GIVEN BY
* IJK. THE NUMBER OF ENTRIES IN ARRAY T IS GIVEN BY NUM.

```
      COMMON/Q/T(50),ALT(50),FTIME(400),AALT(400),IJK,NUM
      ITCALL=0
      DO 30   J=1,IJK
      INCR=0
      IF(ITCALL.EQ.1)  GO TO 10
      I=3
      ITCALL=1
    5 INCR=1
      IM1=I-1
      IM2=I-2
   10 IF(FTIME(J).LT.T(IM2)) WRITE(2,12)
   12 FORMAT("-","TIME LESS THAN LOWEST TRAJECTORY POINT.")
*  LOCATE THE TIME VALUES WHICH BRACKET FTIME(J).
      IF(FTIME(J).LE.T(I))  GO TO 15
      I=I+1
      IF(I.GT.NUM) STOP
      GO TO 5
*  IF PRESENT TIME VALUE FTIME(J) IS IN THE SAME 10 SECOND
*  INTERVAL AS THE PREVIOUS ONE, COMPUTE ALTITUDE WITH OLD
*  COEFFICIENTS.  IF NOT, COMPUTE NEW COEFFICIENTS.
   15 IF(INCR.EQ.1) GO TO 25
   20 AALT(J)= A*FTIME(J)*FTIME(J)+B*FTIME(J)+C
      GO TO 30
   25 BRAC1=(T(I)-T(IM1))*(ALT(IM1)-ALT(IM2))
      BRAC2=(T(IM1)-T(IM2))*(ALT(I)-ALT(IM1))
      TOP=BRAC1-BRAC2
      BRAC1=(T(IM1)-T(IM2))*(T(I)*T(I)-T(IM1)*T(IM1))
      BRAC2=(T(I)-T(IM1))*(T(IM1)*T(IM1)-T(IM2)*T(IM2))
      BOTTOM=BRAC2-BRAC1
      A=TOP/BOTTOM
      B=(ALT(IM1)-ALT(IM2))-A*(T(IM1)*T(IM1)-T(IM2)*T(IM2))
      B=B/(T(IM1)-T(IM2))
      C=ALT(IM2)-A*T(IM2)*T(IM2)-B*T(IM2)
      GO TO 20
   30 CONTINUE
      RETURN
      END


      SUBROUTINE TPGET(U,ARRAY,M,N,NBLOCK)

*  THIS SUBROUTINE IS USED TO TRANSFER ONE RECORD OF TAPE DATA FROM
*  UNIT 'U' TO 'ARRAY', BEGINNING WITH ARRAY ELEMENT M.  THE NUMBER
*  OF 16-BIT WORDS TRANSFERRED ON EACH CALL IS N (TYPICALLY 10, 45,
*  1005, OR 2008). THE NUMBER OF THE RECORD JUST READ IS NBLOCK.

      IMPLICIT INTEGER(A-Z)
      DIMENSION BUFFER(540), ARRAY(1)
      BUFFER IN (U,1)(BUFFER(1),BUFFER(540))
      NBLOCK=NBLOCK+1
      IF(UNIT(U)) 10,20,40
   10 CALL LENGTHX(U,I,J)
*  I IS THE NUMBER OF 60-BIT WORDS READ.
*  J IS THE NUMBER OF BITS IN THE LAST 60-BIT WORD THAT WERE NOT USED.
      N=(60*I-J)/16
```

```
      CALL GBYTES(BUFFER,ARRAY(M),0,16,0,N)
      RETURN
   20 NBLOCK=NBLOCK-1
      WRITE(2,30) NBLOCK
   30 FORMAT(" "/"0","*** END OF FILE ENCOUNTERED. LAST RECORD IS ",I4,
     J". ***")
      STOP 1
   40 WRITE(2,50) NBLOCK
   50 FORMAT(" "/"0","*** PARITY ERROR DETECTED IN RECORD ",I4,". ***")
      STOP 2
      END



      SUBROUTINE FORWRD(U,NBLOCK)

*   THIS SUBROUTINE IS USED TO FORWARD SPACE ONE RECORD ON TAPE UNIT U.
*   THE NUMBER OF THE RECORD SKIPPED IS NBLOCK.

      IMPLICIT INTEGER(A-Z)
      DIMENSION BUFFER(540)
      BUFFER IN (U,1)(BUFFER(1),BUFFER(540))
      NBLOCK=NBLOCK+1
      IF(UNIT(U)) 10,20,40
   10 RETURN
   20 NBLOCK=NBLOCK-1
      WRITE(2,30) NBLOCK
   30 FORMAT(" "/"0","*** END OF FILE ENCOUNTERED. LAST RECORD IS ",I4,
     J". ***")
      STOP 3
   40 WRITE(2,50) NBLOCK
   50 FORMAT(" "/"0","*** PARITY ERROR DETECTED IN RECORD ",I4,". ***")
      STOP 4
      END
/EOR
NIKE APACHE 14.534
1977 AUG 10  05:01:00 UT
X = 126.54 DEGREES
WALLOPS ISLAND, VIRGINIA
WI534L
F008
1
0925
1020
32340.
124
1000
0100
222:05:01:00
   30.0    026.397
   40.0    044.090
   50.0    060.738
   60.0    076.404
   70.0    091.113
   80.0    104.874
```

90.0	117.692
100.0	129.570
110.0	140.507
120.0	150.514
130.0	159.592
140.0	167.738
150.0	174.960
160.0	181.259
170.0	186.632
180.0	191.087
190.0	194.622
200.0	197.240
210.0	198.940
220.0	199.722
230.0	199.588
240.0	198.533
250.0	196.562
260.0	193.678
270.0	189.869
280.0	185.142
290.0	179.494
300.0	172.929
310.0	165.432
320.0	157.013
330.0	147.664
340.0	137.382
350.0	126.171
360.0	114.020
370.0	100.927
380.0	086.893
390.0	071.924
400.0	056.136
410.0	039.885
420.0	023.673
430.0	008.544
440.0	0.0

APPENDIX III.   Program NASA for examining the contents of a digital magnetic
                tape.   Sample output for Nike Apache 14.534 is shown.

```
/*CYBER
JOBROB.
SIGNON(355469629).
ZIMMO.
BILL,ELEC,PS6899.
PRINT/RJE=EE.
FTN,A,L=0.
LABEL,TAPE1,NT,LB=KU,PO=R,VSN=WI534-D404,F=L.
ATTACH,UOILIB/UN=LIBRARY.
LDSET(LIB=SYMLIB/UOILIB).
LGO.
SKIPTO,X.
EXIT.
DAYFILE.
/EOR
      PROGRAM NASA(INPUT,OUTPUT,TAPE1,TAPE2=OUTPUT,TAPE3=INPUT)
* THIS PROGRAM IS USED TO DISPLAY DIGITAL DATA FROM NASA DATA TAPES
* RECORDED AT WALLOPS ISLAND VIRGINIA. THE USER MUST SUPPLY CARDS
* INDICATING THE CHANNEL AND RECORD NUMBER TO BE PRINTED.  THESE
* CARDS MUST BE TYPED IN THE FOLLOWING FORMAT:
*  COLUMNS 1 - 4 RECORD NUMBER.
*  COLUMN  5      COMMA.
*  COLUMN  6      CHANNEL TO BE PRINTED - 1,2,3,4, OR 5.
*  COLUMN  7      COMMA.
*  COLUMN  8      NUMBER OF CONSECUTIVE RECORDS TO PRINT.
* FOLLOWING THE LAST CARD IS A 789 CARD. THIS PROGRAM WILL PRINT DATA
* FOR RECORDS OF LENGTH 10,45,1005, OR 2008 WORDS. EACH WORD IS 16 BITS.
* WRITTEN BY R.K.ZIMMERMAN,JR.       MARCH 1978
* AERONOMY LABORATORY - UNIVERSITY OF ILLINOIS
      IMPLICIT INTEGER(A-Z)
      DIMENSION ARRAY(2008),PARRAY(400)
      DATA (NBLOCK=0)
* THE FOLLOWING LINE LOCATES THE 'FILE ENVIRONMENT TABLE' ADDRESS WHICH
* IS USED LATER IN THE PROGRAM TO BACKSPACE TAPE1.
      NN=FETADR(1)
* WRITE "NASA" BANNER AT TOP OF OUTPUT.
      WRITE(2,5)
    5 FORMAT("0"/"0",6X,"N      N    AAAA     SSSS     AAAA",13X,"AERONOMY"
     J/" ",6X,"NN    N   A    A   S     S   A      A"
     J/" ",6X,"N N   N   A    A   S         A      A",10X,"LABORATORY"
     J/" ",6X,"N  N  N  AAAAAA    SSSS    AAAAAA"
     J/" ",6X,"N   N N  A    A        S   A      A",14X,"ROCKET"
     J/" ",6X,"N    NN  A    A   S    S   A      A"
     J/" ",6X,"N     N  A    A    SSSS    A      A",13X,"PROGRAM"
     J/"0",11X,"-- CDC CYBER VERSION --"/"0"/"0")
* READ CARD INFORMATION.
   10 READ(3,20) RECNUM,CHAN,NUM
   20 FORMAT(I4,1X,I1,1X,I1)
      IF(EOF(3)) 200,25
* SKIP THE PROPER NUMBER OF RECORDS TO GET TO THE RECORDS DESIRED.
   25 ISKIP=RECNUM-NBLOCK-1
```

```
      IF(ISKIP) 30,70,50
   30 ISKIP=-ISKIP
      DO 40 I=1,ISKIP
   40 CALL BACKUP(NN,NBLOCK)
      GOTO 70
   50 DO 60 I=1,ISKIP
   60 CALL FORWRD(1,NBLOCK)
* FILL ARRAY WITH DATA.
   70 DO 190 I=1,NUM
      CALL TPGET(1,ARRAY,1,NWORDS,NBLOCK)
      IF(NWORDS.EQ.2008) GOTO  90
      IF(NWORDS.EQ.1005) GOTO 130
      IF(NWORDS.LE.45)   GOTO 160
      WRITE(2,80) NBLOCK,NWORDS
   80 FORMAT(" "/"0","RECORD ",I4," NON-STANDARD LENGTH, ",I4,
     J" WORDS.")
      GOTO 190
   90 DO 100 N=1,400
      JJ=CHAN+N*5
  100 PARRAY(N)=ARRAY(JJ)
      CALL CALTIM(ARRAY(2006),ARRAY(2007), ARRAY(2008),DAY,HOUR,MIN,SEC,
     JFRCSEC)
      D1=DAY/100
      D2=(DAY-D1*100)/10
      D3=(DAY-D1*100-D2*10)
      H1=HOUR/10
      H2=HOUR-H1*10
      M1=MIN/10
      M2=MIN-M1*10
      S1=SEC/10
      S2=SEC-S1*10
      F1=FRCSEC/1000
      F2=(FRCSEC-F1*1000)/100
      F3=(FRCSEC-F1*1000-F2*100)/10
      F4=(FRCSEC-F1*1000-F2*100-F3*10)
      WRITE(2,110)NBLOCK,ARRAY(2006),ARRAY(2007),ARRAY(2008),D1,D2,D3,
     JH1,H2,M1,M2,S1,S2,F1,F2,F3,F4,CHAN
  110 FORMAT(" "/"0","RECORD ",I4," CONTAINS 2008 WORDS."/" ","TIME CODE
     J (",Z4,":",Z4,":",Z4,") = DAY ",3I1,", ",2I1,":",2I1,":",2I1,".",
     J4I1," U.T."/" ","DIGITAL DATA FROM CHANNEL ",I1,".")
      WRITE(2,120)(PARRAY(N),N=1,400)
  120 FORMAT("0",4X,10I6)
      GOTO 190
  130 WRITE(2,140) NBLOCK,CHAN
  140 FORMAT(" "/"0","RECORD ",I4," CONTAINS 1005 WORDS."/
     J" ","DIGITAL DATA FROM CHANNEL ",I1,".")
      DO 150 N=1,200
      JJ=CHAN+N*5
  150 PARRAY(N)=ARRAY(JJ)
      WRITE(2,120)(PARRAY(N),N=1,200)
      GOTO 190
  160 WRITE(2,170) NBLOCK,NWORDS
  170 FORMAT(" "/"0","RECORD ",I4," CONTAINS ",I2," WORDS.")
* THE FOLLOWING THREE DO-LOOPS ARE NECESSARY TO CONVERT TEXTUAL DATA
```

```
* FROM IBM EBCDIC REPRESENTATION TO CYBER DISPLAY REPRESENTATION.
      DO 173 N=1,NWORDS
      M=2*N-1
  173 CALL GBYTES(ARRAY(N),PARRAY(M),44,8,0,2)
      M=2*NWORDS
      DO 176 N=1,M
  176 PARRAY(N)=CONETD(PARRAY(N))
      DO 178 N=1,M
      IF((PARRAY(N).EQ.00).OR.(PARRAY(N).EQ.42).OR.(PARRAY(N).EQ.50).OR.
     J(PARRAY(N).EQ.63)) PARRAY(N)=45
  178 CONTINUE
      WRITE(2,180)(PARRAY(N),N=1,M)
  180 FORMAT(" ",90R1)
  190 CONTINUE
      GOTO 10
  200 STOP
      END


      SUBROUTINE CALTIM(T2006,T2007,T2008,DAY,HOUR,MIN,SEC,FRCSEC)
      IMPLICIT INTEGER(A-Z)
      DIMENSION I(16)
* SUBROUTINE CALTIM (CALCULATE TIME) CALCULATES TIMES
* BY DECODING THE NASA DIGITAL TIME DATA IN THE LAST
* THREE WORDS OF A TAPE RECORD.   THIS IS UNIVERSAL
* COORDINATED TIME IN DAYS, HOURS, MINUTES, SECONDS,
* AND DECIMAL FRACTIONAL SECONDS.

* CONVERT T2006 INTO FRACTIONAL SECONDS.
      CALL BINARY(T2006,I)
      FRCSEC=(8*I(16)+4*I(15)+2*I(14)+I(13))*1000
     1+(8*I(12)+4*I(11)+2*I(10)+I(9))*100
     2+(8*I(8)+4*I(7)+2*I(6)+I(5))*10
     3+(8*I(4)+4*I(3)+2*I(2)+I(1))

* CONVERT T2007 INTO MINUTES AND SECONDS.
      CALL BINARY(T2007,I)
      MIN=(4*I(15)+2*I(14)+I(13))*10
     1+(8*I(12)+4*I(11)+2*I(10)+I(9))
      SEC=(4*I(7)+2*I(6)+I(5))*10
     1+(8*I(4)+4*I(3)+2*I(2)+I(1))

* CONVERT T2008 INTO DAYS AND HOURS
      CALL BINARY(T2008,I)
      DAY=(2*I(16)+I(15))*100
     1+(8*I(14)+4*I(13)+2*I(12)+I(11))*10
     2+(8*I(10)+4*I(9)+2*I(8)+I(7))
      HOUR=(2*I(6)+I(5))*10
     1+(8*I(4)+4*I(3)+2*I(2)+I(1))
      RETURN
      END


      SUBROUTINE BINARY(IINTGR,I)
      INTEGER I(16)
* SUBROUTINE BINARY GENERATES THE BINARY REPRESENTATION
```

* OF THE NUMBER INTGR, FOR USE IN SUBROUTINE CALTIM.

```
      INTGR=IINTGR
      DO 1 N=1,16
    1 I(N)=0
      DO 2 N=1,16
      J=17-N
      L=2**(J-1)
      IF(INTGR.GE.L) I(J)=1
      IF(INTGR.GE.L) INTGR=INTGR-L
    2 CONTINUE
```

* THE ARRAY I(1-16) IS THE BINARY REPRESENTATION OF
* THE NUMBER INTGR, WITH I(16) BEING THE MOST SIGNI-
* FICANT BIT,2**15, AND I(1) THE LEAST SIGNIFICANT
* BIT,2**0.

```
      RETURN
      END
      SUBROUTINE TPGET(U,ARRAY,M,N,NBLOCK)
```

* THIS SUBROUTINE IS USED TO TRANSFER ONE RECORD OF TAPE DATA FROM
* UNIT 'U' TO 'ARRAY', BEGINNING WITH ARRAY ELEMENT M. THE NUMBER
* OF 16-BIT WORDS TRANSFERRED ON EACH CALL IS N (TYPICALLY 10, 45,
* 1005, OR 2008). THE NUMBER OF THE RECORD JUST READ IS NBLOCK.

```
      IMPLICIT INTEGER(A-Z)
      DIMENSION BUFFER(540), ARRAY(1)
      BUFFER IN (U,1)(BUFFER(1),BUFFER(540))
      NBLOCK=NBLOCK+1
      IF(UNIT(U)) 10,20,40
   10 CALL LENGTHX(U,I,J)
```
* I IS THE NUMBER OF 60-BIT WORDS READ.
* J IS THE NUMBER OF BITS IN THE LAST 60-BIT WORD THAT WERE NOT USED.
```
      N=(60*I-J)/16
      CALL GBYTES(BUFFER,ARRAY(M),0,16,0,N)
      RETURN
   20 NBLOCK=NBLOCK-1
      WRITE(2,30) NBLOCK
   30 FORMAT(" "/"0","*** END OF FILE ENCOUNTERED. LAST RECORD IS ",I4,
     J". ***")
      STOP 1
   40 WRITE(2,50) NBLOCK
   50 FORMAT(" "/"0","*** PARITY ERROR DETECTED IN RECORD ",I4,". ***")
      STOP 2
      END


      SUBROUTINE FORWRD(U,NBLOCK)
```

* THIS SUBROUTINE IS USED TO FORWARD SPACE ONE RECORD ON TAPE UNIT U.
* THE NUMBER OF THE RECORD SKIPPED IS NBLOCK.

```
          DO 80 I = 2,64
            IF(CORE(I-B) .EQ. 0) GOTO 100
            IF((CORE(I-B) .AND. -777777B) .EQ. LFN) GOTO 90
80        CONTINUE
90        FITADR = CORE(I-B) .AND. 777777B
          FETADR = CORE(FITADR-B+1) .AND. 777777B

100       RETURN
          END

          SUBROUTINE BACKUP(FETADR,NBLOCK)

*   THIS ROUTINE IS INTENDED MAINLY FOR BACKING UP 1 BLOCK ON
*   A MAGNETIC TAPE BEING READ BY A FORTRAN PROGRAM. IT IS ASSUMED
*   THAT THE TAPE IS ACCESSED BY THE PROGRAM VIA SOME UNIT NUMBER,
*   SAY 5. THE USER OF THIS ROUTINE SHOULD FIRST USE THE INTEGER
*   FUNCTION "FETADR" TO ESTABLISH THE ADDRESS OF THE "FILE
*   ENVIRONMENT TABLE" FOR THE TAPE, AND SAVE THE VALUE (NEVER MIND
*   WHY, JUST DO IT). THEN THIS ROUTINE MAY BE CALLED AT WILL TO
*   BACKSPACE THE TAPE BY ONE BLOCK. THE SECOND PARAMETER IS SUPPOSED
*   TO BE AN INTEGER VARIABLE WHICH THE USER PRESUMABLY USES TO
*   KEEP TRACK OF WHICH BLOCK THE TAPE IS POSITIONED ON; ALL BACKUP
*   DOES WITH "BLOCK" IS SUBTRACT ONE FROM IT.
*
*   IF THE TAPE IS UNIT 5, THEN THE PROCESS OF USING BACKUP WOULD BE
*   SOMETHING LIKE THIS:
*
*       IADDR = FETADR(5)
*
*           .
*           .
*           .
*       CALL BACKUP(IADDR,NBLOCK)
*           .
*           .
*           .
*       DO 25 I = 1,10
* 25      CALL BACKUP(IADDR,NBLOCK)
*
*       ETCETERA,ETCETERA,ETCETERA
*
*   THIS  ROUTINE IS INTENDED TO RUN ONLY UNDER CYBER FORTRAN AT THE
*   UNIVERSITY OF ILLINOIS. IT USES AN EXTERNAL ROUTINE "SKIPB" FROM
*   SYSTEM LIBRARY SYMLIB TO DO THE ACTUAL BACKSPACE.
*
*   CODED BY STAN KERR AT THE COMPUTING SERVICES OFFICE OF THE UNIVERSITY
*   OF ILLINOIS AT URBANA FOR BOB ZIMMERMAN OF ELECTRICAL ENGINEERING.
*
          IMPLICIT INTEGER(A-Z)
          DIMENSION  CORE(1)

          BIAS = LOCF(CORE(0))

          IN = CORE(FETADR+1-BIAS) .AND. 777777B
          CORE(FETADR+2-BIAS) = (CORE(FETADR+2-BIAS) .AND. MASK(42)) + IN
```

```
         CORE(FETADR+3-BIAS) = (CORE(FETADR+3-BIAS) .AND. MASK(42)) + IN

         CALL SKIPB(CORE(FETADR-BIAS),1,1)
         NBLOCK = NBLOCK-1
         RETURN
         END

         IDENT   CONETD
((       ENTRY   CONETD
**       CONETD - TABLE ORGANIZATION
*
*        THE CONVERSION TABLE USED BY CONETD IS SET UP WITH
*        8 DISPLAY CODE CHARACTERS PER WORD, LEFT-JUSTIFIED, TO
*        SIMPLIFIY THE ARITHMETIC NECESSARY TO ACCESS A WORD
*        WHICH CONTAINS THE DISPLAY CODE CORRESPONDING TO A GIVEN
*        EBCDIC CHARACTER.

CONETD   EQ      0
         SA1     X1          X1 = I
         SX6     -1          X6=-1, DEFAULT VALUE IF I OUT OF RANGE
         NG      X1,CONETD   RETURN IF I<0
         SX2     256
         IX2     X1-X2
         PL      X2,CONETD   RETURN IF I>255
         BX2     X1
         AX2     3           X2=I/8
         SA2     X2+TABLE    X2 = TABLE WORD WITH CONVERTED VALUE
         MX0     57
         BX1     -X0*X1      X1=MOD(I,8)
         SX1     X1+1        X1=MOD(I,8)+1
         LX1     1
         BX3     X1
         LX3     1
         IX1     X1+X3       X1=6*(1+MOD(I,8))
         SB2     X1
         LX2     B2          SHIFT CONVERTED VALUE TO LOW 6 BITS
         MX0     54
         BX6     -X0*X2      AND OUT EXTRANEOUS AND RETURN
         EQ      CONETD

TABLE    DATA    5562646055525565000B,55555545564657500000B
         DATA    33343536555551550000B,43445555615473710000B
         DATA    55555555554742770000B,55555555550067700000B
         DATA    55554155555555530000B,55555553740550000000B
         DATA    55555555555555550000B,55556157725145660000B
         DATA    67555555555555550000B,55556253475277760000B
         DATA    46505555555555550000B,55557556636573710000B
         DATA    55555555555555550000B,55740060747054640000B
         DATA    55010203040506070000B,10115555555555550000B
         DATA    55121314151617200000B,21225555555555550000B
         DATA    55762324252627300000B,31325555555555550000B
         DATA    55555555555555550000B,55555555555555550000B
         DATA    72010203040506070000B,10115555555555550000B
         DATA    66121314151617200000B,21225555555555550000B
```

```
          DATA    75552324252627300000B,31325555555555550000B
          DATA    33343536374041420000B,43445555555555550000B
          END
/EOR


JOB ACTIVE.



          N     N   AAAA     SSSS     AAAA                AERONOMY
          NN    N   A    A   S    S   A    A
          N N   N   A    A   S        A    A               LABORATORY
          N  N  N   AAAAAA    SSSS    AAAAAA
          N   N N   A    A        S   A    A                 ROCKET
          N    NN   A    A   S    S   A    A
          N     N   A    A    SSSS    A    A                PROGRAM

                 -- CDC CYBER VERSION --
```

RECORD   1 CONTAINS 45 WORDS.
     AMQ1 NIKE APACHE 14.534

RECORD   2 CONTAINS 10 WORDS.
     AMQ1

RECORD   3 CONTAINS 45 WORDS.
     AMQ1 NIKE APACHE 14.534   CALS

RECORD   4 CONTAINS 10 WORDS.
     AMQ1 6   H

RECORD   5 CONTAINS 1005 WORDS.
DIGITAL DATA FROM CHANNEL 1.

          182   174   171   167   170   171   163   157   155   159

          166   167   167   165   170   175   178   180   173   169

          167   168   169   161   158   156   162   169   167   168

          164   174   179   179   178   172   169   169   172   164

          158   157   159   162   165   169   163   164   173   174

181	173	169	167	168	173	163	159	159	159
166	167	167	161	169	177	179	177	174	171
167	171	170	163	158	155	160	163	168	164
164	171	177	180	178	172	169	168	174	167
161	157	157	163	169	169	167	165	174	179
182	178	171	167	169	171	167	159	155	157
164	166	167	164	167	174	179	178	175	169
168	169	171	163	160	155	161	165	167	168
163	169	176	179	182	174	173	168	172	170
159	159	155	163	164	170	167	163	173	178
179	179	173	169	167	173	169	163	158	155
162	165	170	166	166	175	179	179	176	170
167	170	171	164	159	157	159	160	167	170
162	168	174	178	179	175	171	170	171	171
162	159	157	159	165	168	166	165	170	178

APPENDIX IV.   Program CALIB for providing the telemetry calibration for digital
               magnetic tapes. Sample output for Nike Apache 14.534 is shown.

```
/*CYBER
JOBZIM.
SIGNON(355469629).
ZIMMO.
CHARGE,ELEC,PS6899.
PRINT/RJE=EE.
FTN,ER,T,A,L=0.
LABEL,TAPE1,NT,LB=KU,PO=R,VSN=WI534-D404,F=L.
ATTACH,UOILIB/UN=LIBRARY.
LDSET(LIB=UOILIB).
LGO.
SKIPTO,X
EXIT.
ENDSKIP,X.
DAYFILE.
/EOR
      PROGRAM CALIB(INPUT,OUTPUT,TAPE1,TAPE2=INPUT,TAPE3=OUTPUT)
      IMPLICIT INTEGER (C-Z)
      DIMENSION CARRAY(2008),PARRAY(90),D(8)
      DATA (NBLOCK=0),(INT=0),(TNI=0)
      REWIND 1
      WRITE(3,10)
   10 FORMAT("0"/"0",7X,"CCCC",4X,"AAAA",3X,"L",7X,"III  BBBBB",12X,
     J"AERONOMY"/" ",6X,"C    C A    A L",8X,"I    B    B"/7X,"C",7X,
     J"A    A L",8X,"I    B    B",9X,"LABORATORY"/" ",6X,"C",7X,"AAAAAA"
     J," L",8X,"I    BBBBB"/" ",6X,"C",7X,"A    A L",8X,"I    B    B",
     J13X,"ROCKET"/7X,"C",4X,"C A    A L",8X,"I    B    B"/" ",7X,
     J"CCCC  A    A LLLLLL  III  BBBBB",13X,"PROGRAM"/"0")
      CALL DATE(A)
      CALL GBYTES(A,D(1),6,6,0,8)
      WRITE(3,20) D(4),D(5),D(7),D(8),D(1),D(2)
   20 FORMAT(" ","TODAYS DATE: ",2R1,"/",2R1,"/",2R1)
      READ(2,30) AA,AB,AC
   30 FORMAT(3A10)
      WRITE(3,40) AA,AB,AC
   40 FORMAT(" ","TELEMETRY CALIBRATION FOR ",3A10)
      READ(2,50)AD,AE
   50 FORMAT(A10/A10)
      WRITE(3,60)AD,AE
   60 FORMAT(" ","DIGITAL TAPE NAME = ",A6,", RACK NUMBER = ",A4,".")
   70 CALL TPGET(1,CARRAY,1,NWORDS,NBLOCK)
      IF(NWORDS.LE.0045) GOTO  90
      IF(NWORDS.EQ.1005) GOTO 140
      IF(NWORDS.EQ.2008) GOTO 230
      WRITE(3,80) NBLOCK,NWORDS
   80 FORMAT(" ","RECORD ",I2," NON-STANDARD LENGTH. ",I4," WORDS.")
      STOP1
   90 TNI=TNI+1
      DO 100 N=1,NWORDS
      M=2*N-1
  100 CALL GBYTES(CARRAY(N),PARRAY(M),44,8,0,2)
```

```
      M=2*NWORDS
      DO 110 N=1,M
110   PARRAY(N)=CONETD(PARRAY(N))
      IF(TNI.EQ.1) WRITE(3,120)
120   FORMAT(" ")
      DO 125 N=1,M
      IF((PARRAY(N).EQ.00).OR.(PARRAY(N).EQ.42).OR.(PARRAY(N).EQ.50).OR.
     J(PARRAY(N).EQ.63)) PARRAY(N)=45
125   CONTINUE
      WRITE(3,130) NBLOCK,(PARRAY(N),N=1,M)
130   FORMAT(" ","RECORD ",I2,1X,90R1)
      GOTO 70
140   INT=INT+1
      IF((INT.EQ.1).AND.(TNI.EQ.0)) WRITE(3,150) AD
150   FORMAT("0","NO ID HEADER RECORDS ON TAPE ",A6,".")
      SUM1=SUM2=SUM3=SUM4=SUM5=0
      DO 160 N=5,1000,5
      N1=N+1 $ N2=N+2 $ N3=N+3 $ N4=N+4 $ N5=N+5
      SUM1=SUM1+CARRAY(N1)
      SUM2=SUM2+CARRAY(N2)
      SUM3=SUM3+CARRAY(N3)
      SUM4=SUM4+CARRAY(N4)
160   SUM5=SUM5+CARRAY(N5)
      A1=SUM1/200. $ A2=SUM2/200. $ A3=SUM3/200. $ A4=SUM4/200.
      A5=SUM5/200.
      IF(INT.EQ.1) WRITE(3,170) NBLOCK,A1,A2,A3,A4,A5
      IF(INT.EQ.2) WRITE(3,180) NBLOCK,A1,A2,A3,A4,A5
      IF(INT.EQ.3) WRITE(3,190) NBLOCK,A1,A2,A3,A4,A5
      IF(INT.EQ.4) WRITE(3,200) NBLOCK,A1,A2,A3,A4,A5
      IF(INT.EQ.5) WRITE(3,210) NBLOCK,A1,A2,A3,A4,A5
      IF(INT.GE.6) WRITE(3,220) NBLOCK,A1,A2,A3,A4,A5
      GOTO 70
170   FORMAT("0",26X,"CHAN 1   CHAN 2   CHAN 3   CHAN 4   CHAN 5"/
     J        " ","RECORD ",I2,"  LBE (-7.50%)",5F9.1)
180   FORMAT(" ","RECORD ",I2,"  LBH (-3.75%)",5F9.1)
190   FORMAT(" ","RECORD ",I2,"  BAND CENTER ",5F9.1)
200   FORMAT(" ","RECORD ",I2,"  UBH (+3.75%)",5F9.1)
210   FORMAT(" ","RECORD ",I2,"  UBE (+7.50%)",5F9.1)
220   FORMAT(" ","RECORD ",I2,"             ",5F9.1)
230   IF((TNI.GE.1).AND.(INT.EQ.0)) WRITE(3,240) AD
      IF((TNI.EQ.0).AND.(INT.EQ.0)) WRITE(3,250) AD
240   FORMAT("0","NO TELEMETRY CALIBRATION RECORDS ON TAPE ",A6,".")
250   FORMAT("0","NO HEADER ID RECORDS OR TELEMETRY"/
     J        " ","CALIBRATION RECORDS ON TAPE ",A6,".")
      WRITE(3,260) NBLOCK,AD
260   FORMAT("0","RECORD ",I2," IS THE FIRST DATA RECORD ON TAPE ",
     JA6,".")
      STOP4
      END

      SUBROUTINE TPGET(U,ARRAY,M,N,NBLOCK)

*  THIS SUBROUTINE IS USED TO TRANSFER ONE RECORD OF TAPE DATA FROM
*  UNIT 'U' TO 'ARRAY', BEGINNING WITH ARRAY ELEMENT M.  THE NUMBER
```

```
*  OF 16-BIT WORDS TRANSFERRED ON EACH CALL IS N (TYPICALLY 10, 45,
*  1005, OR 2008). THE NUMBER OF THE RECORD JUST READ IS NBLOCK.

       IMPLICIT INTEGER(A-Z)
       DIMENSION BUFFER(540), ARRAY(1)
       BUFFER IN (U,1)(BUFFER(1),BUFFER(540))
       NBLOCK=NBLOCK+1
       IF(UNIT(U)) 10,20,40
    10 CALL LENGTHX(U,I,J)
*  I IS THE NUMBER OF 60-BIT WORDS READ.
*  J IS THE NUMBER OF BITS IN THE LAST 60-BIT WORD THAT WERE NOT USED.
       N=(60*I-J)/16
       CALL GBYTES(BUFFER,ARRAY(M),0,16,0,N)
       RETURN
    20 NBLOCK=NBLOCK-1
       WRITE(2,30) NBLOCK
    30 FORMAT(" "/"0","*** END OF FILE ENCOUNTERED. LAST RECORD IS ",I4,
      J". ***")
       STOP 1
    40 WRITE(2,50) NBLOCK
    50 FORMAT(" "/"0","*** PARITY ERROR DETECTED IN RECORD ",I4,". ***")
       STOP 2
       END


       SUBROUTINE FORWRD(U,NBLOCK)

*  THIS SUBROUTINE IS USED TO FORWARD SPACE ONE RECORD ON TAPE UNIT U.
*  THE NUMBER OF THE RECORD SKIPPED IS NBLOCK.

       IMPLICIT INTEGER(A-Z)
       DIMENSION BUFFER(540)
       BUFFER IN (U,1)(BUFFER(1),BUFFER(540))
       NBLOCK=NBLOCK+1
       IF(UNIT(U)) 10,20,40
    10 RETURN
    20 NBLOCK=NBLOCK-1
       WRITE(2,30) NBLOCK
    30 FORMAT(" "/"0","*** END OF FILE ENCOUNTERED. LAST RECORD IS ",I4,
      J". ***")
       STOP 3
    40 WRITE(2,50) NBLOCK
    50 FORMAT(" "/"0","*** PARITY ERROR DETECTED IN RECORD ",I4,". ***")
       RETURN
       END


       IDENT  CONETD
((     ENTRY  CONETD
**     CONETD - TABLE ORGANIZATION
*
*      THE CONVERSION TABLE USED BY CONETD IS SET UP WITH
*      8 DISPLAY CODE CHARACTERS PER WORD, LEFT-JUSTIFIED, TO
*      SIMPLIFIY THE ARITHMETIC NECESSARY TO ACCESS A WORD
```

```
*           WHICH CONTAINS THE DISPLAY CODE CORRESPONDING TO A GIVEN
*           EBCDIC CHARACTER.

CONETD      EQ      0
            SA1     X1              X1 = I
            SX6     -1              X6=-1, DEFAULT VALUE IF I OUT OF RANGE
            NG      X1,CONETD       RETURN IF I<0
            SX2     256
            IX2     X1-X2
            PL      X2,CONETD       RETURN IF I>255
            BX2     X1
            AX2     3               X2=I/8
            SA2     X2+TABLE        X2 = TABLE WORD WITH CONVERTED VALUE
            MX0     57
            BX1     -X0*X1          X1=MOD(I,8)
            SX1     X1+1            X1=MOD(I,8)+1
            LX1     1
            BX3     X1
            LX3     1
            IX1     X1+X3           X1=6*(1+MOD(I,8))
            SB2     X1
            LX2     B2              SHIFT CONVERTED VALUE TO LOW 6 BITS
            MX0     54
            BX6     -X0*X2          AND OUT EXTRANEOUS AND RETURN
            EQ      CONETD

TABLE       DATA    55626460555256650000B,55555545564657500000B
            DATA    33343536555551550000B,43445556154737100000B
            DATA    55555555554742770000B,55555555550067700000B
            DATA    55555415555555555300000B,55555555374055000000B
            DATA    55555555555555550000B,55556157725145660000B
            DATA    67555555555555550000B,55556253475277760000B
            DATA    46505555555555550000B,55557556636573710000B
            DATA    55555555555555550000B,55740607470546400000B
            DATA    55010203040506070000B,10115555555555550000B
            DATA    55121314151617200000B,21225555555555550000B
            DATA    55762324252627300000B,31325555555555550000B
            DATA    55555555555555550000B,55555555555555550000B
            DATA    72010203040506070000B,10115555555555550000B
            DATA    66121314151617200000B,21225555555555550000B
            DATA    75552324252627300000B,31325555555555550000B
            DATA    33343536374041420000B,43445555555555550000B
            END
```

```
 CCCC      AAAA    L           III   BBBBB              AERONOMY
C     C    A    A  L            I    B     B
C          A    A  L            I    B     B            LABORATORY
C          AAAAAA  L            I    BBBBB
C          A    A  L            I    B     B            ROCKET
C     C    A    A  L            I    B     B
 CCCC      A    A  LLLLLL      III   BBBBB              PROGRAM
```

TODAYS DATE: 07/19/78
TELEMETRY CALIBRATION FOR NIKE APACHE 14.534
DIGITAL TAPE NAME = WI534 , RACK NUMBER = D404.

RECORD 1   AMQ1   NIKE APACHE 14.534
RECORD 2   AMQ1
RECORD 3   AMQ1   NIKE APACHE 14.534   CALS
RECORD 4   AMQ1 6   H

	CHAN 1	CHAN 2	CHAN 3	CHAN 4	CHAN 5
RECORD 5 LBE (-7.50%)	168.0	151.0	169.1	154.1	166.9
RECORD 6 LBH (-3.75%)	1101.0	1098.8	1106.8	1088.3	1113.3
RECORD 7 BAND CENTER	2033.8	2039.6	2050.8	2030.0	2055.1
RECORD 8 UBH (+3.75%)	2967.2	2986.6	2985.8	2971.8	2998.5
RECORD 9 UBE (+7.50%)	3903.3	3932.0	3931.3	3911.2	3944.1

RECORD 10 IS THE FIRST DATA RECORD ON TAPE WI534 .

APPENDIX V. Subroutine CRUNCH as used in the analysis of Nike Apache 14.533.
Seventeen points are averaged to smooth the data and remove 60 Hz hum.

```
      SUBROUTINE CRUNCH(M,WORD,SPREAD,TIME,TEMP)
*  SUBROUTINE CRUNCH OPERATES ON THE LOG ELECTROMETER
*  DATA AT THE POSITION INDICATED BY THE POINTER WORD
*  FROM SUBROUTINE TRSHLD. CRUNCH EXAMINES 60 CONSECUTIVE
*  POINTS, FITTING A LINE TO THE POINTS BY A LEAST SQUARES
*  PROCEDURE (TAKING 5 CONSECUTIVE POINTS AT A TIME).

*  R. K. ZIMMERMAN, JR.              MARCH 1978
*  AERONOMY LABORATORY - UNIVERSITY OF ILLINOIS

      COMMON LOG(3,400),RECNUM(3).RECTIM(3),OFFSET,CALIB,KMAX,KMIN
      INTEGER LOG,RECNUM,OFFSET,WORD,LLOG(60)
      DIMENSION TE(52),SLOPEZ(56)

*  FIRST THE ARRAY LLOG(60) MUST BE FILLED WITH LOG
*  ELECTROMETER DATA.

      N =WORD+OFFSET+ 1
      NN=WORD+OFFSET+60
      L=1
*  SEVENTEEN POINT AVERAGE.
      T17=0.0
      NX=WORD+OFFSET
      DO 5 NZIM=1,17
      JJ=NZIM-9+NX
      MM=M
      IF(JJ.LT.1)   GOTO 3
      IF(JJ.GT.400) GOTO 4
      T17=T17+LOG(MM,JJ)
      GOTO 5
   3 JJ=JJ+400 $ MM=LAST(M)
      T17=T17+LOG(MM,JJ)
      GOTO 5
   4 JJ=JJ-400 $ MM=NEXT(M)
      T17=T17+LOG(MM,JJ)
   5 CONTINUE

      IF(N.GT.400)  GO TO 20
      IF(NN.GT.400) GO TO 40
      DO 10 J=N,NN
      JLSS=J-9 $ JPLS=J+8
      MLSS=MPLS=M
      IF(JLSS.LT.1) MLSS=LAST(M)
      IF(JLSS.LT.1) JLSS=JLSS+400
      IF(JPLS.GT.400) MPLS=NEXT(M)
      IF(JPLS.GT.400) JPLS=JPLS-400
      T17=T17-LOG(MLSS,JLSS)+LOG(MPLS,JPLS)
      LLOG(L)=T17/17.0
  10 L=L+1
*  ARRAY LLOG(60) IS NOW FILLED WITH AVERAGED DATA FROM FILE M.
*  PROCEED TO LEAST SQUARE FIT.
```

```
          GO TO 80
    20 N =N -400
       NN=NN-400
       DO 30 J=N,NN
       JLSS=J-9 $ JPLS=J+8
       MLSS=MPLS=NEXT(M)
       IF(JLSS.LT.1) MLSS=M
       IF(JLSS.LT.1) JLSS=JLSS+400
       T17=T17-LOG(MLSS,JLSS)+LOG(MPLS,JPLS)
       LLOG(L)=T17/17.0
    30 L=L+1
* ARRAY LLOG(60) IS NOW FILLED WITH AVERAGED DATA FROM FILE NEXT(M).
* PROCEED TO LEAST SQUARE FIT.
       GO TO 80
    40 DO 50 J=N,400
       JLSS=J-9 $ JPLS=J+8
       MLSS=MPLS=M
       IF(JPLS.GT.400) MPLS=NEXT(M)
       IF(JPLS.GT.400) JPLS=JPLS-400
       T17=T17-LOG(MLSS,JLSS)+LOG(MPLS,JPLS)
       LLOG(L)=T17/17.0
    50 L=L+1
       NN=NN-400
       DO 60 J=1,NN
       JLSS=J-9 $ JPLS=J+8
       MLSS=MPLS=NEXT(M)
       IF(JLSS.LT.1) MLSS=M
       IF(JLSS.LT.1) JLSS=JLSS+400
       T17=T17-LOG(MLSS,JLSS)+LOG(MPLS,JPLS)
       LLOG(L)=T17/17.0
    60 L=L+1
* ARRAY LLOG(60) IS NOW FILLED WITH AVERAGED DATA FROM FILE M AND FILE
* NEXT(M). PROCEED TO LEAST SQUARE FIT.
    80 DO 170  J=1,56
THE REMAINDER OF SUBROUTINE CRUNCH IS IDENTICAL
WITH THAT GIVEN IN APPENDIX II.
```

REFERENCES

Barbier, D. [1958], The auroral activity at low latitudes, *Ann. Geophys.*, *14*, 334-355.

Blamont, J. E., and C. de Jager [1961], Upper atmosphere turbulence near the 100 km level, *Ann. Geophys.*, *17*, 134-144.

Boggess, R. L., L. H. Brace, and N. W. Spencer [1959], Langmuir probe measurements in the ionosphere, *J. Geophys. Res.*, *64*, 1627-1630.

Boyd, R. L. F. [1968], Langmuir probes on spacecraft, in *Plasma Diagnostics*, Chap. 12, ed. W. Lochte-Holtgreven, North-Holland Publishing Company.

Brace, L. H., W. R. Hoegy, H. G. Mayr, G. A. Victor, W. B. Hanson, C. A. Reber, and H. E. Hinteregger [1976], Discrepancy between electron heating and cooling rates derived from Atmosphere Explorer-C measurements, *J. Geophys. Res.*, *81*, 5421-5429.

Butler, S. T., and K. A. Small [1963], The excitation of atmospheric oscillations, *Proc. Roy. Soc.*, *Ser. A*, *274*, 91-121.

Carpenter, D. L. [1971], Ogo 2 and 4 VLF observations of the asymmetric plasmapause near the time of SAR arc events, *J. Geophys. Res.*, *76*, 3644-3650.

Carru, H., M. Petit, G. Vasseur, and P. Waldteufel [1967a], Résults ionosphériques obtenus par diffusion de Thomson, *Ann. Geophys.*, *23*, 455-465.

Carru, H., M. Petit, and P. Waldteufel [1967b], Mesures de températures électroniques et ioniques par diffusion incohérente, *J. Atmos. Terr. Phys.*, *29*, 351-366.

Chandra, S., E. J. Maier, B. E. Troy, Jr., and B. C. Narasinga Rao [1971], Subauroral red arcs and associated ionospheric phenomena, *J. Geophys. Res.*, *76*, 920-925.

Chang, J. S., and J. G. Laframboise [1976], Theory of electrostatic probes in a flowing continuum low-density plasma, *Technical Note 30*, Center de Recherche en Physique de l'environnement Terrestre et Planetaire, Orleans-La-Source, France.

Chappell, C. R., K. K. Harris, and G. W. Sharp [1971], Ogo 5 measurements of the plasmasphere during observations of stable auroral red arcs, *J. Geophys. Res.*, *76*, 2357-2365.

Clark, W. L., J. R. McAfee, R. B. Norton, and J. M. Warnoch [1969], Radio wave reflections from large horizontal gradients in topside ionosphere, *Proc. IEEE, 57,* 493-496.

Cole, K. D. [1975], Coulomb collisions of ring current particles - Indirect source of heat for the ionosphere, *Report X-621-75-108,* Goddard Space Flight Center, Greenbelt, MD.

Cornwall, J. M., F. V. Coroniti, and R. M. Thorne [1971], Unified theory of SAR arc formation at the plasmapause, *J. Geophys. Res., 76,* 4428-4445.

Dalgarno, A. [1969], Inelastic collisions at low energy, *Can. J. Chem., 47,* 1723-1729.

Dalgarno, A., M. B. McElroy, M. H. Rees, and J. C. G. Walker [1968], The effect of oxygen cooling on the ionospheric electron temperatures, *Planet. Space Sci., 16,* 1371-1380.

Davis, T. N., K. Burrows, and J. D. Stolarik [1967], A latitude survey of the equatorial electrojet with rocket-borne magnetometers, *J. Geophys. Res., 72,* 1845-1861.

Edwards, B. [1977] (Ed.), Research in Aeronomy: October 1, 1976 - March 31, 1977, *Prog. Rep. 77-1,* Aeron. Lab., Dep. Elec. Eng., Univ. Ill., Urbana-Champaign, 28-34.

Evans, J. V. [1967], Electron temperature and ion composition in the F_1 region, *J. Geophys. Res., 72,* 3343-3355.

Evans, J. V. [1973], Millstone Hill Thomson scatter results for 1966 and 1967, *Planet. Space Sci., 21,* 763-792.

Fillinger, R. W., Jr., E. A. Mechtly, and E. K. Walton [1976], Analysis of sounding rocket data from Punta Chilca, Peru, *Aeron. Rep. 73,* Aeron. Lab., Dep. Elec. Eng., Univ. Ill, Urbana-Champaign.

Hasegawa, A., and K. Mima [1978], Anomalous transport produced by kinetic Alfven wave turbulence, *J. Geophys. Res., 83,* 1117-1123.

Herman, J. R., and S. Chandra [1969a], The influence of varying solar flux on ionospheric temperatures and densities: A theoretical study, *Planet. Space Sci., 17,* 815-840.

Herman, J. R., and S. Chandra [1969b], The role of atomic oxygen in the ionospheric *E* and *F*-region behavior, *Planet. Space Sci., 17,* 1247-1256.

Hines, C. O. [1965], Dynamical heating of the upper atmosphere, *J. Geophys. Res., 70,* 77-183.

Hirao, K., and K. Oyama [1970], An improved type of electron temperature probe, *J. Geomag. Geoelect.*, *22*, 393-402.

Hirao, K., and K. Oyama [1972], A critical study on the reliability of electron temperature measurements with a Langmuir probe, *J. Geomagn. Geoelec.*, *24*, 415-427.

Hoch, R. J., and L. L. Smith [1971], Location in the magnetosphere of field lines leading to SAR arcs, *J. Geophys. Res.*, *76*, 3079-3086.

Hoegy, W. R. [1976], New fine structure cooling rate, *Geophys. Res. Lett.*, *3*, 541-544.

Holmes, J. C., and E. P. Szuszczewicz [1975], Versatile plasma probe, *Rev. Sci. Instrum.*, *46*, 592-598.

King, G. A. M., and F. E. Roach [1961], Relationship between red auroral arcs and ionospheric recombination, *J. Res. Nat. Bur. Stand.*, *Sect. D*, *65*, 129-135.

Klaus, D. E., and L. G. Smith [1978], Rocket observations of electron-density irregularities in the equatorial ionosphere below 200 km, *Aeron. Rep. 80*, Aeron. Lab., Dep. Elec. Eng., Univ. Ill, Urbana-Champaign.

Lane, N. F., and A. Dalgarno [1969], Electron cooling by vibrational excitation of O_2, *J. Geophys. Res.*, *74*, 3011-3012.

Lindzen, R. S., and S. Chapman [1969], Atmospheric tides, *Space Sci. Rev.*, *10*, 3-188.

Marovich, E. [1966], Peak observations of stable auroral red arcs, Summary 1955-1965, *Tech. Rep. IER 16-ITSA 16*, 68 pp., NOAA, Boulder, CO.

Marovich, E., and F. E. Roach [1963], Distribution of latitude of red arcs, *J. Geophys. Res.*, *68*, 1885-1888.

Mott-Smith, H. M., and I. Langmuir [1926], The theory of collectors in gaseous discharges, *Physical Review*, *28*, 727-763.

Nagy, A. F., W. B. Hanson, R. J. Hoch, and T. L. Aggson [1972], Satellite and ground-based observation of a red arc, *J. Geophys. Res.*, *77*, 3613-3617.

Norton, R. B., and J. A. Findlay [1969], Electron density and temperature in the vicinity of the 29 September 1967 middle latitude red arc, *Planet. Space Sci.*, *17*, 1867-1877.

Norton, R. B., and E. Marovich [1969], Alouette observations taken during a middle-latitude red arc, *Proc. IEEE*, *57*, 1158-1160.

Pharo, M. W., III, L. R. Scott, H. G. Mayr, L. H. Brace, and H. A. Taylor, Jr. [1971], An experimental study of the ion chemistry and thermal balance in the *E-* and *F*-regions above Wallops Island, *Planet. Space Sci., 19,* 15-25.

Reed, E. I., and J. E. Blamont [1968], Ogo 4 observations of the September 1967 M-arc, *EOS Trans. AGU, 49,* 731 only.

Rees, M. H., and R. G. Roble [1975], Observations and theory of the formation of stable auroral red arcs, *Rev. Geophys. Space Phys., 13,* 201-242.

Roach, F. E., and J. R. Roach [1963], Stable 6300 A auroral arcs in midlatitudes, *Planet. Space Sci., 11,* 523-545.

Roble, R. G., R. B. Norton, J. A. Findlay, and E. Marovich [1971], Calculated and observed features of stable auroral red arcs during three geomagnetic storms, *J. Geophys. Res., 76,* 7648-7662.

Salah, J. E., and R. W. Wand [1974], Tides in the temperature of the lower thermosphere at mid-latitudes, *J. Geophys. Res., 79,* 4295-4304.

Salah, J. E., J. V. Evans, and R. H. Wand [1975], *E*-region temperature measurements at Millstone Hill, *J. Atmos. Terr. Phys., 37,* 461-489.

Schunk, R. W., and J. C. G. Walker [1973], The theory of charged particle temperatures in the upper atmosphere, *Progress in High Temperature Physics and Chemistry, 5,* Ed. C. A. Rouse, 2-62, Pergamon, New York.

Schutz, R. S., L. G. Smith, and H. D. Voss [1975], Electron heating rates in the *E* and *F* regions, *Radio Sci., 10,* 289-295.

Smith, L. G. [1963], Electron density in the ionosphere, *Final Report NASw-98,* Geophysics Corporation of America.

Smith, L. G. [1969], Langmuir probes in the ionosphere, *Small Rocket Instrumentation Techniques,* North-Holland Publ.,Amsterdam, 1-15.

Smith, L. G., M. A. Geller, and H. D. Voss [1974], Energetic electrons in the midlatitude nighttime *E*-region, *J. Atmos. Terr. Phys., 36,* 1601-1612.

Smith, L. G., and D. E. Klaus [1978], Rocket observations of electron density irregularities in the equatorial *E* region, *COSPAR: Space Research Vol. XVIII,* ed. M. J. Rycroft and A. C. Stickland, 261-264, Pergamon, New York.

Smith, L. G., L. H. Weeks, and P. J. McKinnon [1968], Rocket observations of electron temperature in the *E* region, *J. Atmos. Terr. Phys., 30,* 1301-1312.

Smith, L. G., R. K. Zimmerman, Jr., K. Hirao, K. Oyama, and C. Calderon [1978], Electron temperature in the equatorial E region measured by two rocket experiments and by incoherent scatter, *COSPAR: Space Research Vol. XVIII*, ed. M. J. Rycroft and A. C. Stickland, 265-268, Pergamon, New York.

Sugiura, M., and J. C. Cain [1966], A model equatorial electrojet, *J. Geophys. Res.*, *71*, 1869-1877.

Szeszczewicz, E. P., and J. C. Holmes [1975], Surface contamination of active electrodes in plasmas: Distortion of conventional Langmuir probe measurements, *J. Appl. Phys.*, *46*, 5134-5139.

Szuszczewicz, E. P., and J. C. Holmes [1977], Observations of electron temperature gradients in the midlatitude E_s layers, *J. Geophys. Res.*, *82*, 5073-5080.

Tohmatsu, T., and F. E. Roach [1962], Morphology of mid-latitude 6300 Å arcs, *J. Geophys. Res.*, *67*, 1817-1821.

Voss, H. D., and L. G. Smith [1979], Nighttime ionization by energetic particles at Wallops Island in the altitude region 120 to 200 km, *Geophys. Res. Lett.*, *6*, 93-96.

Wand, R. H., and F. W. Perkins [1968], Radar Thomson scatter observations of temperature and ion-neutral collision frequency in the E region, *J. Geophys. Res.*, *73*, 6370-6372.

Wand, R. H., and F. W. Perkins [1970], Temperature and composition of the ionosphere: diurnal variations and waves, *J. Atmos. Terr. Phys.*, *32*, 1921-1943.

Wehner, G., and G. Medicus [1952], Reliability of probe measurements, *J. Appl. Phys.*, *23*, 1035-1046.